The Philosophical Magazine

FIRST PUBLISHED IN 1798

A Journal of Theoretical Experimental and Applied Physics

Vol. 6 June 1961 No. 66
Eighth Series

25s. 0d., plus postage
Annual Subscription £13 10s. 0d., payable in advance

Printed and Published by
TAYLOR & FRANCIS LTD
RED LION COURT, FLEET STREET, LONDON, E.C.4

THE PHILOSOPHICAL MAGAZINE

Authors wishing to submit papers for publication in the Journal should send manuscripts directly to the Publishers.

Manuscripts should be typed in *double* spacing on one side of quarto (8 × 10 in.) paper, and authors are urged to aim at absolute clarity of meaning and an attractive presentation of their texts.

References should be listed at the end in alphabetical order of authors and should be cited in the text in terms of author's name and date. Diagrams should normally be in Indian ink on white card, with lettering in soft pencil, the captions being typed on a separate sheet.

A leaflet giving detailed instructions to authors on the preparation of papers is available on request from the Publishers.

Authors are entitled to receive 25 offprints of a paper in the Journal free of charge, and additional offprints can be obtained from the Publishers.

The *Philosophical Magazine* and its companion journal, *Advances in Physics*, will accept papers for publication in experimental and theoretical physics. The *Philosophical Magazine* publishes contributions describing new results, letters to the editor and book reviews. *Advances in Physics* publishes articles surveying the present state of knowledge in any branch of the science in which recent progress has been made. The editors welcome contributions from overseas as well as from the United Kingdom, and papers may be published in English, French and German.

Thermoremanent Magnetization
I. Experiments on Single Domain Grains†

By C. W. F. Everitt
Imperial College, London

[Received February 6, 1961]

Abstract

This paper describes an attempt to test certain predictions by Néel concerning the properties of thermoremanent magnetization in fine-grained materials. The method of investigation was to examine the effects of alternating-field demagnetization on a specimen which had been given partial and total thermoremanences.

A positive correlation was found between the blocking temperature and coercive force of individual magnetic grains in accordance with a prediction of Néel's. In confirmation of another of Néel's predictions, the ratio j_T/j_s of thermoremanence to spontaneous magnetization in grains with a particular blocking temperature T_B was found to be proportional to the hyperbolic tangent of the magnetizing field; whilst in apparent disagreement with a third prediction j_T/j_s was found to be independent of the coercive force of the grains. In addition the blocking temperatures were found to be almost independent of the magnetizing field up to 50 oersteds.

§ 1. Introduction

1.1. *Background*

The aim of the present work has been to investigate the relationship between the coercive properties of a magnetic material and its thermal properties, by examining the effects of alternating fields on the thermoremanent magnetizations acquired in various fields and temperature ranges.

The properties of thermoremanent magnetization have been investigated experimentally in some detail by Thellier (1941) and other workers whose observations may be summarized as follows:

(1) In many magnetic materials the moments acquired on cooling in a field H from above the Curie temperature (T_C), are directly proportional to H if H is less than 1–2 oersted, and proportional to $H^{1/2}$ if H is 2–30 oersted (Néel 1955, pp. 227 and 240).

(2) If the field is only applied over part of the temperature range during cooling, a partial thermoremanence is produced. A partial thermoremanence acquired between temperatures T_1, T_2 ($T_1 < T_2 < T_C$) is unaffected by heating to T_1 but completely destroyed by heating to T_2. It

† Communicated by the Author.

is also quite independent of other magnetizations acquired in temperature interval outside $T_1 T_2$, even if they are due to fields that are different in magnitude and direction. These facts are epitomized by Thellier's statement: "All the moments are added geometrically but paradoxical as it might seem each is quite independent and preserves a sort of exact memory of the temperatures and field which produced it."

When a magnetization is acquired over a very narrow temperature interval, the mean of the temperature interval is frequently referred to as the 'blocking temperature' for that particular partial thermoremanence. Three different theoretical models, based on the conception of blocking temperatures have been proposed by Néel (1955, pp. 210–212, 225–226, 240–241) to account for thermoremanence in both single domain and multi-domain grains.

For single domains the essential idea is that the blocking temperature is a unique quantity associated with each magnetic grain. Above the blocking temperature the spontaneous magnetization undergoes rapid fluctuations in direction owing to thermal agitation; below this temperature it is very stable in direction. The blocking temperature is given by

$$T_B = \text{const.}\, v j_s(T_B) H_c(T_B) \quad . \quad . \quad . \quad . \quad . \quad . \quad (1)$$

where v is the volume of the grain concerned, and $j_s(T_B)$ and $H_c(T_B)$ are respectively its spontaneous magnetization per unit volume and coercive force, each measured immediately below the blocking temperature†. This formula implies *inter alia* that any bulk magnetic material should exhibit a spectrum of blocking temperatures owing to variations in grain size.

In a small external field a bulk material acquires a thermoremanence, because the moments in individual grains tend to become aligned with the field above the blocking temperature, and then locked into place below that temperature. The properties of partial thermoremanence can evidently be explained easily enough in this way. In § 2.2, an experiment to test eqn. (1) will be described.

Equation (1) is derived from an expression given by Néel for the relaxation time τ_0 of fluctuations in direction of the spontaneous magnetization in zero external field:—

$$\frac{1}{\tau_0} = C \exp\left\{-\frac{v j_s H_c}{2kT}\right\} \quad . \quad . \quad . \quad . \quad . \quad . \quad (2)$$

(C, constant, k, Boltzmann's constant); the blocking temperature being the temperature at which τ_0 becomes of the order of the duration of experiments. In an external field, h, Néel calculates that each grain should

† It is supposed that at the blocking temperature the coercive force of the particle suddenly jumps from zero to an appreciable finite value. This value is itself dependent on the temperature.

exhibit two relaxation times, $\tau(0, \pi)$ and $\tau(\pi, 0)$ for magnetizations parallel and anti-parallel to the field:

$$\frac{1}{\tau(0, \pi)} = C\left(1 + \frac{h}{H_c}\right)\left(1 - \frac{h^2}{H_c^2}\right)\exp\left\{-\frac{vj_s(H_c+h)^2}{2H_c kT}\right\}, \quad (3)$$

$$\frac{1}{\tau(\pi, 0)} = C\left(1 - \frac{h}{H_c}\right)\left(1 - \frac{h^2}{H_c^2}\right)\exp\left\{-\frac{vj_s(H_c-h)^2}{2H_c kT}\right\}. \quad (4)$$

These equations imply that if a specimen is magnetized between two temperatures T_1, T_2 ($T_1 < T_2$) in a sufficiently high field, some grains with blocking temperatures higher than T_2 will become magnetized along the field. On re-heating in zero field the magnetization should start to disappear at T_1 but a substantial residual moment should remain above T_2. Since the exponential terms dominate these equations, the relation between the temperature (T_M) at which the magnetization becomes locked in direction in an external field h, and the blocking temperature in zero field (T_B) should be, equating the exponents in (2) and (3):

$$\frac{T_B}{T_M} = \left(\frac{H_c+h}{H_c}\right)^2. \quad \ldots\ldots\ (5)$$

An experiment to test the effect of the external field on the blocking temperatures will be described in § 2.2.

For a single grain in zero field, the magnetic moment acquired below the blocking temperature will be the spontaneous magnetizations j_s, and may lie in a purely fortuitous way along either of the easy directions in the grain. In an external field, on the other hand, the moment has a bias towards the easy direction nearest to the field. According to Néel, for a statistically large number of grains aligned with their axes parallel to the field, all with blocking temperature T_B, the ratio of the net thermoremanence j_T to the spontaneous magnetization j_s at any temperature is

$$\frac{j_T}{j_s} = \tanh\left[\frac{vj_s(T_B)}{kT_B}.h\right]$$

where k is Boltzmann's constant and h is the applied field.

Substituting from (1), we obtain

$$\frac{j_T}{j_s} = \tanh\left[\text{const.}\,\frac{h}{H_c(T_B)}\right]. \quad \ldots\ldots\ (6)$$

It must be emphasized that j_T is the thermoremanence in grains with a particular blocking temperature T_B. It should be carefully distinguished from J_T the overall thermoremanence for an assemblage of grains with different blocking temperatures; although, as we shall see, the two quantities are sometimes closely related. An experiment to test eqn. (6) will be described in § 2.3.

1.2. *Aim and Arrangement of the Experiments*

A series of experiments to investigate the relationships given in the preceding section were performed on a sample of laterite lent to me by Dr. R. L. Wilson. This was chosen because it was known to have very fine

grains; electron microscope photographs taken by the research department of E.M.I. having shown that the grains ranged in diameter from 0·01 to 0·1 microns and were therefore probably single domains (Néel 1955, p. 206). The magnetic material consisted of impure hematite (Curie point 665°C), and a form of maghemite containing titanium and aluminium, which had a Curie point in a high field of 600°C. Preliminary measurements showed that the maghemite was unaffected by heating to 670°C, but above that temperature gradually underwent inversion to hematite. Figure 1 contains the distribution of partial thermoremanences between room temperature and 665°C, obtained from the intensities of magnetization produced by applying fields of 10 oersteds over various temperature intervals. It shows that there was hardly any partial thermoremanence between 470°C and 600°C: that is to say the maghemite effectively losts its coercive force at a temperature well below the Curie point (600°C), while the hematite had almost no blocking temperatures below about 600°C.

Fig. 1

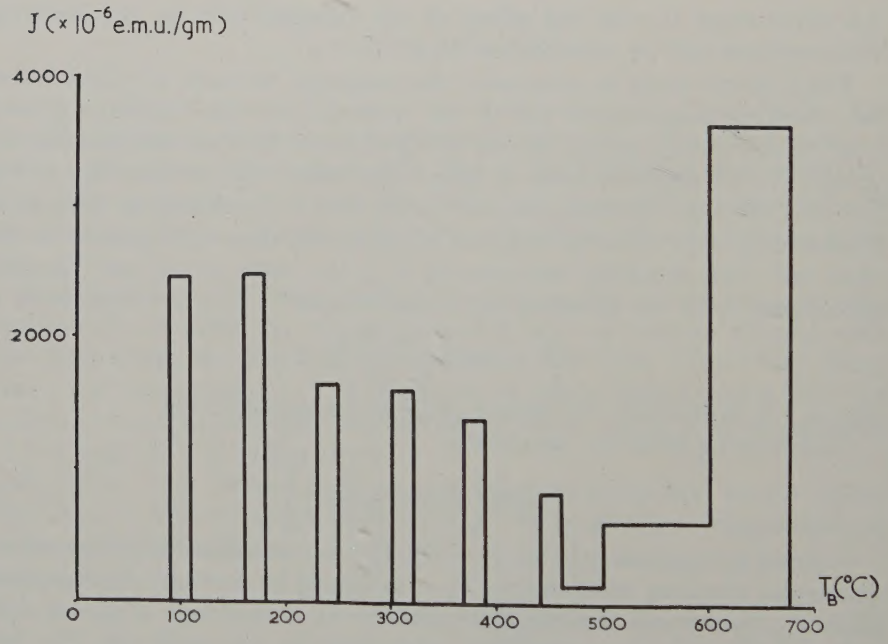

Distribution of blocking temperatures.

The specimen, being in powder form, was packed into a cylindrical duralumin box ($\frac{3}{8}$ in. diameter, $\frac{3}{8}$ in. long) with a screwed lid. Partial thermoremanences were given to this specimen over very narrow temperature intervals, by inserting it in a metal block inside a furnace, and so controlling the temperature closely. The temperature was measured by a thermocouple inserted into a hole in the metal block. In view of the

distribution of partial thermoremanences, and to avoid crystalline changes during heating, all the experiments were carried out between room temperature and 470°C.

Demagnetization by alternating fields was performed in an apparatus consisting essentially of a pair of air-cored coils carrying fifty cycle currents, within which the specimen was rotated about two perpendicular axes simultaneously with respective frequencies of one and two cycles/second. The field was first raised to a value H_a peak oersteds and then reduced smoothly to zero through a motor-driven water resistance.

Demagnetization curves, obtained by raising the value of H_a in progressive steps, were used to deduce the intensities of magnetization associated with grains of different coercive forces. Alternating field demagnetization has been used for this purpose by Johnson and Brown (1958, 1959) in determining the shape distributions of magnetic particles; but the interpretation of the results has been considerably simplified in the present work by rotating the specimen. The effect of rotation is to present the specimen to the field in almost all possible orientations. Hence, grains with coercive forces less than H_a become remagnetized with random directions, giving an overall demagnetization; whilst grains with coercive forces greater than H_a are virtually unaffected. Thus the spectrum of magnetization as a function of coercive force can be determined. It should be observed that the coercive forces in these measurements are the values at room temperature, not at the blocking temperature.

The aim of the experiments has been fourfold:

(1) to investigate the significance of alternating field demagnetization (§ 2.1);

(2) to examine the effect of the magnetizing field on the blocking temperature and to test eqn. (5) (§ 2.2);

(3) to examine alternating field demagnetization curves of partial thermoremanences to test eqn. (1) (§ 2.2);

(4) to examine alternating field demagnetization curves of total thermoremanences to test eqn. (6) (§ 2.3).

§ 2. Results

2.1. *The Significance of Alternating Field Demagnetization*

Three experiments were carried out to test the significance of alternating field demagnetization curves.

For the first experiment the specimen was initially saturated in a field of 10 000 oersteds, and demagnetized to obtain the main curve in fig. 2(*a*). Next, subsidiary demagnetization curves were obtained after the specimen had been resaturated and partially demagnetized at three specific values of the field. The curves show that after demagnetization in a certain field, repetition in fields up to about five oersteds lower had no effect. Experiments similar to this, but different in object and result have been reported by Hajko and Daniel-Szabo (1959).

The second experiment was based on the phenomenon of anhysteretic magnetization. An anhysteretic moment is produced in a material if an alternating field sufficient to cause saturation is applied and reduced to zero in the presence of a constant direct field. For the present work, partial anhysteretic moments, analogous to partial thermoremanences, were produced by applying a direct field of 10 oersteds only over small

Fig. 2

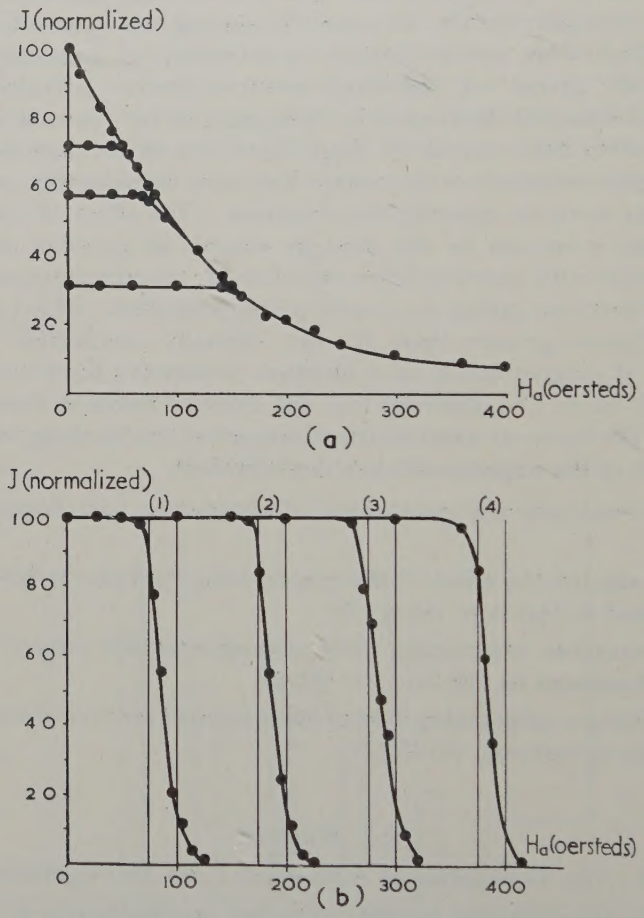

(*a*) Alternating field demagnetization of saturation remanence. Partial demagnetizations carried out at 60, 90 and 150 peak oersteds.

(*b*) Alternating field demagnetization of partial anhysteric magnetizations. Magnetizations produced in direct field of 10 oersteds and alternating fields ranging from :

(1) 100–75 oersteds.
(2) 200–175 oersteds.
(3) 300–275 oersteds.
(4) 400–375 oersteds.

ranges of alternating fields 25 oersteds wide. Figure 2(*b*) shows the effect of alternating field demagnetization on these partial anhysteretic moments. Up to a few oersteds below the lower value of the original field the moment was almost unaffected, whereas by the upper value it was almost completely destroyed. Thus partial anhysteretic magnetization has properties closely analogous to partial thermoremanence.

The aim of the third experiment was to investigate whether demagnetization at 50 cycles might modify the apparent coercive forces as compared with steady field values. The specimen was magnetized isothermally in direct fields and then demagnetized in alternating fields. The moment produced by a direct field of 100 oersteds disappeared in an alternating field of 95 oersteds, and that produced by 200 oersteds disappeared in 190 oersteds. This suggests that the coercive force at 50 cycles was approximately the same as that measured in the normal way with a steady current. Similar results to this have been reported by Mlle. Rimbert (1959).

These three experiments show that:

(1) a given alternating field demagnetizes a unique proportion of the material after which no lower value of the field had any appreciable effect;

(2) the properties of partial anhysteretic magnetization are strictly analogous to these of partial thermoremanence;

(3) time effects on the coercive force are negligible at 50 cycles.

2.2. *Experiments on Partial Thermoremanences*

Partial thermoremanences were produced in the specimen for the temperature interval 265° to 245°C, in fields of 2, 10 and 50 oersteds. Figure 3 shows normalized heating curves for these three magnetizations. In each case the moments largely disappeared between 245 and 265°C. The mean coercive force associated with this magnetization at room temperature was found experimentally to be about 70 oersteds (see fig. 5). It follows, from eqn. (5) that a field of 10 oersteds should have magnetized all grains with blocking temperatures up to 430°C. The heating curve for the thermoremanence acquired in 50 oersteds between 430°C and 245°C, shown by the pecked line on fig. 3, indicates the curve to be expected if this prediction were correct. It will be seen that in fact, even a field of 50 oersteds only magnetized a small proportion of grains with blocking temperatures above 265°C; so there seems to be a serious discrepancy with Néel's formulae. It is especially remarkable that the blocking temperature should have an experimentally well-defined meaning even in fields up to 50 oersteds, considering that a field of 50 oersteds applied over the whole range from 470°C to room temperature produced a magnetization equal to the saturation remanence (see § 2.3).

Figure 4(*a*) shows alternating field demagnetization curves for partial thermoremanences produced by applying fields of 10 oersteds over six separate temperature intervals 20°C wide. The curves are systematically displaced towards higher fields with increasing temperature, and therefore

demonstrate a strong correlation between the room temperature coercive force and the blocking temperature. In fig. 5 the value of H_a corresponding to the steepest part of the demagnetization curve is plotted against the mean of each temperature range. It is almost a straight line. Provided the coercive force at room temperature is related monotonically to the value at the blocking temperature, this confirms the linear relationship contained in eqn. (1).

Fig. 3

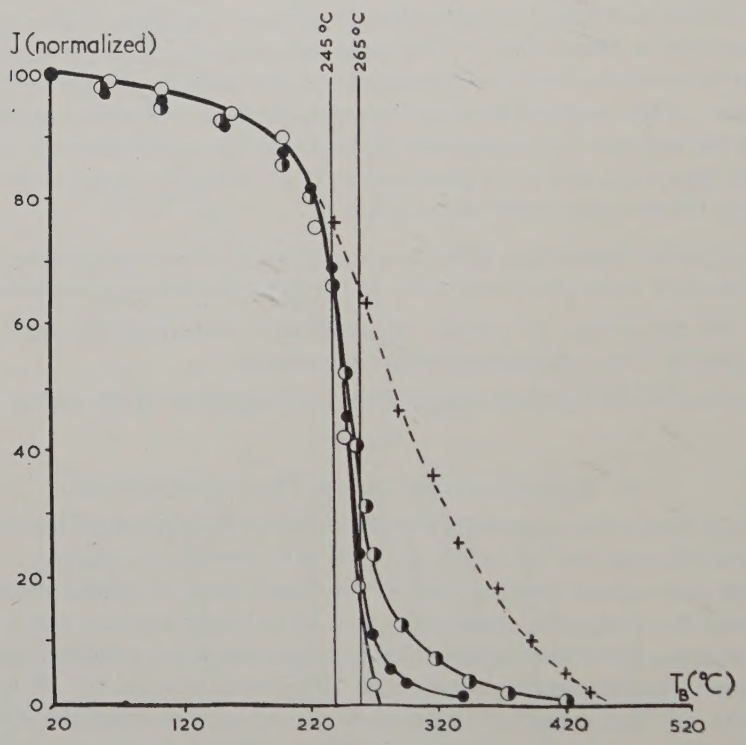

Heating curves for partial thermoremanences produced in different fields applied between 265°c to 245°c.

○ 2 oersteds.
● 10 oersteds.
◑ 50 oersteds.
\+ Moment produced by cooling in 50 oersteds from 430°c to 245°c.

The curves of fig. 4 (*a*) also show that at least one further parameter must occur in the equation between blocking temperature and coercive force, since there is a complete spectrum of coercive forces associated with each blocking temperature. Equation (1) suggests that this parameter is the grain size. If so the spectrum of grain sizes associated with each blocking temperature can be determined from the shape of the demagnetization curves.

Figure 4 (*b*) shows demagnetization curves for the thermoremanence produced in steady fields of 2, 10 and 50 oersteds applied over the same temperature interval of 250°–230°c. As might be expected from the similarity of the heating curves in fig. 3, these three demagnetization curves are almost identical.

Fig. 4

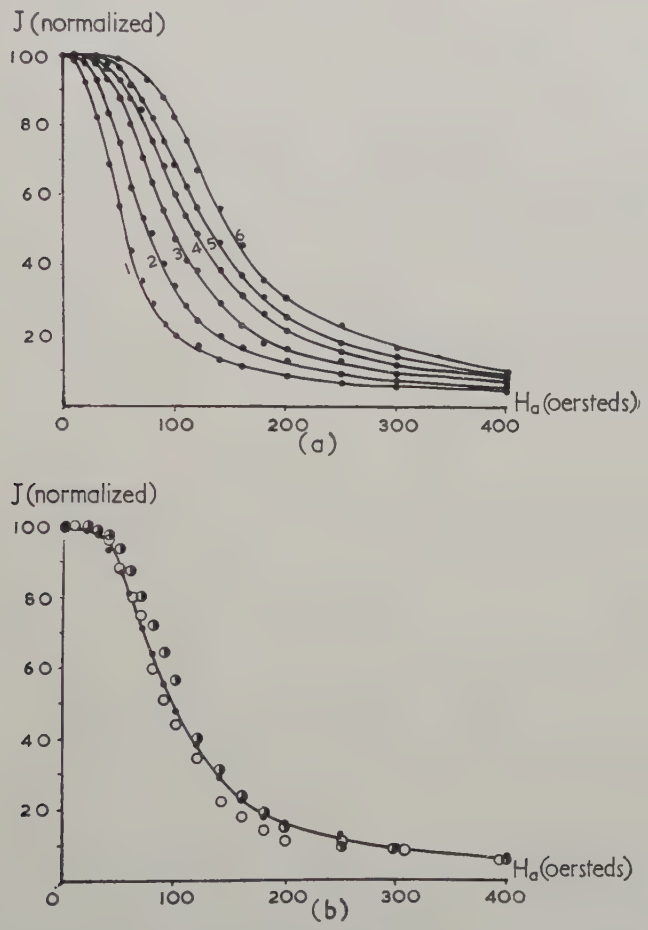

Alternating field demagnetization of partial thermoremanences.

(*a*) Moments produced in field of 10 oersteds applied between the following temperatures:

(1) 110°– 90°c.
(2) 180°–160°c.
(3) 250°–230°c.
(4) 320°–300°c.
(5) 390°–370°c.
(6) 460°–440°c.

(*b*) Moments produced between 250°c and 230°c in the following fields:

○ 2 oersteds.
● 10 oersteds.
◑ 50 oersteds.

2.3. *Alternating Field Demagnetization of Total Thermoremanences*

In order to test eqn. (6) a series of demagnetization curves were made on the total thermoremanences acquired in fields of 2, 10 and 50 oersteds and also on the remanence after saturation at room temperature in a field of 3000 oersteds.

Fig. 5

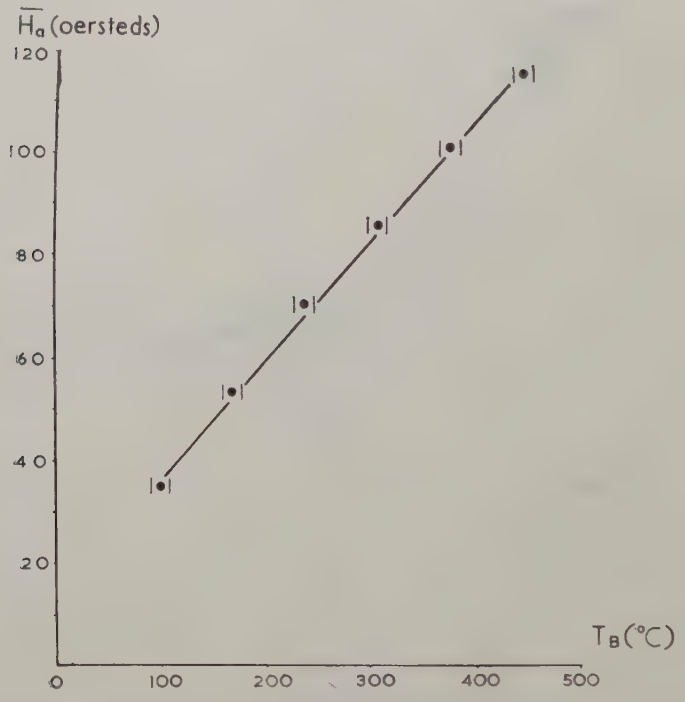

Effective coercive force versus blocking temperature.

The slope $\partial J/\partial H_a$ of any alternating field demagnetization curve at some particular value H_a gives the intensity of magnetization associated with grains of coercive force H_a. In particular, provided there are no complications due to self-demagnetizing fields, the slope of the curve for demagnetization of the saturation remanence J_R is

$$\frac{\partial J_a}{\partial H_a} = v(H_a) \cdot j_s'$$

where j_s' is the spontaneous magnetization per unit volume of all grains with coercive force H_a and $v(H_a)$ is their total volume. Similarly the slope of the curve for thermoremanence J_T is

$$\frac{\partial J_T}{\partial H_a} = v(H_a) \cdot j_T'$$

where j_T' is the thermoremanence per unit volume in grains with coercive force H_a. Therefore

$$\frac{\partial J_T}{\partial H_a} \Big/ \frac{\partial J_R}{\partial H_a} = j_T'/j_s'.$$

In view of the strong correlation revealed in § 2.2 between H_a and the blocking temperature T_B, there should be a close relation between j_T'/j_s' the ratio of magnetizations in grains with a particular coercive force H_a, and the corresponding ratio j_T/j_s in grains with a particular blocking temperature T_B. Hence measurements of j_T'/j_s' as function of H_a allow a partial test of the dependence of j_T/j_s on $H_c(T_B)$ given in eqn. (6).

Figure 6 shows the values of j_T'/j_s' plotted against H_a for thermoremanences acquired in fields of 2, 10 and 50 oersteds. They are straight lines parallel to the H_a axis (in other words the original alternating field demagnetization curves were all the same shape). Thus the ratio j_T'/j_s' is independent of the room temperature coercive force. It follows that so long as there is a monotonic relationship between the coercive forces at the blocking temperature and at room temperature, these results fail to confirm eqn. (6), which predicts that j_T/j_s depends strongly on $H_c(T_B)$.

Fig. 6

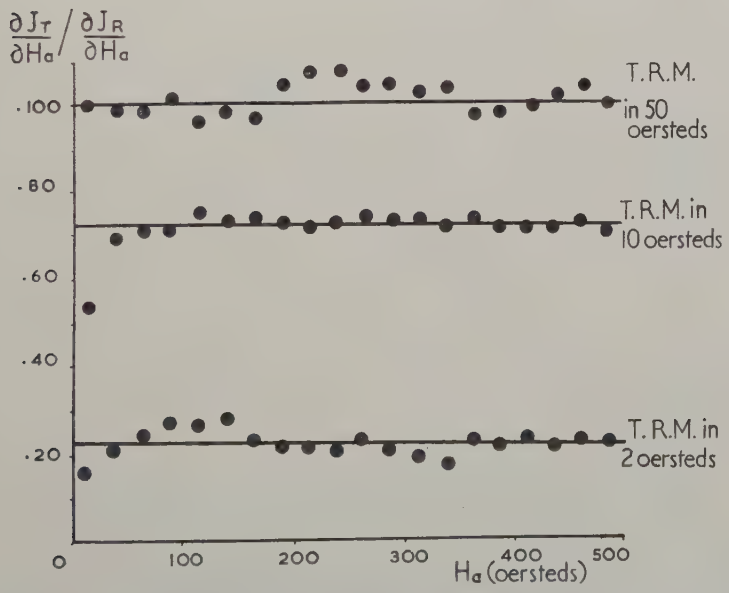

Ratio j_T'/j_s' versus alternating field for different thermoremanences.

Since j_T'/j_s' is independent of H_a, its magnitude for any magnetizing field h is simply equal to the ratio of total thermoremanence J_T in that field to the saturation remanence J_R. In fig. 7, $\tanh^{-1}(J_T/J_R)$ is plotted against h. It is a straight line of slope 0·098 showing that j_T'/j_s' depends on the hyperbolic tangent of h as does j_T/j_s in eqn. (6).

An alternative test of eqn. (6) may be derived from the following argument based on the demagnetization curves in fig. 4 (*b*) of partial thermoremanences produced in different fields. We have seen that the moment acquired between 265° and 245°C was a true partial thermoremanence, disappearing almost entirely by 265° on reheating. Now since a field of 50 oersteds applied between 470°C and room temperature produced a moment equal to the saturation remanence, it follows that the partial thermoremanence in 50 oersteds corresponds to saturation of all grains with blocking temperatures between the temperatures of magnetization.

Fig. 7

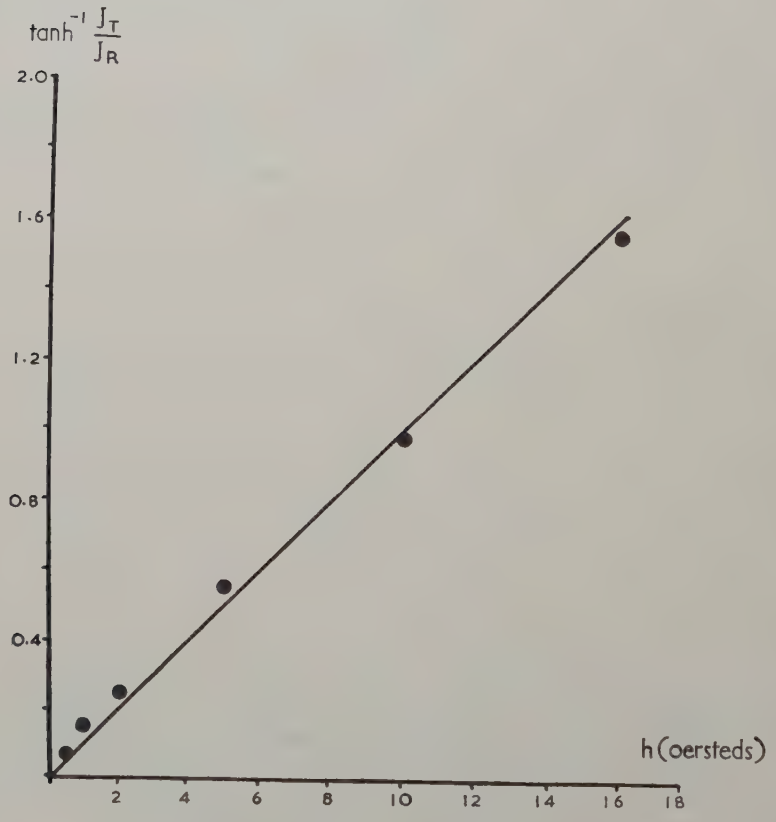

Tanh^{-1} J_T/J_R versus magnetizing field.

Therefore j_T/j_s can be derived for grains with blocking temperatures between 250° and 230°C from the slopes of the curves in fig. 4 (*b*), in exactly the same way as j_T'/j_s' is derived from fig. 6. Since the curves have identical shape, j_T/j_s is independent of H_a.

These experiments therefore show that j_T/j_s depends on the field h in accordance with eqn. (6):

$$\frac{j_T}{j_s'} = \tanh \frac{h}{H_c(T_B)}$$

but on the other hand, j_T/j_s is independent of the coercive force $H_c(T_0)$.

§ 3. Conclusion

The work described in this paper proceeds a step nearer to a direct test of Néel's formulae. The chief defects are that there is an unknown distribution of grain volumes, and an unknown relationship between the coercive forces at room temperature and the blocking temperature. These defects could be overcome by using a series of samples with narrow ranges of grain sizes; but they would be extremely difficult to prepare.

The conclusions are most conveniently summarized by a table comparing Néel's theory with the experimental measurements.

Theory	Experiment
1. $T_B = \text{const. } v j_s(T_B) H(T_B)$ (eqn.(1))	(*a*) $T_B \propto H_c(T_0)$ (*b*) T_B depends on at least one other parameter besides $H_C(T_0)$—presumably the volume of the grain.
2. In an external field h, some grains become magnetized, even though their blocking temperatures are higher than the temperature of magnetization. The maximum blocking temperature affected is given by $\frac{T_B}{T_M} = \left(\frac{H_c+h}{H_c}\right)^2$ (eqn. (5))	For moments acquired between 265° and 245°C, very few grains with blocking temperatures above 265° become magnetized, even in fields up to 50 oersteds; whereas according to eqn. (5) a field of only 10 oersteds should magnetize all grains with blocking temperatures up to 430°C
3. $\frac{j_T}{j_s} = \tanh\left[\text{const}\frac{h}{H_c(T_B)}\right]$ (eqn. (6))	(*a*) $\frac{j_T'}{j_s'} = \tanh(A \cdot h)$ where $A = 0{\cdot}098$ per oersted (*b*) $\frac{j_T'}{j_s'}$ and $\frac{j_T}{j_s}$ are independent of $H_c(T_0)$

T_B, blocking temperature; v, volume of grain; $H_c(T_B)$ and $H_c(T_0)$ coercive force at blocking temperature and room temperature respectively; j_T/j_s, ratio of mean thermoremanence to spontaneous magnetization in all grains with a particular blocking temperature T_B; j_T'/j_s, analogous ratio in all grains with a particular coercive force $H_c(T_0)$; h, external field.

Thus the linear relationship between blocking temperature and coercive force derived by Néel is confirmed; but the blocking temperature depends much less markedly on the external field than expected, and the ratio of

thermoremanence is spontaneous magnetization in grains with particular blocking temperatures is independent of their coercive forces contrary to the relationship derived from Néel's formulae.

In addition this work demonstrated the existence of a partial anhysteretic magnetization closely analogous in behaviour to partial thermoremanence.

In a further paper I hope to describe an extension of this work to material with multidomain grains.

Acknowledgment

I wish to thank Dr. R. L. Wilson for lending me the material used for this study and for several helpful suggestions.

APPENDIX

On the Value of the Constant A

Since the experiments appear to contradict eqn. (6), it is not strictly logical to attempt a comparison of the measured constant A in

$$j_T/j_s = \tanh(A \,.\, h)$$

with the theory. However, Dr. E. P. Wohlfarth has pointed out to me that there is an interesting agreement between the measured value of A and the quantities in Néel's original equation

$$j_T/j_s = \tanh \frac{v j_s(T_B)}{kT_B} \,.\, h.$$

Taking the mean diameter of the grains as 5×10^{-6} cm. (measured by electron microscope); j_s for maghemite as 200 gauss; k as $1{\cdot}4 \times 10^{-16}$ ergs/°C, and T_B as 600°K, we find

$$\left[\frac{v j_s(T_B)}{kT_B}\right] = 0{\cdot}12 \text{ per oersted.}$$

The measured value of A is 0·098 per oersted.

It is clear that a comparison of this kind is not satisfactory; but the agreement between the two figures is remarkably good.

References

Hajko, V., and Daniel-Szabo, J., 1959, *Czech. J. Phys.*, **9**, 37.
Johnson, C. E., and Brown, W. F., 1958, *J. appl. Phys.*, **29**, 313; 1959, *Ibid.*, **30**, 136 S.
Néel, L., 1955, *Advanc Phys.*, **4**, 191.
Rimbert, F., 1959, *Rev. Inst. franç. Pétrole*, **14**, 1.
Thellier, E., 1941, *C.R. Acad. Sci., Paris*, **223**, 319.

The Fermi Surfaces of the Noble Metals†

By J. F. Cornwell
Mathematics Department, Imperial College, London

[Received January 10, 1961]

Abstract

The energy band structure of the noble metals is calculated using a plane wave pseudo-potential method, and the properties of the Fermi surfaces so obtained are compared with those deduced from experimental observations.

§ 1. Introduction

There has recently been a considerable amount of experimental work aimed at determining the Fermi surfaces of the noble metals. No really satisfactory energy band calculation for these metals has, however, yet been published, although B. Segall (private communication) is working on a calculation for copper. The best published calculation on the noble metals is probably that by Howarth (1953) on copper, which demonstrated the sensitiveness of the calculated energy levels to the assumed potential field. Howarth's calculation indicated a nearly spherical Fermi surface, but an increasing amount of experimental evidence (Pippard 1957, Morse and Gavenda 1959, Langenberg and Moore 1959, Morse *et al.* 1960, Shoenberg 1960) has led to the conclusion that the Fermi surfaces in copper, silver and gold probably all deviate considerably from the spherical and have considerable contact with the Brillouin zone (B.Z.) boundaries. It is of interest therefore to see how far the present experimental observations can be correlated using a simple pseudo-potential plane wave approach.

Ziman (1961) has recently used this approach in a calculation in which the B.Z. is replaced by eight circular cones with vertices at the centre of the B.Z. and having the same volume as the B.Z. Ziman represents the pseudo-potential by a single adjustable parameter, V_{111}, the first Fourier coefficient of the pseudo-potential. In the calculations to be described here the peculiarities of such a zone model have been avoided, and the second Fourier coefficient, V_{200}, which might be expected to play a significant role, has been introduced. Also, symmetrized triple Fourier expansions of $E(\mathbf{k})$ with 15 terms have been employed in the course of the calculations and these might give a useful representation of the Fermi surface for calculations on, for example, the anomalous skin effect. Such an expansion containing only two terms has been used by Garcia-Moliner (1958).

† Communicated by Dr. E. P. Wohlfarth.

§ 2. Calculations

Pseudo-potential methods have been applied quite successfully to a number of metals and semiconductors. For the lighter metals, such as lithium and beryllium, an 'l-dependent' pseudo-potential is needed (Cornwell and Wohlfarth 1960, Cornwell 1961), but for heavier metals such as the noble metals it is probably quite satisfactory to use the same pseudo-potential in the calculation of the energy levels of any state, whatever its symmetry. In this latter approach (see, for example, Phillips and Kleinmann 1959, Harrison 1960), the Fourier coefficients of the pseudo-potential are taken as adjustable parameters. The most important are the first two, which for the face-centred cubic structure are V_{111} and V_{200}, and in the present calculation only these have been considered, all the others being taken as zero. Near the centre of the B.Z. it may be assumed that

$$E(\mathbf{k}) = \alpha k^2,$$

where $\alpha = m/m^*$ is the ratio of the free electron mass m to an effective mass m^*. This ratio determines the energy scale of the band structure, and as it is not known *a priori*, it could be taken as a further adjustable parameter if necessary (Harrison 1960).

As the effects of the core electrons are not considered explicitly in this approach, but only appear implicitly in the pseudo-potential, the metals copper, silver and gold may, by using the following notation, be considered together. Let a be the lattice constant for the metal, and define vectors $\boldsymbol{\varkappa}$ by $\boldsymbol{\varkappa} = (a/2\pi)\mathbf{k}$, where the $\mathbf{k}$ vectors are defined in the usual way. The energy $\epsilon(\boldsymbol{\varkappa})$ and the parameters U_{111}, U_{200} may also be expressed in non-dimensional units by $\epsilon(\boldsymbol{\varkappa}) = E(\mathbf{k})/\alpha(2\pi/a)^2$, $U_{111} = V_{111}/\alpha(2\pi/a)^2$, $U_{200} = V_{200}/\alpha(2\pi/a)^2$, ($E(\mathbf{k})$, V_{111}, V_{200} being in rydbergs). In the pseudo-potential calculations mentioned above it was found unnecessary to employ more than a small number of terms in the plane wave expansions of the valence electron wave functions. As it was not considered worth while to be too elaborate in the present calculations, the number of terms used in obtaining an energy level at a symmetry point of the B.Z. was taken to be equal to the degeneracy of the corresponding level in the free electron approximation, so that, for example, with the notation described above, the energy of the s-like state at L, L_1, is given by

$$\epsilon(L_1) = U_{111} + 0{\cdot}75,$$

and the energy of the p-like state at L, L_2', by

$$\epsilon(L_2') = -U_{111} + 0{\cdot}75,$$

taking the energy zero to coincide with the bottom of the band at Γ. The labelling of the states is that of Bouckaert *et al.* (1936). For $\alpha = 1$ and several values of the parameters U_{100} and U_{111}, energy levels were then calculated at 85 non-equivalent points in the B.Z., using an appropriate small number of plane waves, and a symmetrized triple Fourier expansion of $\epsilon(\boldsymbol{\varkappa})$ with 15 independent coefficients was fitted to these calculated

levels by least squares. For small values of U_{111} and U_{200}, small discontinuous truncation errors appear as a result of taking different numbers of plane waves at different points in the B.Z., and these were smoothed out by taking this Fourier expansion. For large values of U_{111} and U_{200}, i.e. $|U_{111}|>0{\cdot}25$ approximately, and $|U_{200}|>0{\cdot}15$ approximately, these truncation errors become serious and the approximation breaks down. Although this difficulty could be alleviated to some extent by using more plane waves, such a course was not considered worth while. The volumes $C(\epsilon)$ contained in $\boldsymbol{\kappa}$ space by surfaces of constant energy ϵ were calculated by numerical integration from the Fourier expansion to obtain the reduced Fermi energy ϵ_F and the density of states at ϵ_F, $N(\epsilon_F)=[dC(\epsilon)/d\epsilon]_{\epsilon_F}$. The extremal areas and radii of the electron orbits obtained by the intersection with the Fermi surface of planes perpendicular to the [100] and [111] directions were also calculated, as was the rate of change of these areas with ϵ. This latter quantity gives the cyclotron resonance effective mass $(1/\pi)(dA/dE)$, where A is in reciprocal atomic units and E in rydbergs. The results of the calculations for $\alpha=1$ are shown in the table. For other values of α, the corresponding results are easily obtained as the extremal areas and radii of the electron orbits are independent of α, while the cyclotron resonance effective mass and $N(\epsilon_F)$ are inversely proportional to α; ϵ_F and the energy gap at L, $\{\epsilon(L_1)-\epsilon(L_2')\}$, are also independent of α. Comparison is made in the table with the corresponding values obtained from experimental observations, and, where appropriate, with the free electron values.

§ 3. Discussion

Measurements of the Knight shift in alloys suggest that $\{\epsilon(L_1)-\epsilon(L_2')\}$ is positive for copper and negative for gold, while for silver the situation is uncertain (Cohen and Heine 1958). Mott's (1953) interpretation of the x-ray spectrum apparently confirms that $\epsilon(L_1)>\epsilon(L_2')$ for copper. The calculations of Segall (1961 a, b) give this ordering of the levels for copper and silver. The parameter U_{111} has been taken as positive to conform to this situation, although taking the corresponding negative values does not change the shape of the Fermi surface appreciably.

The extremal areas given by the de Haas–van Alphen effect measurements of Shoenberg (1960) are shown in columns 3, 4 and 5 of the table. It is very difficult to conceive a Fermi surface which, although having considerable contact with the eight [111] B.Z. boundaries, has larger *absolute* belly areas perpendicular to both the [111] and [100] directions than the free electron Fermi sphere of the same volume. (It has been shown by Luttinger (1961) that interactions between the electrons do not affect the periods of the de Haas–van Alphen oscillations which thus continue to be related to the areas by Onsager's theorem.) The *relative* values of the [100] and [111] belly areas, (A_{100}/A_{111}), are also impossible to fit in this pseudo-potential model, as Shoenberg has found that $(A_{100}/A_{111})>1$, and the results of the calculations show the opposite. It may be noted in

U_{111}	U_{200}	Extremal cross-sectional areas of Fermi surface			Cyclotron resonance effective masses			Extremal radii of electron orbits			Gap at L	ϵ_F	$N(\epsilon_F)$
		[100] belly	[111] belly	[111] neck	[100] belly	[111] belly	[111] neck	[100] belly	[111] belly	[111] neck			
0·195	0·00	1·849	1·923	0·017	1·21	1·68	1·08	0·767	0·782	0·074	0·39	0·55	4·03
0·195	−0·10	1·858	1·916	0·002	1·05	1·56	0·95	0·769	0·781	0·025	0·39	0·55	4·14
0·195	0·10	1·876	1·910	0·015	1·05	1·32	0·62	0·773	0·780	0·069	0·39	0·55	3·97
0·205	0·10	1·859	1·910	0·021	1·13	1·37	0·79	0·769	0·780	0·082	0·41	0·54	4·21
0·250	0·00	1·789	1·919	0·076	1·23	1·77	1·10	0·755	0·781	0·156	0·50	0·52	4·51
0·250	0·15	1·806	1·916	0·062	1·08	1·68	0·90	0·758	0·781	0·140	0·50	0·52	4·36
Free electrons		1·919	1·919	—	1·00	1·00	—	0·781	0·781	—	—	0·61	2·46
Experimental													
Copper		2·018	1·954	0·083	1·38	1·30	—	0·765	—	0·130	0·39	0·4 to 0·6	3·36
		(1·850)	(1·869)	—	(1·32)	(1·30)							
Silver		2·046	2·005	0·039	0·71	—	—	0·763	0·775	0·111	0·42	—	2·33
Gold		2·057	1·956	0·065	—	0·9	0·9	0·775	—	0·135	0·28	—	2·84

this connection that from the Fermi surface deduced by Pippard (1957) from anomalous skin effect measurements on copper, Shoenberg has calculated the cross-sectional areas given in parentheses in columns 3 and 4 of the table. These agree with the present calculations in that $(A_{100}/A_{111})<1$ and both A_{100} and A_{111} are not greater than the corresponding cross-sectional area A_{fe} of the free electron Fermi sphere.

The ultrasonic attenuation measurements of Morse (1960), Morse *et al.* (1960) and Bohm (1960) (given in columns 9, 10 and 11 of the table) suggest that $A_{100}<A_{fe}$ for all three metals, and, moreover, that for silver, $A_{100}<A_{111}<A_{fe}$. Also, for all three metals these measurements give neck radii perpendicular to the [111] direction that are consistent with the neck areas obtained by Shoenberg. The magneto-resistance measurements of Alekseevski and Gaidukov (1959) and Gaidukov (1959) for copper, silver and gold have been shown by Priestley (1960) to be also consistent with the neck areas measured by Shoenberg.

Shoenberg has also obtained from the de Haas–van Alphen effect the effective masses shown in columns 6, 7 and 8 of the table, although for silver and gold these are only rough values. The results for copper agree well with the cyclotron resonance data of Langenberg and Moore (1959), given in parentheses in columns 6 and 7.

The experimental values of $N(\epsilon_F)$ given in column 14 have been taken directly from the low temperature electronic specific heat measurements of Corak *et al.* (1955), no account being taken of the effects of electron–phonon interactions (see, for example, Jones 1957) or of electron–electron interactions (Fletcher and Larson 1958), both of which would, if included, make these measurements correspond to lower values of $N(\epsilon_F)$. The value of the occupied band width given by the soft x-ray emission spectrum of copper is about 5 to 7 ev (Cauchois 1953), no measurements having been made on silver and gold.

The internal photoelectric absorption band edges give the value of the energy gap at L. The early experimental data of Meier (1910) have been interpreted by Mott and Jones (1936), who suggest that this energy gap is 4·25 ev for copper, 4·0 ev for silver and approximately 2·5 ev for gold. A similar interpretation of the recent experimental results of Biondi and Rayne (1959) gives for copper an energy gap at L of 4·5 ev, and those of Taft and Philipp (1961) and Rhodin and Fromhold (1961) give for silver a gap of $3{\cdot}8 \pm 0{\cdot}3$ ev.

As the table shows, for the range of U_{200} for which the approximations used are valid, the calculated properties of the Fermi surface are much more sensitive to U_{111} than to U_{200}. For each metal, agreement of the observed and calculated neck areas can be obtained for a U_{111} within a narrow range by a suitable choice of U_{200}. In this narrow range of U_{111}, however, the other calculated properties do not change appreciably, and so one needs only to take a particular pair of values of U_{111} and U_{200} that give agreement between the observed and the calculated neck areas and discuss the other calculated properties of the Fermi surface that correspond to this pair.

For copper, with an energy gap at L of 4·5 ev (corresponding to $\{\epsilon(L_1)-\epsilon(L_2')\}=0{\cdot}39$ with $\alpha=1$), the Fermi surface does just touch the [111] B.Z. boundaries, but the contact areas are small. The best agreement of calculated and observed neck areas is given by $U_{111}=0{\cdot}25$ and $U_{200}=0{\cdot}0$, which, with $\alpha=1$, corresponds to an energy gap at L of 5·7 ev (cf. Ziman's (1961) estimate of 7 ev for $\alpha=1$) and too high a value of $N(\epsilon_F)$. Choosing $\alpha=1{\cdot}30$ to give agreement with the observed $N(\epsilon_F)$ gives an energy gap at L of 7·5 ev, and cyclotron resonance effective masses for the [100] and [111] belly orbits of 0·95 and 1·36 respectively.

For silver the best agreement of the calculated and observed neck areas and radii corresponds to $U_{111}=0{\cdot}22$ approximately, with $U_{200}=0{\cdot}0$. Choosing $\alpha=1{\cdot}93$ to give agreement with the observed $N(\epsilon_F)$ gives an energy gap at L of 7·7 ev, and cyclotron resonance effective masses for the [100] and [111] belly orbits of 0·60 and 0·78 respectively.

For gold the best agreement of the calculated and observed neck areas and radii is given by $U_{111}=0{\cdot}25$ and $U_{200}=0{\cdot}15$. Choosing $\alpha=1{\cdot}54$ to give agreement with the experimental $N(\epsilon_F)$ gives an energy gap at L of 7·0 ev and cyclotron resonance effective masses for the [111] belly and neck orbits of 1·09 and 0·58 respectively.

From this discussion one concludes that, within the limits of validity of the model used here, for copper, silver and gold the optical data are inconsistent with the low temperature specific heats and the [111] neck areas given by the de Haas–van Alphen effect, the cyclotron resonance effective masses being, however, roughly correct. The calculations were performed on the Ferranti Mercury Computer of the University of London, and could be extended to further cases should more extensive experimental data become available.

Acknowledgments

My thanks are due to the Senate of the University of London for the award of a University Postgraduate Studentship. I am also indebted to Dr. E. P. Wohlfarth for much useful advice, and to Dr. J. C. Phillips and Dr. D. Shoenberg, F.R.S. for useful discussions, and to Dr. J. M. Ziman for a copy of his paper prior to publication.

References

Alekseevski, N. E., and Gaidukov, Yu. P., 1959, *J. exp. theor. Phys.*, **37,** 672.

Biondi, M. A., and Rayne, J. A., 1959, *Phys. Rev.*, **115,** 1522.

Bohm, H. V., 1960, *Cooperstown Proceedings*, p. 245.

Bouckaert, L. P., Smoluchowski, R., and Wigner, E. P., 1936, *Phys. Rev.*, **50,** 58.

Cauchois, Y., 1953, *Phil. Mag.*, **44,** 173.

Cohen, M. H., and Heine, V., 1958, *Advanc. Phys.*, **7,** 395.

Corak, W. S., Garfunkel, M. P., Satterthwaite, C. B., and Wexler, A., 1955, *Phys. Rev.*, **98,** 1699.

Cornwell, J. F., 1961, *Proc. roy. Soc.* A, **261,** 551.

Cornwell, J. F., and Wohlfarth, E. P., 1960, *Nature, Lond.*, **186,** 379.

Fletcher, J. G., and Larson, D. C., 1958, *Phys. Rev.*, **111,** 455.
Gaidukov, Yu. P., 1959, *J. exp. theor. Phys.*, **37,** 1281.
Garcia-Moliner, F., 1958, *Phil. Mag.*, **3,** 207.
Harrison, W. A., 1960, *Phys. Rev.*, **118,** 1182.
Howarth, D. J., 1953, *Proc. roy. Soc.* A, **220,** 513.
Jones, H., 1957, *Proc. roy. Soc.* A, **240,** 321.
Langenberg, D. N., and Moore, T. W., 1959, *Phys. Rev. Letters*, **3,** 328.
Luttinger, J. M., 1961, *Phys. Rev.*, **121,** 1251.
Meier, W., 1910, *Ann. Phys. Lpz.*, **31,** 1017.
Morse, R. W,. 1960, *Cooperstown Proceedings*, p. 214.
Morse, R. W., Myers, A., and Walker, C. T., 1960, *Phys. Rev. Letters*, **4,** 605.
Mott, N. F., 1953, *Phil. Mag.*, **44,** 187.
Mott, N. F., and Jones, H., 1936, *The Theory of the Properties of Metals and Alloys* (Oxford: Clarendon Press).
Phillips, J. C., and Kleinmann, L., 1959, *Phys. Rev.*, **116,** 287.
Pippard, A. B., 1957, *Phil. Trans.* A, **250,** 325.
Priestley, M. G., 1960, *Phil. Mag.*, **5,** 111.
Rhodin, T. N., and Fromhold, A. T., 1961, *Bull. Amer. phys. Soc.*, **6,** 146.
Segall, B., 1961 a, *Bull. Amer. phys. Soc.*, **6,** 10 ; 1961 b, *Ibid.*, **6,** 145.
Shoenberg, D., 1960, *Phil. Mag.*, **5,** 105.
Taft, E. A., and Philipp, H. R., 1961, *Phys. Rev.*, **121,** 1100.
Ziman, J. M., 1961, *Advanc. Phys.*, **10,** 1.

The Flow Stress of Aluminium and Copper at High Temperatures

By P. B. Hirsch and D. H. Warrington
Crystallographic Laboratory, Cavendish Laboratory, Cambridge

[Received April 28, 1961]

Abstract

The ratio of the flow stress at a high temperature to that at 0°c has been measured for polycrystalline Al and Cu, and for single crystals of Al. In Al the flow stress decreases ratio strongly with temperature above a certain critical temperature (about 250°c). In Cu a similar but more gradual decrease in the flow stress ratio is observed. The results are interpreted in terms of a model based on sessile vacancy jogs in screw dislocations, which has also been used by Hirsch (1960) and Mott (1960) to explain linear hardening. Below a certain critical temperature the screw dislocations advance with the aid of stress leaving a dipole or a row of vacancies behind; in this region the flow stress will be nearly temperature independent. Above the critical temperature the jogs advance with the aid of thermal activation, vacancies being emitted by and moving away from the jogs in the same thermally activated process, and the flow stress decreases strongly with temperature. The activation energy for this process is that of self-diffusion. An analysis of the experimental results in terms of this model shows that the mean vacancy jog height for Al is 2–5 Burgers vectors, and for Cu only 1–2 Burgers vectors. Models involving the climb of edge dislocations are also discussed and found to be less satisfactory, although they cannot be ruled out completely.

§ 1. Introduction

The reversible temperature dependence of the flow stress of face-centred cubic metals for temperatures below that at which self-diffusion becomes important has been studied by a number of workers (Cottrell and Stokes 1955, Adams and Cottrell 1955, Haasen 1958, Diehl 1956, Rebstock 1957, Basinski 1959). Figure 1 shows the temperature dependence for Al, after correction for the temperature variation of the shear modulus. On the basis of these measurements the flow stress τ has been interpreted as the sum of two terms; i.e. $\tau = \tau_g + \tau_s$, where τ_g is independent of temperature after correction for the temperature dependence of the shear modulus, and τ_s is the temperature dependent contribution. In Al τ_s is important only in region A on fig. 1; in region B, τ is almost entirely due to τ_g (Seeger 1955). Current theories of flow stress attribute τ_g to the long-range elastic stresses from piled-up groups of dislocations (Seeger *et al.* 1957) or to the elastic stresses due to forest dislocations (Thornton and Hirsch 1958, Thornton 1958, Hirsch 1958, Basinski 1959, Bailey and Hirsch 1960, Saada 1960a, b, Carrington *et al.* 1960). τ_s is thought to be due to the stress required to make jogs during intersection of forest dislocations.

The experiments described in this paper were aimed at investigating the temperature dependence of the flow stress at higher temperatures, where self-diffusion might be important. Ball (1957) measured this temperature dependence for polycrystalline Al, and found that the flow stress decreases at temperatures above 200°C. This decrease was attributed tentatively to the onset of grain boundary sliding and consequent redistribution of stresses. To test this suggestion single crystals of Al have now been studied in addition to polycrystals of Al and Cu. All the experiments were carried out by deforming first at the high temperature and then at a lower temperature, to minimize possible recovery effects.

Fig. 1

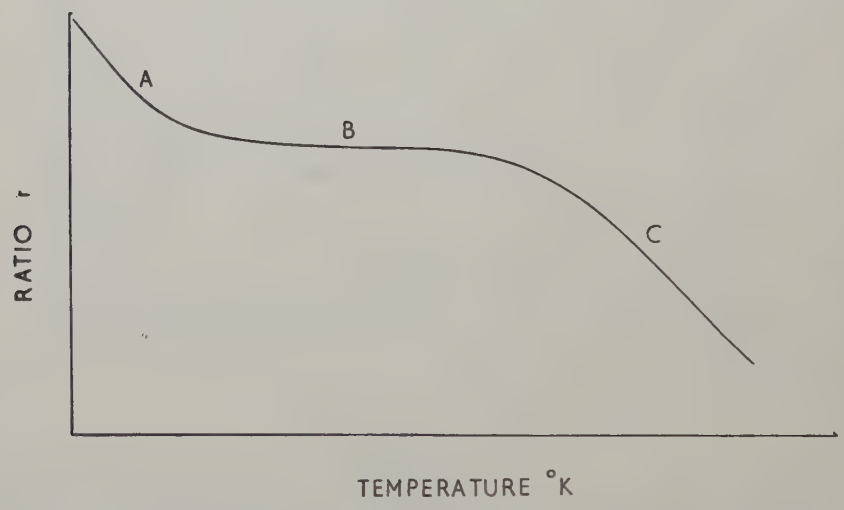

Schematic variation of flow stress ratio r.

§ 2. Experimental Results

2.1. *Aluminium*

Polycrystalline specimens of two purities (99·8, 99·99%) were prepared with a 400 μ grain size in a form suitable for tensile test with a reduced cross section over a 5 cm gauge length. They were strained in a Polanyi-type machine at the high temperature of strain rates of $0{\cdot}8 \times 10^{-4}$ and $0{\cdot}7 \times 10^{-3}\,\mathrm{sec}^{-1}$, and excursions were made to 0°C to determine the flow stress ratio. During each low temperature deformation the extension was kept to a minimum (about 0·3%), while the intermediate strains at the higher temperature were about 3 to 5%. Measurements on the stress–strain curves at the slower strain rate were made by reading by eye the two dial gauges determining stress and strain. At the faster strain rate the dial gauges were photographed at the rate of one frame every two seconds.

Single crystal specimens were prepared by the strain anneal method and by growth from the melt. They were gripped between small steel plates containing a serrated groove. Initially the diameter of the specimen was uniform over its whole length, but a reduced gauge section developed naturally during the deformation.

The high temperatures were obtained by means of a salt bath controlled to $\pm 2°$C.

2.2. *Copper*

Copper specimens of two purities were used: Johnson-Matthey spectroscopically pure material with grain size $100\,\mu$, and O.F.H.C. copper with grain size $50\,\mu$.

The specimens used at the high temperatures were in the form of a wire 2 mm in diameter. They were pulled in an induction furnace under a vacuum of 2×10^{-5} mm Hg, and cooled from temperature by radiation. (The furnace consisted of an induction coil about $2\frac{1}{2}$ in. diameter and 6 in. long, surrounding a Hysil glass cylinder with O ring sales on its ground end surfaces. The specimen load was measured by a bending beam situated outside the vacuum.) A gauge length of 3 cm of uniform extension was cut from the centre of the specimen and pulled between serrated grips in the low temperature stress–strain machine. Intermediate temperature specimens ($< 500°$C) were of the shaped gauge length type and were extended in the salt bath.

2.3. *Determination of the Flow Stress Ratio*

The values of the flow stress ratio were always obtained by transition from the higher to the lower temperature. Except for the results described in § 3.4, the lower temperature was always 0°C. The flow stress at the high temperature, τ_T, was taken to be the stress at which the specimen was unloaded. The flow stress at 0°C, τ_0, was defined by drawing a tangent to the stress–strain curve at 0·2% extension and noting the stress at which this intersects the extrapolated elastic portion of the curve. This occurred typically at a stress corresponding to an extension of about 0·03%.

In order to compare the temperature variation of the flow stress ratio with that of the elastic modulus, the flow stress ratio has been divided by the ratio of Young's moduli (Y_T) at the two temperatures, using Koster's (1948) measurements. The results are shown in figs. 2–6, where the flow stress ratio $r = \tau_T Y_0 / \tau_0 Y_T$ has been plotted against temperature. It should be emphasized that the procedure of dividing by the ratio of Young's moduli has been adopted merely to demonstrate the deviation of the temperature variation of the flow stress ratio from that of the elastic modulus. Whether this procedure is appropriate for the detailed interpretation of the results depends on the particular model adopted. This point will be discussed again in § 4.2.2.

Fig. 2

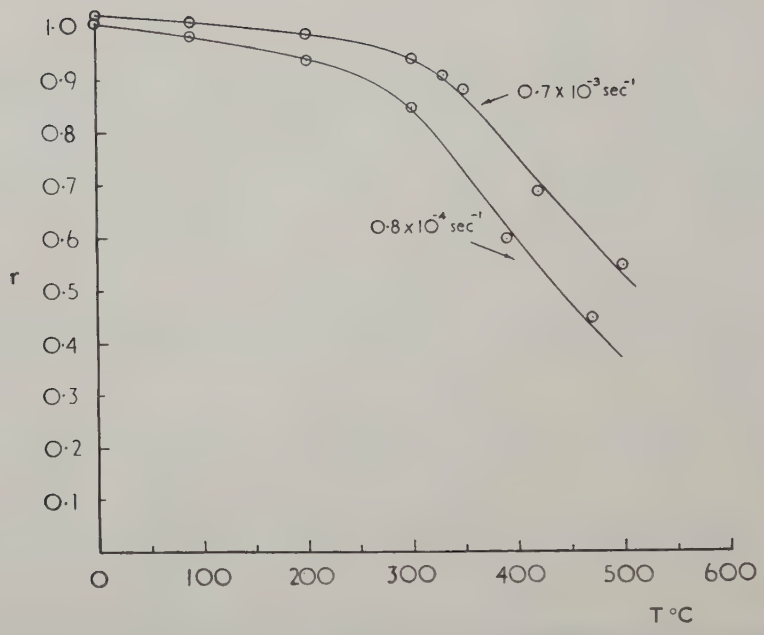

Temperature dependence of r for 99·99% pure polycrystalline Al for two strain rates.

Fig. 3

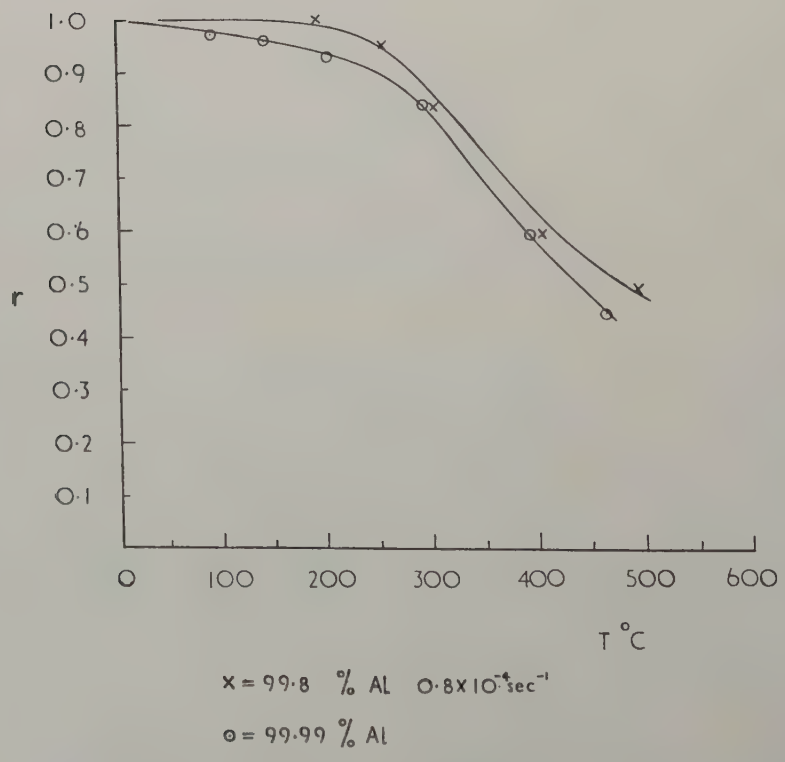

Temperature dependence of r for two purities of polycrystalline Al (99·8% and 99·99%).

Fig. 4

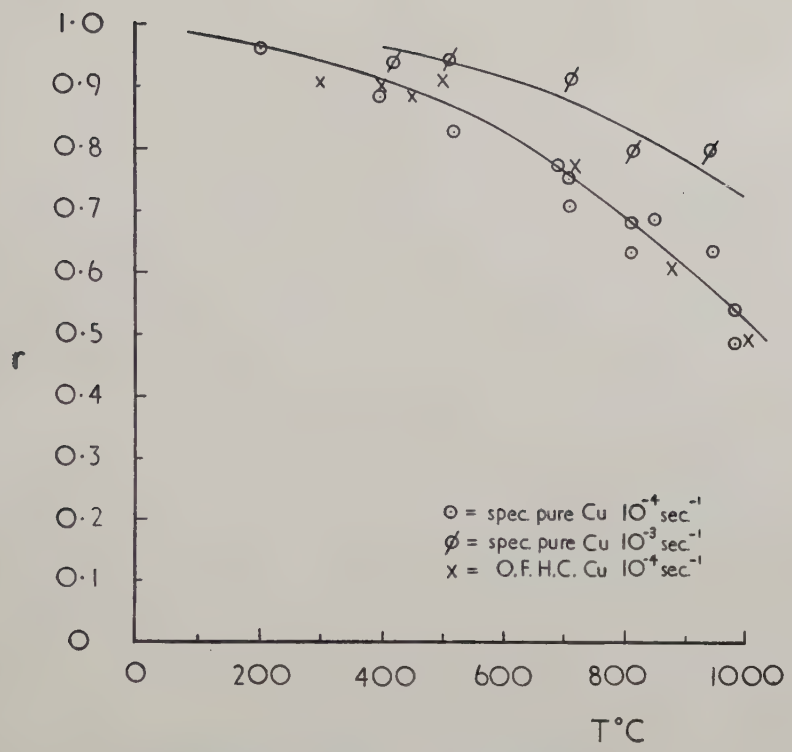

Temperature dependence of r for polycrystalline Cu.

Fig. 5

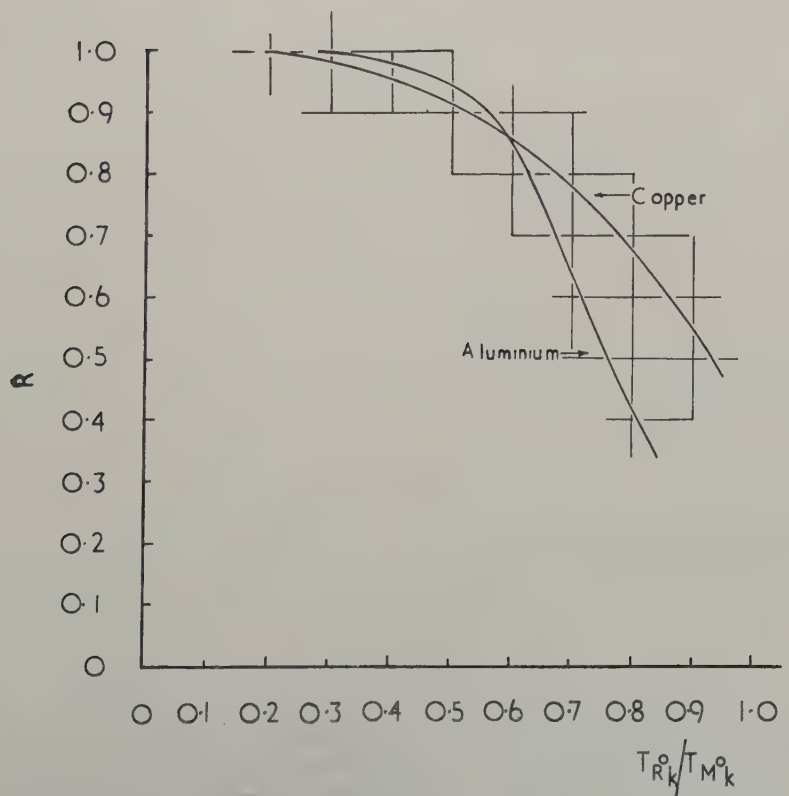

Comparison of temperature dependence of R for polycrystalline Al and Cu (for strain-rate of 10^{-4} sec^{-1}) plotted on a scale of temperature relative to that of the melting point.

Fig. 6

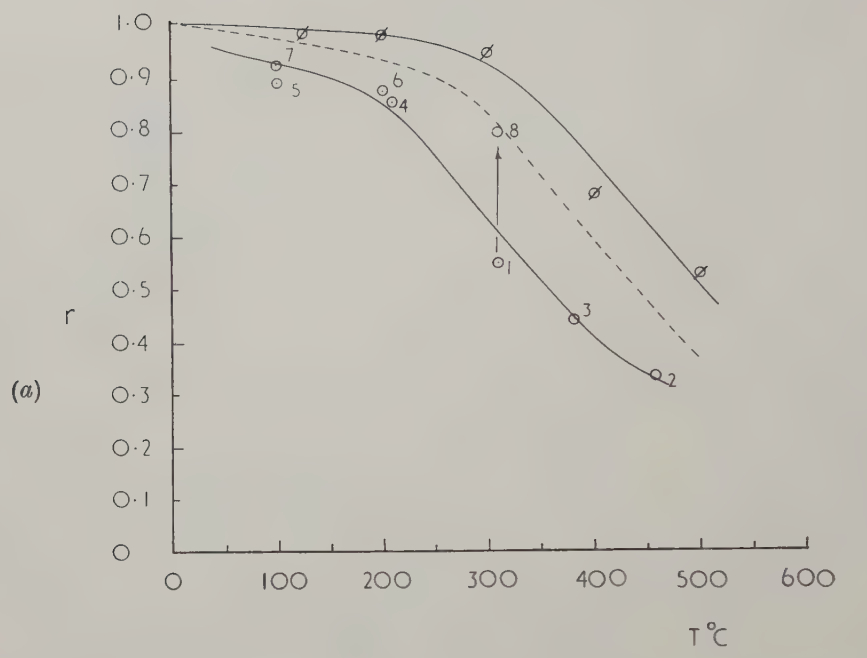

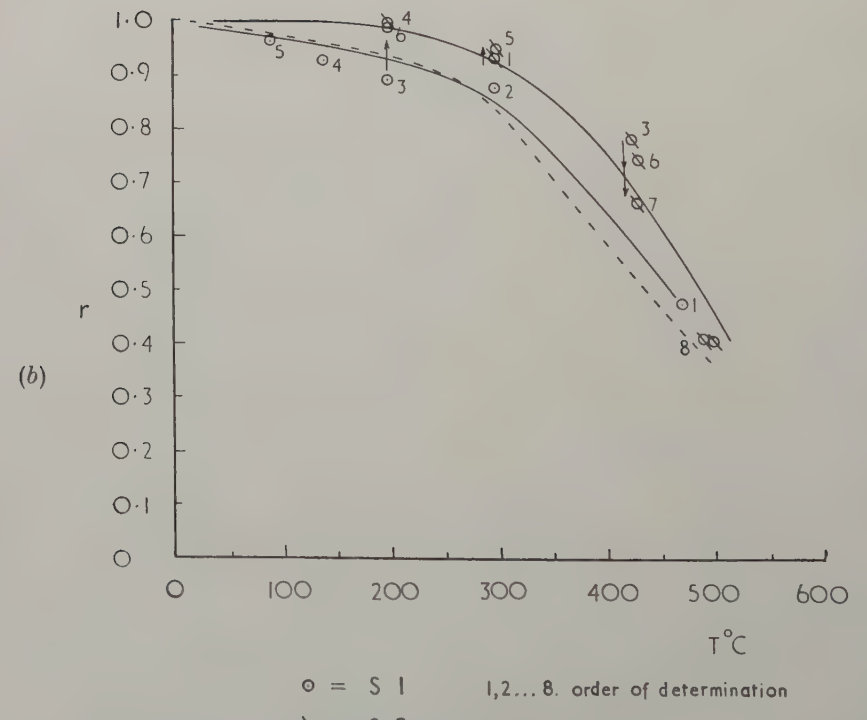

(*a*) Temperature dependence of r for single crystals of Al of two orientations grown from the melt. The dotted curve for polycrystalline Al at the same strain-rate ($0{\cdot}8 \times 10^{-4}$ sec^{-1}) is shown for comparison.

(*b*) Temperature dependence of r for single crystals of Al grown by the strain anneal method. The dotted curve for polycrystalline Al at the same strain rate ($0{\cdot}8 \times 10^{-4}$ sec^{-1}) is shown for comparison.

§ 3. Results

3.1. *Aluminium Polycrystals*

The results for 99·99% Al for two strain rates are shown in fig. 2. It is evident that the flow stress ratio r decreases sharply with increasing temperature above about 250°C, thus confirming Ball's results (1957).

It is seen that the increase in the strain rate shifts the decrease in the flow stress ratio, r, to higher temperatures as would be expected for a temperature activated phenomenon. At 0°C the ratio of the stresses for a change of strain rate was found to be 1·02.

Because of the restricted number of specimens (and the inaccuracies of the determinations) the shape of the curve of r above 300°C is not precisely determined, but it is evident that the plateau in the curve above about 400°C, as reported by Ball (1957), is not present. It is suggested that this arose from his technique of using higher reference temperatures than 0°C for specimens deformed above 400°C. The specimens were kept at these reference temperatures (300–450°C) for 15 min before restraining. Although these were about 100°C below the original temperature of straining they are well above the temperature at which recovery by self-diffusion can be important during the test and it is suggested that this process led to too high a value of the flow stress ratio. The present results do not however rule out the possibility of a plateau above about 500°C.

r was determined for a range of values of stress at the high or low temperatures. Table 1 gives a typical set of results. Below about 300°C the range of stress extended over a factor of two, but at the higher temperatures the low work-hardening rates only allowed a variation of 10–20% in stress. For all the ranges of stresses investigated no significant variations of r were detected at any temperature.

The results obtained with 99·8% Al are shown in fig. 3, where the corresponding curve for 99·99% Al is shown for comparison. The general behaviour is similar, but the onset of the decrease in r has been raised to slightly higher temperatures and the knee in the curve has been sharpened.

3.2. *Copper Polycrystals*

The results are shown in fig. 4; they differ in form from those for aluminium in that the decrease in r with temperature is more gradual; this is partly due to the large slope in the curve at 0°C. The existence of the comparatively greater slope around 0°C is in agreement with the results of previous workers (Adams and Cottrell 1955, Diehl 1956, Basinski 1959). Nevertheless the increasing rate of decrease of r with temperature is etablished, and by comparing the results for Cu and Al on a reduced temperature scale (i.e. by plotting r against T/T_m, where T_m is the melting-point temperature), the general behaviour for the two metals is seen to be rather similar (fig. 5).

The experimental points for Cu show a large scatter (fig. 4); this is partly due to the fact that only one value of r could be determined from each specimen, and partly to the large work-hardening rate on restraining at

0°C, leading to an appreciable experimental error. The second effect was very noticeable for specimens deformed at 10^{-3} sec, and not much reliance can be placed on these points. All the specimens were deformed to about 4% at the high temperature in order to avoid complications which might arise in the interpretation of the results if intercrystalline cracking should occur. Since this cracking is dependent upon purity and the two purities of copper gave approximately the same value of r it is believed that these difficulties have been avoided. The elongation to fracture at high temperature was typically about 15%. Since the specimens were deformed to approximately only one stress at any temperature, the dependence of r on stress is not known.

Table 1. Results for 99·99% Al extended at a rate of $0{\cdot}7 \times 10^{-3}\,\mathrm{sec}^{-1}$

Temp. °C	Ratio (τ_T/τ_0)	Stress (kg/mm²) at 0°C	Work-hardening rate at 0°C (arbitrary units)
100	0·895	1·9	12
	0·933	3·0	12
	0·925	3·8	11
200	0·845	1·5	14
	0·845	2·1	14
	0·87	2·4	14
300	0·77	1·1	16
	0·79	1·3	15
	0·78	1·4	14
350	0·69	0·91	13
	0·715	1·06	13
420	0·482	0·84	12
	0·485	0·89	13
500	0·36	0·57	19
	0·36	0·59	20
	0·40	0·65	18
	0·36	0·60	18

3.3. *Aluminium Single Crystals*

The results quoted are for the ratio of loads to extend the specimen; the resolved shear stresses were not in general determined. The flow stress ratio depends upon crystal orientation and also apparently more upon the deformation than for polycrystals.

Crystal S7 was grown from the melt. Five separate specimens of the same orientation (near the centre of the stereographic triangle, fig. 7) were pulled to various stages of the stress strain curve and fig. 6*a* shows the results obtained at 10% extension.

Table 2 gives the values of r for various values of resolved shear stress at room temperature. Up to and including 400°c the range of stress extended over a factor of 2, but even at 500°c the stress varied by 30%.

On the whole the flow stress ratio shows a larger variation with stress than for polycrystals, particularly at the higher temperatures, although for the range of stresses given in table 2 the maximum variation is only about 10%.

Fig. 7

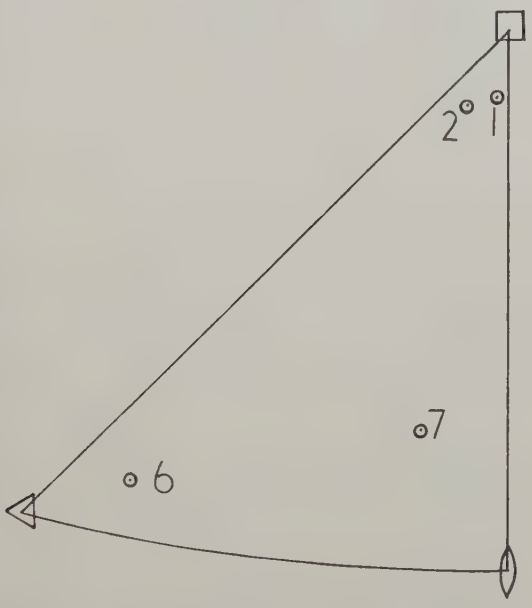

Orientations of single crystals of Al used in the experiments.

Crystal S6 was also grown from the melt. Its orientation was very close to [111] and favourable for '(100)' slip (fig. 7). The points were obtained from one specimen in the sequence shown, and are abnormally low, especially for low deformations. This may be connected with the abnormally high work-hardening characteristics of this orientation at room temperature. The decrease in temperature during the measurement of r effectively takes the crystal from stage III conditions of parabolic hardening to a pseudo stage II condition of high linear work hardening, and irregularities might be expected. Certainly this effect requires further study. Point 8 was determined after a 3% strain at 0°c followed by a further 3% strain at 310°c and demonstrates clearly that the flow stress ratio is dependent upon the flow stress.

Crystals S1 and S2 had orientations 5° from [100] (fig. 7) and were prepared by the strain anneal method. The results are shown in fig. 6*b*. The value of the flow stress ratio varied with deformation as indicated by the arrows. The corresponding curve for polycrystals is shown dotted.

Although the results are more complicated than for polycrystalline specimens, the ratio r does decrease in a similar manner in the same temperature range and the curves have approximately the same value of the slope.

Table 2. Results of single crystal (S7) of Al extended at a rate of $0{\cdot}8 \times 10^{-4}\,\mathrm{sec}^{-1}$

Temp. °C	Ratio (τ_T/τ_0)	Resolved shear stress (kg/mm²) at 0°C.	Work-hardening rate at 0°C (arbitrary units)
100	0·94	0·31	26
	0·935	0·61	26
	0·935	0·97	28
200	0·87	0·31	33
	0·91	0·46	31
	0·88	0·66	32
	0·89	0·87	33
300	0·81	0·23	22
	0·79	0·29	26
	0·82	0·41	34
	0·80	0·54	32
400	0·58	0·11	14
	0·48	0·19	27
	0·52	0·24	24
	0·52	0·25	24
500	0·43	0·14	26
	0·43	0·155	21
	0·38	0·195	29

3.4. *Discussion*

The similarity in the results obtained with single and polycrystals of Al implies at once that the decrease in r with temperature cannot be due to grain boundary sliding, but must result from a real change in r for slip within a single crystal or grain.

The determinations of flow stress ratio at high temperatures differ from those previously reported at low temperatures, in that in the former case the work-hardening rates at the two test temperatures are quite different. Thus, whereas the work-hardening rates at the high temperatures are usually low, those at 0°C in the present tests are generally high. The possibility therefore arises that the flow stress determinations at 0°C might be affected by different work-hardening rates after deformations at different high temperatures. Figure 8 shows a set of flow stress determinations at 0°C for polycrystalline Al deformed at a strain rate of

$0{\cdot}7 \times 10^{-3}\,\mathrm{sec}^{-1}$, for different initial deformation temperatures. The value of the load on the specimen at the flow stress is given together with a load scale for each curve. In fact the work-hardening rate at 0·2% extension shows only a small variation for the complete range of temperatures. Table 1 gives the work-hardening rates in arbitrary units; it is clear that apart from the values at 500°C the work-hardening rates are reasonably constant and can therefore not be expected to have a direct effect on the value of the flow stress determined. Table 2 gives the work-hardening rates at 0°C for the Al single crystal S7; in this case the work-hardening rates are seen to be similar after deformation at all temperatures and consequently again the variation of flow stress at 0°C with temperature of pre-straining cannot be attributed to change in the work-hardening rates at 0°C.

Fig. 8

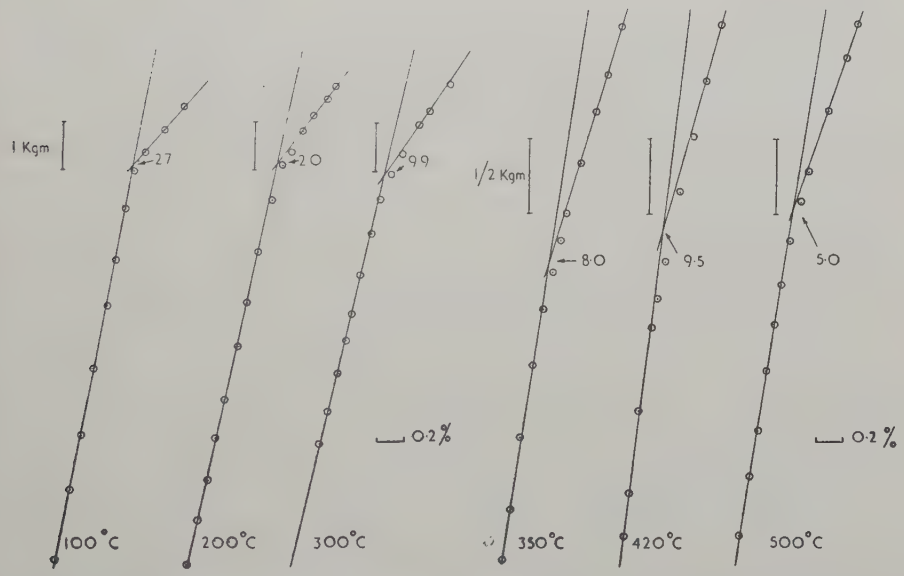

Load-strain curves at 0°C for 99·99% Al, strained at a rate of $0{\cdot}7 \times 10^{-3}\,\mathrm{sec}^{-1}$, showing flow stress determinations at this temperature after prior deformation at various temperatures.

Figure 8 also shows that the stress–strain curve does not depart abruptly from the elastic extension curve, and after initial prestrains at the higher temperatures measurable microstrain occurs at stresses 5–10% below those of the determined flow stresses. This effect might be due to recovery during the period of cooling from the high temperature. It is also possible that such recovery may affect the value of the flow stress; in that case the flow stress determined experimentally will be too low, and therefore the flow stress ratio too high. Recovery therefore cannot explain the observed

decrease in flow stress with temperature. If it is important at all in these measurements it will have the effect of reducing the true decrease in flow stress with temperature.

It should be emphasized however that recovery is likely to be important during the deformation at high temperatures. The low *work-hardening rates* at these temperatures are probably due to recovery during the test. However, the flow stress at the high temperature is uniquely determined by the actual stress on the specimen when the test is stopped and the temperature lowered. The flow stress at the low temperature should therefore correspond to the stress required to move dislocations in crystals with dislocation structures either identical to those at the high temperature or, if recovery occurs during cooling, softer than these.

All the considerations suggest that the observed decrease in r is due to a real decrease of the flow stress with temperature for a given dislocation structure.

There is however still the possibility that the dislocation structure at 0°c is changed materially during the microstrain period preceding the determination of the flow stress. It is difficult to rule out this possibility completely as relatively little is known about the nature of the changes occurring during microstrain. Nevertheless, from general experience of the changes in dislocation distribution with strain it seems rather unlikely that the dislocation distribution could be changed materially by only about 0·2% strain.

Table 3. Ratio of flow stress at low temperature to that at 0°c, for polycrystalline Al

	Flow stress ratio r −73°c	Flow stress ratio r −196°c
Present results	1·02	1·18
Basinski (1959)	1·02	1·15

To give another check on the results, measurements of the flow stress for polycrystalline Al were made at 0°c, −73°c and −196°c after prior deformation at a high temperature, 400°c. Table 3 shows the flow stress ratios calculated from these results, expressed relative to a value of unity at 0°c, compared with Basinski's (1959) results obtained for specimens deformed at or below 0°c. The agreement between these sets of data is quite good, indicating that the method of determination of flow stress used in the present experiments is satisfactory, and also that dislocation structures introduced at high temperatures have the same effect on the low-temperature flow stress as those introduced at low temperatures.

The discussion given in the following section is based upon the assumption, justified by the above arguments, that the experimental results

reported in this paper represent reasonably correctly the variation of the flow stress ratio with temperature for crystals containing the same dislocation structures at the high and low temperatures.

§ 4. Interpretation

4.1. *Possible Models for the Flow Stress*

The results reported in the previous section show that at high temperatures the flow stress decreases in a manner shown in fig. 1 (region C). The following facts must be explained:

(1) The flow stress changes from one which is temperature independent (region B) to one which is strongly temperature dependent above a certain critical temperature (region C), although the actual transition is gradual.

(2) The ratio of the flow stress at the high temperature to that at the low temperature is independent of the actual value of the flow stress for strains exceeding about 5%. A similar law for low temperatures has been enumerated by Cottrell and Stokes (1955) over the limited range of stresses available.

Electron microscope observations and x-ray diffraction studies of polycrystalline specimens of Al and Cu deformed at high temperatures show that the dislocations are arranged in well formed sub-boundaries (Warrington 1961). Dislocations passing through the crystal will have to overcome the local elastic stresses due to the dislocation boundaries during the process of intersection (Thornton and Hirsch 1958, Hirsch 1958, Basinski 1959, Bailey and Hirsch 1960, Saada 1960 a, b, Carrington *et al.* 1960), and possibly long-range stresses from other dislocations (Seeger *et al.* 1957). The first of these elastic stresses should be the same (after correction for the temperature variation of the shear modulus) at the high and low temperatures, and therefore cannot account for the decrease in flow stress with increasing temperature. There is however the possibility that at the high temperatures the strain is produced entirely by sub-grain boundary migration. If the boundaries migrate as a whole, the dislocations would not have to overcome their mutual elastic stresses. In order to test this possibility measurements were made of the sub-grain boundary migration and these are discussed in Appendix A. It is shown there that sub-grain boundary migration can account only for about 6% of the strain at all temperatures and this effect can therefore not explain the decrease in the flow stress ratio.

The second type of elastic stress, i.e. long-range stress, could only possibly explain the decrease in flow stress if such stresses are built up at the low temperatures during the microstrain period. These long-range strains could be due to interactions between edge dislocations; screw dislocations, at least in Al, should be able to cross slip to overcome any obstacles at all

stresses at the temperatures considered (Seeger *et al.* 1959). The decrease of the flow stress could then be due to edge dislocations surmounting barriers by climb.

Fig. 9

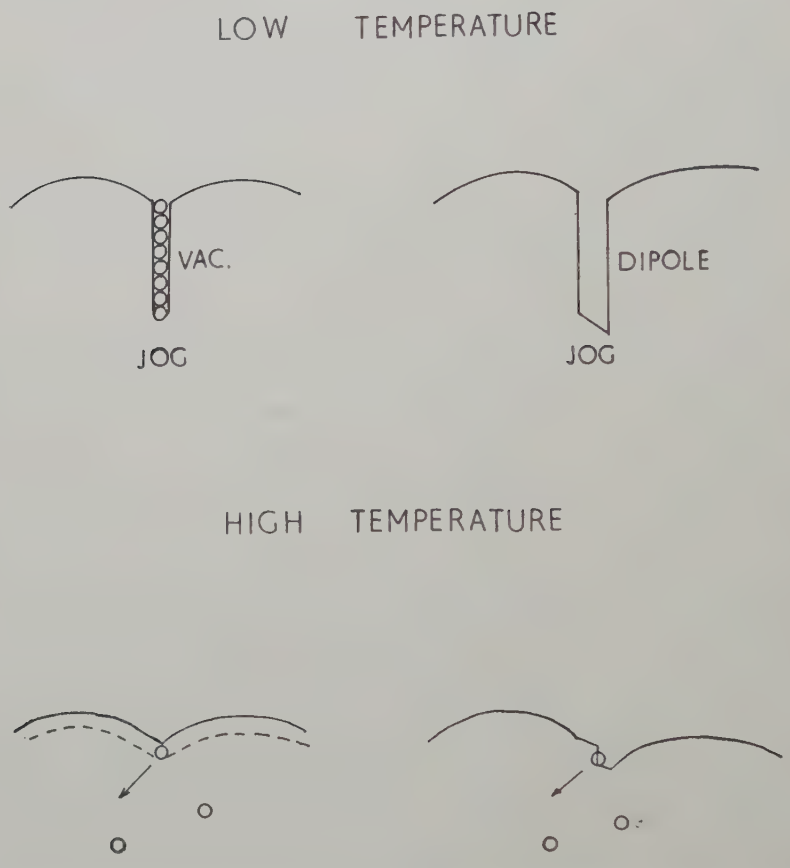

Diagram illustrating the low and high temperature behaviour of jogs in screw dislocations.

Alternatively however the flow stress may be controlled by jogs in screw dislocations, if it is assumed that the jogs cannot move conservatively. At low temperatures the dislocations move forward, leaving a string of defects or a dislocation dipole (see fig. 9); at higher temperatures the jogs are dragged with the dislocation with the aid of thermal activation, vacancies being emitted by and moving away from the jogs in the same thermally activated process. The activation energy for this process is that of self-diffusion. This mechanism was proposed many years ago (Mott 1952, van Bueren 1957), but discarded because it was believed that

jogs could move easily conservatively along the screw dislocation (Friedel 1955). In a face-centred cubic lattice however the jogs may be dissociated (Thompson 1953, Friedel 1956), and this may cause them to be sessile (Hirsch, unpublished). Recently, considerable evidence has been obtained that dislocation dipoles are produced at least by *long* jogs in screw dislocations in fatigued Cu, Ag, Au, Ni (Segall 1960), Segall *et al.* 1961), Zn deformed in tension (Price 1960), Mg deformed by tension or by quenching (Lally, unpublished), MgO (Washburn *et al* 1960) and to some extent in single crystals of Cu and CuAl alloys deformed in tension (Howie 1960), and polycrystalline Cu (Warrington 1961) and Al deformed in tension (Fourie and Wilsdorf 1960, Warrington 1961).

In the following section the analysis of flow stress in terms of sessile jogs will be developed; that in terms of climb of edge dislocations will be discussed in § 4.3.

4.2. *The Model Based on Jogs in Screw Dislocations*

4.2.1. *Formulation of the problem*

Consider a screw dislocation held back by sessile jogs (i.e. jogs which are dissociated and cannot glide conservatively along the dislocation) p Burgers vectors high, spaced at a mean distance l_j along the dislocation. The dislocation could advance either with the aid of elastic stress alone leaving a line of point defects or a dipole (as shown in fig. 9), or with the aid of thermal activation in a process in which a point defect is created and moved away from the jog in the same jump. This latter condition is essential, as otherwise the jog would move back again annihilating the point defect created. These mechanisms have already been discussed in some detail by Seeger (1955) and Friedel (1956).

At low temperatures the first of these processes will occur, giving rise to a flow stress (τ_1) which is temperature independent except for the variation of shear modulus (for a dislocation) or of the free energy of a line of point defects with temperature. Above a sufficiently high temperature corresponding to a given rate of strain the second process will become rate-determining and the flow stress (τ_2) will then be strongly temperature dependent. The jog model therefore explains at once how τ_g can decrease with temperature at high temperatures, above a critical temperature determined by the condition that $\tau_2 < \tau_1$. In general of course τ_g could have a contribution also from elastic stresses, τ_e say; we shall write therefore

$$\tau_g = \tau_j + \tau_e \qquad (1)$$

where τ_j is the stress necessary to overcome resistance from jogs. This term τ_j will now be considered in detail.

If $U_0(T)$ is the free energy of the defect created at temperature T for every Burgers vector of advance of the dislocation, the flow stress for the low temperature process is given by

$$\tau_1 = U_0(T)/b^2 l_j = U_0(T)/pv \qquad (2)$$

where v is the activation volume, equal to $b^2 l_j/p$ (see below).

In the high temperature process we shall assume that the defects created by non-conservative motion of the jogs are vacancies, not interstitials. An examination of the extension of jogs in face centred cubic crystals suggests that if the jogs are small only vacancy producing jogs should be sessile (Hirsch, unpublished). We shall consider therefore only vacancy jogs in this section. The activation energy for formation and moving the defect will therefore be assumed to be that of self-diffusion, U_D, (enthalpy). Multiple jogs will tend to take up some steady-state form, for which the work done during the activation for every point on the jog will be equal to the average value of $v\tau_2 = \tau_2 l_j b^2/p$ where τ_2 is the flow stress for the high temperaure process and v is the activation volume.

Friedel's analysis for climb (1956), when applied to this process, gives a strain rate $\dot{\epsilon}$ at temperature T

$$\dot{\epsilon} = N l_j b^2 z A \exp(-U_D/kT)[\exp(v\tau_2/kT) - c/c_0] \quad . \quad . \quad . \quad (3)$$

where N is the number of elements activated per unit volume, ν an atomic frequency, z the coordination number, $A = \exp(s/k)$, where s is the entropy of activation, k the Boltzmann factor, c the actual concentration of vacancies, and c_0 the equilibrium concentration of vacancies at temperature T. The second term in the bracket of eqn. (3) represents the chemical stress due to any possible supersaturation of vacancies present. In the steady state there will be a certain concentration of vacancies for a given stress and strain rate; i.e. for every vacancy emitted at a jog, another will be absorbed somewhere else in the crystal, for example at interstitial jogs. The steady-state concentration of vacancies will depend on the distribution of sources and sinks in the crystal. Before the flow stresses τ_1 and τ_2 can be compared, the effect of supersaturation of vacancies must be considered. This will be discussed in Appendix B; we quote here the result that in general

$$\tau_2 = U_D/v - (kT/v)\log(f N l_j b^2 \nu z A/\dot{\epsilon}) \quad . \quad . \quad . \quad (4)$$

where f is a constant. From (2) and (4) we obtain therefore

$$\tau_2/\tau_1 = pU_D/U_0 - (pkT/U_0)\log(f N l_j b^2 \nu z A/\dot{\epsilon}). \quad . \quad . \quad (5)$$

This relation predicts that the flow stress will decrease linearly with temperature above a critical temperature T_c given by the condition $\tau_2/\tau_1 = 1$, while

$$T_c = [U_D - U_0(T_c)/p]/k\log(f N l_j b^2 \nu z A/\dot{\epsilon}). \quad . \quad . \quad . \quad (6)$$

(It will be assumed that the enthalpy U_D is approximately independent of temperature.)

In practice there is likely to be a distribution of jog heights; for this and other reasons the transition will be gradual rather than abrupt. For small jogs (a few Burgers vectors) U_0 will be proportional to p; with increasing p the values of U_0/p will gradually decrease; thus, the critical temperature will gradually increase with increasing size of jog.

Equation (5) also shows at once that the flow stress ratio is independent of the amount of prestrain, except for a possible change in p/U_0 and a slow variation of the log term through changes in the product $Q = fNl_j$. At present we do not know anything about the variation of p/U_0 with strain. With regard to Q, since N can be written in the form ρ_m/l_j, where ρ_m is the density of moving dislocations, $Q = f\rho_m$. This parameter would have to vary by a factor of 10 to cause a change by 10% in the ratio τ_2/τ_1 (see §4.2.2.). There is at present no independent information on the variation of Q with prestrain. However, if p/U_0 is constant, and if Q does not vary by more than about a factor of 10 for the ranges of prestrain considered, the Cottrell–Stokes law follows at once.

It is clear therefore that the jog model can account at least qualitatively for the nature of the flow stress variation at high temperatures. The quantitative interpretation will be discussed in the next section.

4.2.2. *Application to experiments*

Experimentally the ratio R of the flow stress at a high temperature (T) to that at a low temperature (in this case usually 273°K) is measured, i.e.

$$R = \frac{\tau_2(T) + \tau_e(T)}{\tau_1(273) + \tau_e(273)} = \frac{\tau_2(T)/\tau_1(273) + \tau_e(T)/\tau_1(273)}{1 + \tau_e(273)/\tau_1(273)} \qquad (7)$$

where $\tau_2(T)/\tau_1(273)$ is given by (5). We have assumed in (7) that the temperature dependent part of the flow stress at low temperatures, τ_s, is negligible at 273°K and above. Below the critical temperature, T_c, given by (6), $\tau_2(T)$ should be replaced by $\tau_1(T)$ in (7). In this region the temperature dependence of R will be that of $\{\tau_1(T) + \tau_e(T)\}$; $\tau_1(T)$ depends on temperature through the entropy term of U_0, $\tau_e(T)$ depends on temperature through the shear modulus G. For long jogs the temperature dependence of U_0 will be equal to that of the shear modulus; for single jogs present estimates of the entropy terms (Simmons and Balluffi 1960) suggest a temperature dependence rather similar to that of the elastic moduli. It seems reasonable therefore to expect the temperature dependence of R to be that of the elastic moduli below T_c. Above T_c, R decreases more strongly with temperature, because of the large temperature dependence of $\tau_2(T)$. In analysing the data, the experimentally determined ratio R will be discussed directly, not the quantities plotted in figs. 2–6 which were divided by the ratios of the elastic moduli at the two temperatures. The temperature T_c is found by intersection of the straight line fitted to the curve at high temperatures, with the line representing the temperature variation of the elastic moduli, passing through the experimental point at 273°K (see figs. 10, 11).

Above T_c the slope of the line R versus T is given by

$$dR/dT = \frac{\left[\dfrac{d\{\tau_2(T)/\tau_1(273)\}}{dT} + \dfrac{\tau_e(273)}{\tau_1(273)G(273)}\left(\dfrac{dG}{dT}\right)\right]}{[1 + \tau_e(273)/\tau_1(273)]}$$

$$= -[pk/\{U_0(273)(1 + \tau_e(273)/\tau_1(273))\}]\log(fNl_jb^2\nu zA/\dot{\epsilon}) + \{[1 + \tau_1(273)/\tau_e(273)]G(273)\}^{-1}(dG/dT) \qquad (8)$$

and the strain-rate dependence of this slope is found to be

$$\frac{\Delta(dR/dT)}{(dR/dT)_1 - [(1+\tau_1(273)/\tau_e(273))G(273)]^{-1}(dG/dT)} = -\frac{\log(\dot{\epsilon}_2/\dot{\epsilon}_1)}{\log(fNl_jb^2vzA/\dot{\epsilon}_1)} \quad . \quad . \quad . \quad (9)$$

where it is assumed that variations in f, N and l_j are small compared with the change in $\dot{\epsilon}$. Thus from the strain-rate dependence the log term can be determined directly, if $\tau_e(273)/\tau_1(273)$ is known. Then $U_0(273)/p$, and therefore $U_0(T_c)/p$, can be obtained from the slope, and hence U_D from the critical temperature (6). However, if $\tau_e(273)/\tau_1(273)$ is not known, a value of U_D can be assumed, and U_0/p and $\tau_e(273)/\tau_1(273)$ can then be calculated from (6), (8) and (9).

To obtain good data on the strain-rate dependence, a wide range of strain rates must be used. If such data are not available, it is necessary to assume values for $\tau_e(273)/\tau_1(273)$ and U_D, and U_0/p can then be determined. It is convenient to use instead of (6) the ratio R_0 obtained on extrapolating (4) to $T=0°K$, i.e.

$$R_0 = [pU_D/U_0(273) + \tau_e(0)/\tau_1(273)]/[1+\tau_e(273)/\tau_1(273)]. \quad (10)$$

These equations will now be used to analyse the experimental data.

(*a*) *Aluminium*

The best curves were obtained for polycrystalline specimens; single crystals give similar curves, but the temperature dependence varies somewhat with pre-strain (see § 3). Figures 2, 3 show the curves of $r = RY(273)/Y(T)$ against T for the two types of polycrystalline specimen used; fig. 10 gives the data R corresponding to fig. 2 for polycrystalline Al examined at two different strain rates. Straight lines have been fitted to the curves of fig. 10 to pass through the same point R_0, at $T=0$. The lines are shown on fig. 10, and the relevant data from them are given in table 4.

From the values of R recorded at the highest temperature we can deduce that $\tau_e(273)/\tau_1(273)$ cannot exceed about 0·4. Using the data on strain-rate dependence and eqn. (9) the log term is found to be 27·5(±20%) and 25·5(±20%), taking the average for the two strain rates, for $\tau_e(273)/\tau_1(273) = 0$ and 0·4 respectively. The accuracy of these values is rather low owing to the lack of precision in determining the slopes. With these values of the log terms the activation energy U_D can be estimated from (6) and (9), and is found to be 2·0 ev(±20%) and 1·6 ev(±20%) respectively. The The latter value is in agreement to within the accuracy of the measurements with the generally accepted value of $U_D = 1{\cdot}35 \pm 0{\cdot}1$ ev (Federighi 1959, De Sorbo and Turnbull 1959, Silcox and Whelan 1960, Simmons and Balluffi 1960).

The use of the strain-rate dependence in analysing the data may however not be valid since the measurements were not made by changing the strain rate for a given specimen, but by using different specimens. Thus the other parameters in the log term may have different values at the two strain rates.

If we now assume $U_D = 1{\cdot}35$ ev, the log terms can be found from (9) and (10) to be 18·6 and 16·5 respectively for the two strain rates for $\tau_e/\tau_1 = 0$, and 23 and 26 for $\tau_e/\tau_1 = 0{\cdot}4$. (Again, these latter values agree, to within the experimental accuracy, with the log terms deduced from the strain

Fig. 10

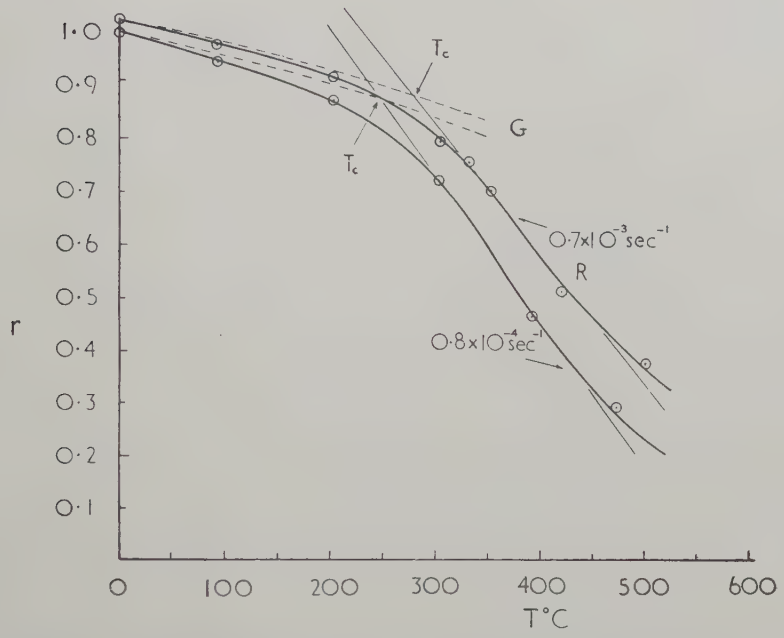

Temperature dependence of R for 99·99% polycrystalline Al for two strain rates. The dotted curves describe the variation of shear modulus, G, with temperature. The full straight lines have been fitted to the experimental curves. The critical temperatures, T_c, are at the points of intersections of the straight lines and the curves of the shear modulus variation.

Table 4. Data from the curves of R against T

Polycrystalline (99·99%) aluminium		
Strain rate	$0{\cdot}8\times10^{-4}$ sec^{-1}	$0{\cdot}7\times10^{-3}$ sec^{-1}
Slope	$2{\cdot}8\times10^{-3}$ °K^{-1} ($\pm$10%)	$2{\cdot}5\times10^{-3}$ °K^{-1} ($\pm$10%)
T_c	513°K	553°K
R_0	$2{\cdot}3\pm0{\cdot}1$	$2{\cdot}3\pm0{\cdot}1$
Polycrystalline copper		
Strain rate	$0{\cdot}8\times10^{-4}$ sec^{-1}	
Slope	$1{\cdot}1\times10^{-3}$ °K^{-1}	
R_0	$1{\cdot}6\pm0{\cdot}15$	

rate dependence. It should also be noted that the values of the log term found in this way are consistent with a logarithmic dependence on strain rate). Using mean values of the log terms equal to 17·5 and 24·5 respectively for the two values of τ_e/τ_1, upper and lower limits of U_0/p can be determined from (8) or (10). Writing $U_0=\alpha Gb^3$, where α is a constant, the limits can be given in terms of α/p. They are found to be 0·16 and 0·12 respectively, and can be used to determine the nature of the defects produced by stress. U_0 for vacancies would be 0·76 ev (Bradshaw and Pearson 1957, Simmons and Balluffi 1960); hence $\alpha/p=0{\cdot}21$.

Table 5. Theoretical values of α/p for vacancy jogs

Aluminium	
Length of jog in Burgers vectors	α/p
1	0·21 (single vacancy)
2	0·178
3	0·149
4	0·128
5	0·113
10	0·072
For comparison: single interstitial jog	0·8
Copper	
Length of jog in Burgers vectors	$\alpha\ p$
1	0·264 (single vacancy)
2	0·210
3	0·171
4	0·144
5	0·126
10	0·078
For comparison: single interstitial jog	1·0

For jogs whose length exceeds several Burgers vectors a dislocation dipole is produced. For this we take

$$U_0=[Gb^3/2\pi(1-\nu)]\log p+2\times\text{core energy}, \quad . \ . \ (11)$$

where the core radius has been taken as b. The core energy will be taken as $\frac{1}{2}\times 0{\cdot}76$ ev, so that for $p=1$, U_0 has the value appropriate to a single vacancy. Table 5 gives some values of α/p calculated in this way. It should be emphasized that the values for $p<5$ are suspect because of the uncertainty about the value of the core energy. The experimental limits on α/p suggest that the mean effective jog length lies between 2 and 5 Burgers vectors.

The values of the log term (17·5–24·5) deduced above are rather larger than those (14–15) found by Basinski (1959) for Al in the low temperature region. It it is assumed that the strain rate is emission-controlled (see Appendix B), an estimate of the moving dislocation density ρ_m can be made from the value of the log term. Since $N=\rho_m/l_j$, and taking $f=1$, the log term becomes $\log(\rho b^2 \nu z A/\dot{\epsilon})$, which is independent of l_j. Putting

Fig. 11

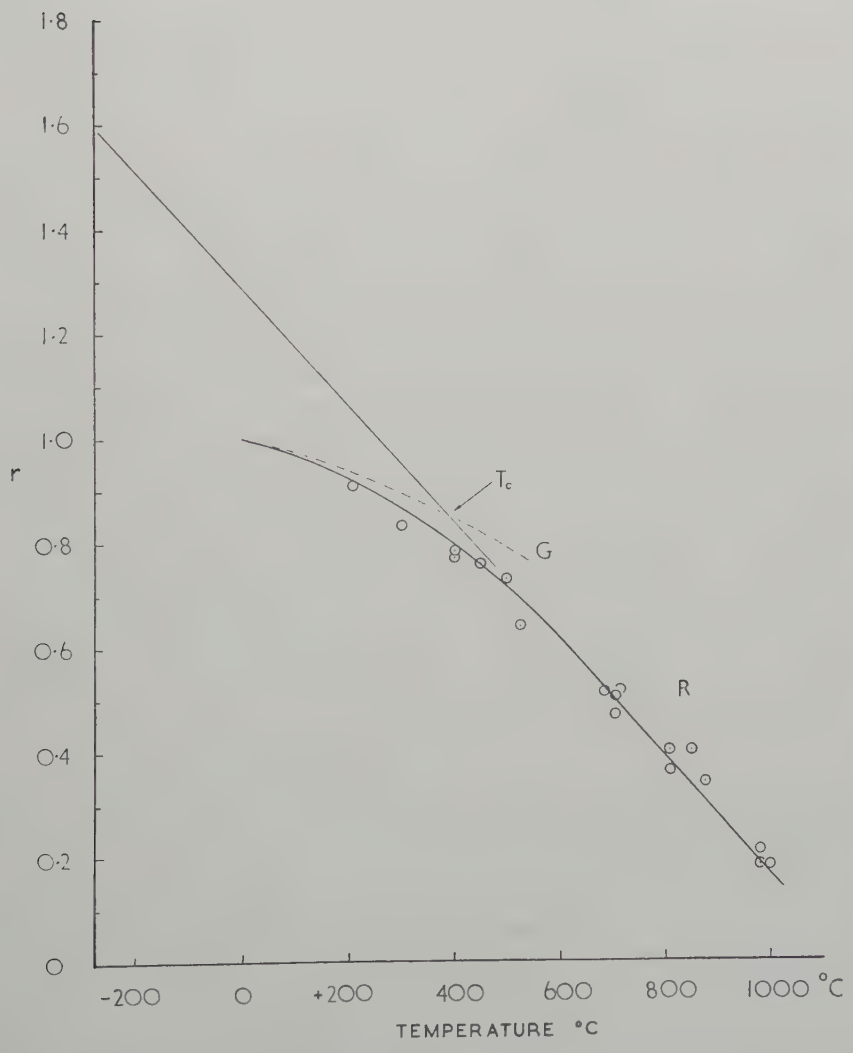

Temperature dependence of R for polycrystalline Cu strained at 10^{-4} sec^{-1}. The full straight line has been fitted to the experimental curve; the dotted curve describes the variation of shear modulus, G, with temperature.

$\nu = 10^{12}\,\mathrm{sec}^{-1}$, $z = 11$, $b = 2{\cdot}86 \times 10^{-8}\,\mathrm{cm}$, $A \sim 10$, $\dot{\epsilon} = 0{\cdot}8 \times 10^{-4}\,\mathrm{sec}^{-1}$, and taking the log term to be equal to 21, ρ_m is found to be $\sim 10^6/\mathrm{cm}^2$, which seems quite a reasonable value.

Equation (6) will be automatically satisfied with the values of the log term and U_0/p deduced above, and the experimental value of T_c. This equation may be considered to mean that the flow stress will begin to decrease when the average thermal energy available for activation to maintain the correct strain rate is equal to $U_D - U_0/p$. As has already been mentioned in § 4.2.1, this average thermal energy must be equal or greater than the activation energy for movement of the vacancy away from the jog. This condition is always automatically satisfied by condition (6), since $U_D - U_0/p$ is always greater or equal to its value for $p = 1$.

(*b*) *Copper*

The results for polycrystalline Cu are not so extensive as for Al, but show a similar variation with temperature (figs. 4, 5). In fig. 11 the values of R derived from the data obtained at the strain rate of $10^{-4}\,\mathrm{sec}^{-1}$ have been plotted against T. A straight line has been fitted to this curve in the highest temperature range, where the curve is approximately linear. Table 4 gives the data taken from this curve.

Proceeding as before and using $U_D = 2{\cdot}05\,\mathrm{ev}$ (Kuper *et al.* 1954) we obtain upper and lower limits for the log term, equal to 22 and 17 respectively. In this case we have assumed that $\tau_e(273)/\tau_1(273)$ cannot exceed 0·5. In the low temperature region Basinski (1959) finds values of 13·4 and 10·5 for the log term at 20–30°K and 200°K respectively. The high temperature value is again rather greater than those obtained by Basinski.

A difficulty arises in the determination of α p. The flow stress is not temperature independent in region B (figs. 1, 4), i.e. τ_s may not be negligible. However, around room temperature, the temperature dependence is small and this temperature will be taken as the low temperature reference point. The uncertainty in τ_s, however, cannot materially affect the range of values of α/p deduced by assuming values of $\tau_e(273)/\tau_1(273)$ between 0 and 0·5; the limits of α/p are found to be 0·28 and 0·21 respectively. Table 5 shows theoretical values of α/p for Cu calculated using eqn. (11), the core energy being taken as $\frac{1}{2} \times 1{\cdot}2\,\mathrm{ev}$. The experimental range of values of α/p corresponds to single or double vacancy jogs in this case.

4.2.3. *The role of interstitial jogs*

Although small interstitial jogs are expected to be glissile, large interstitial jogs might be sessile (Hirsch, unpublished). It is interesting therefore to examine whether the experimental results might be explained in terms of interstitial jogs.

The low temperature process will be similar to that for vacancy jogs, except of course that rows of interstitials rather than vacancies would be produced by single jogs. The flow stress will be given by a relation similar to (2).

At high temperatures two processes may be considered. Interstitial jogs might either advance by interstitial diffusion, or by absorbing vacancies produced by vacancy jogs. The former process may be ruled out because the activation energy for interstitial diffusion is likely to be unreasonably high (~ 3 ev) for Al).

For the latter process, the strain rate will be given by the relation

$$\dot{\epsilon} = N_i l_i b^2 \nu z A [c/c_0 - \exp(-v_i \tau_2/kT)] \exp(-U_D/kT) \quad . \quad . \quad (12)$$

where v_i is the activation volume for the interstitial jogs, N_i the number of interstitial jogs per unit volume, spaced at distance l_i.

The strain rate will therefore be determined by the supersaturation produced by the vacancy jogs and the second term in the bracket can be neglected. The supersaturation c/c_0 will be some fraction (say γ) of the maximum supersaturation $\exp(v_v \tau_2/kT)$ (see Appendix B), where v_v is the activation volume for vacancy jogs. Hence we obtain for τ_2

$$\tau_2 = U_D/v_v - (kT/v_v) \log(\gamma N_i l_i b^2 \nu A/\dot{\epsilon}), \quad . \quad . \quad . \quad . \quad (13)$$

a relation of precisely the same form as for vacancy jogs, except for the parameters appearing in the log term. Hence we obtain

$$\tau_2/\tau_1 = pU_D l_i/v_i l_v - (pkTl_i/U_i l_v) \log(\gamma N_i l_i b^2 \nu z A/\dot{\epsilon}) \quad . \quad . \quad (14)$$

where l_v is the average spacing of vacancy jogs p Burgers vectors high, U_i the energy per atom length of an interstitial dipole. Writing $U_i = \beta G b^3$, the parameter α/p appearing in the vacancy jog model must be replaced by the parameter $\beta l\sigma/pl_i$ for interstitial jogs. There are enough unknown quantities in this parameter to satisfy any of the experimental values. Thus, for example, if $l_v \sim l_i$, the experimental results can be explained in terms of single interstitial jogs if the vacancy jogs are several Burgers vectors long, or in terms of multiple interstitial jogs if $p = 1$.

Equation (14) would also give rise to a Cottrell–Stokes law if $pl_i/v_i l_v$ is independent of prestrain. It is clear therefore that the present experimental results could be explained either in terms of the small vacancy jogs discussed in the previous section, or in terms of interstitial jogs of indeterminate size.

4.2.4. *Effect of stress concentrations*

The dislocations introduced in polycrystals by deformation at high temperatures are arranged in the form of a well-developed substructure (e.g. Ball 1957, Warrington 1960). The flow stress at room temperature of specimens containing this sype of sub-structure has been found to be proportional to $t^{-1/2}$, where t is the sub-grain diameter. This result has been established for Al (Ball 1957, Warrington 1961), Cu (Warrington 1961), and Fe (Ball 1957, Warrington 1961). Such a law suggests the presence of stress concentrations due to groups of dislocations piled up at the sub-boundaries (Gay *et al.* 1954). The question arises as to whether the observed temperature dependence of the flow stress is consistent with such a model.

Suppose that the criterion for the flow stress is that a dislocation must penetrate the boundary, and that the stress must be sufficient to overcome the resistance of the jogs formed by intersection. When the dislocation has moved a certain distance, at least, some of the jogs might be annihilated and the dislocation could move more freely. The flow stress would be determined by the stress necessary to drag the jogs near the boundary and stress concentrations could therefore be important. Alternatively the criterion for the flow stress could be the operation of a jogged source near the boundary. In either case eqns. (2) and (4) could be rewritten in the form

$$\tau_1 k_1 = U_0/pv \qquad . \quad . \quad . \quad . \quad . \quad . \quad . \quad . \quad . \quad . \quad . \quad (15)$$

and

$$\tau_2 k_2 = U_D/v - (kT/v)\log(fNl_j g' vzA/\dot{\epsilon}) \qquad . \quad . \quad . \quad (16)$$

where k_1, k_2 are the stress concentration factors and g' a parameter taking into account the fact that after dragging the jogs for a certain distance the dislocation can glide freely till it is held up at the next boundary.

If the flow determining stress is that which acts at a distance $x \leqslant t$ from the boundary, $k_1 = k_2 \sim \sqrt{(t/x)}$, and hence the flow stress ratio τ_2/τ_1 will be unaffected by the stress concentration, but the log term will depend on g'. If on the other hand the flow determining stress is that acting on the leading dislocation of the pile-up, $k_{1,2} \sim \pi t \tau_{1,2}/Gb$ (Eshelby *et al.* 1951), and hence

$$(\tau_2/\tau_1)^2 = pU_D/U_0 - (pkT/U_0)\log(fNl_j g' vzA/\dot{\epsilon}) \qquad . \quad . \quad (17)$$

The form of the decrease of τ_2/τ_1 with temperature will no longer be linear, but the expression for the critical temperature would still be the same. The experimental results could equally well be explained in terms of the parabolic relation (17). In this case some of the parameters derived from the experimental data, e.g. the log term, or p/U_0, will differ from those deduced assuming no stress concentrations; the effective jog length would be found to be larger, by perhaps a factor of 2.

It is clear therefore that the observed temperature dependence is consistent with a model involving stress concentrations, and that the detailed interpretation would depend on the particular model assumed.

4.2.5. *Density of jogs*

The jog density corresponding to the observed flow stresses depends also on the particular model assumed. For Al, for example, the stresses range from about $0{\cdot}1\,\mathrm{kg/mm^2}$ to about $5\,\mathrm{kg/mm^2}$; if there are no stress concentrations the corresponding jog spacings are $1{\cdot}3 \times 10^4$ and $2{\cdot}6 \times 10^2$ Burgers vectors respectively. If on the other hand stress concentrations of the type discussed in § 4.2.4 are operative, the jog spacings will be much smaller. Thus, using a stress concentration factor $k_{1,2} \sim \pi t \tau_{1,2}/Gb$, and using Warrington's (1961) data on the relation between τ and t, the jog spacing is found to be only ~ 5 Burgers vectors for all stresses.

At present it is not possible to decide which of these jog densities is more reasonable. If the jogs are produced by dislocation intersection the spacings deduced assuming no stress concentrations would seem to be of the correct order of magnitude when compared with the dislocation densities. On the other hand jogs could be created and destroyed continuously by cross slip and the smaller jog spacing could be quite reasonable. The problem is further complicated by the fact that according to theory and experiment the smallest jogs are expected to be glissile in Al in the temperature range of the present experiments. The density of sessile jogs would therefore depend both on the rate of production and of annihilation of jogs.

4.3. *Models Based on Climb of Edge Dislocations*

4.3.1. *Formulation of the problem*

The difficulty in this case is to decide on a suitable model for the low temperature process. We shall discuss as an example a model in which parallel edge dislocations of opposite sign pass each other on glide planes a distance h apart. At low temperatures the stress required to overcome the elastic interaction is of the form

$$\tau_1 k_1 = \alpha_1 Gb/h \qquad . \; . \; . \; . \; . \; . \; . \; . \quad (18)$$

where k_1 is the stress concentration factor due to the pile-up and α_1 is a constant ($=\{8\pi(1-\nu)\}^{-1}$).

At high temperatures the dislocations can climb towards each other to annihilate, and another dislocation can then be emitted by the source. This model is similar to that used in Mott's theory of creep (1953), extended by Weertman (1955). Each dislocation has to climb a distance of the order h, and for each annihilation an area a of slip plane is swept out. Applying Friedel's theory of climb (1956) the strain rate is given by

$$\dot{\epsilon} = Nagbvz A \exp(-U_D/kT)[\exp(b^3 k_2 \tau_2/kT) - c/c_0] \quad . \; . \quad (19)$$

where g is a factor involving the number of jumps which have to be made before slip over the area a takes place, N is the number of jogs per unit volume, k_2 is the stress concentration factor which also takes into account that the normal stress rather than the shear stress should be used here.

As in the case of jogs in screw dislocations, the form of the equation is similar whether the climb is emission or diffusion controlled (see Appendix B). We have in general

$$\tau_2/k_2 = U_D/b^3 - (kT/b^3)\log(f Nagbzv A/\dot{\epsilon}). \qquad . \; . \; . \quad (20)$$

This relation differs basically from that for jogs in screws in that the activation volume (b^3) is much smaller and independent of prestrain. Any hardening in the high temperature region must involve a decrease of the stress concentration factor, e.g. due to shortening of the pile-up length, since the log term cannot be expected to vary over wide limits.

From (18) and (20) we obtain

$$\tau_2 k_2/\tau_1 k_1 = U_D h/\alpha_1 G b^4 - (kTh/\alpha_1 G b^4) \log (f N a g b v z A/\dot{\epsilon}). \quad (21)$$

The flow stress ratio now depends on h, so that a Cottrell–Stokes law can only be obeyed if h is constant during the deformation. If $k_1 \sim k_2$, putting $\alpha_1 = [8\pi(1-\nu)]^{-1}$, the experimental values of $\alpha_1 b/h$ imply a value of $b \sim h$. This means that in (18) $\tau_1 k_1$ is of the order of the theoretical shear strength, and a more reasonable model satisfying this condition would be one in which the dislocations annihilate by forced climb (Friedel 1956), i.e.

$$\tau_1 k_1 = U_v/b^3. \quad . \quad . \quad . \quad . \quad . \quad . \quad (22)$$

Using (20) and (22) a Cottrell–Stokes Law is obtained and the temperature variation is explained satisfactorily. However, both models are rather unlikely, since the stress concentrations (k_1 and k_2) must be extremely large ($\gtrsim 100$) to explain the actual values of the stresses.

If the $k_{1,2}$'s are proportional to the stresses, relation (21) will be replaced by

$$(\tau_2/\tau_1)^2 = U_D h/\alpha_1 G b^4 - (kTh/\alpha_1 G b^4) \log (f N a g b v z A/\dot{\epsilon}) \quad (23)$$

and h would now be increased by at most a factor of 2. Nevertheless, the stress concentrations would still have to be unreasonably large to explain the observed values of τ_1.

The same objections also apply if the edge dislocations are held up by the long prismatic loops known to be produced by the deformation (for references see § 4.1).

We conclude therefore that although models can be found which explain the temperature dependence of τ satisfactorily in terms of climb of edge dislocations, those considered in this section seem rather unlikely ones. In order to compensate for the small activation volumes in these models, unreasonably large stress concentrations are required.

4.3.2. *Nabarro–Herring and related types of creep*

In the previous section it was assumed that the stress concentration is large so that $b^3 k_2 \tau_2 > kT$. For small values of k_2 this is not satisfied, so that the second term in (19) cannot be ignored. In the extreme case when $k_2 = 1$, and taking $c = c_0$, for most stresses $b^3 \tau_2 < kT$ so that

$$\dot{\epsilon} = N A g a b v z (b^3 \tau_2/kT) \exp(-U_D/kT). \quad . \quad . \quad . \quad (24)$$

This relation is of the same form as that for Nabarro–Herring creep (Nabarro 1947, Herring 1950) except that in the latter case the creep is considered to be diffusion-controlled. It is quite clear from comparing (3) with (19) and (24) that creep due to sessile jogs in screws should occur at a lower temperature than that due to climb of edges, since the activation volume is so much larger in the first case (usually 100 times or more).

It also follows, as has already been pointed out in the previous section, that assuming the accepted values for U_D climb of edges can only account for the results if k_2 is very large, i.e. of the same order as l_j/b in eqn. (3). If, on the other hand, k_2 is assumed to be small, so that (24) applies, the activation energy deduced from a plot of $\log \tau_2$ against $1/T$ is found to be much smaller than U_D. Furthermore, the experimentally observed strain rate dependence (fig. 2) cannot be explained in terms of eqn. (24). According to this law τ_2 should be proportional to strain rate; in practice fig. 2 shows clearly that a change in strain rate by a factor of 9 changes the flow stress ratio only by 10–20%. On these grounds Nabarro creep cannot explain the experimental results.

If some of the parameters multiplying τ_2 in eqn. (24) are stress dependent, the general creep equation

$$\dot{\epsilon} = \text{const.}\, \tau_2^{\,n} \exp(-U_D/kT) \quad . \quad . \quad . \quad . \quad . \quad (25)$$

is obtained, where n can take several values (Weertman 1955, Friedel 1956). To explain the small strain-rate dependence n would have to be about 10; such a power law is extremely unlikely.

We conclude therefore that Nabarro–Herring creep cannot account for the experimental results, and that explanations in terms of more complicated creep laws involving climb of edge dislocations appear to be rather improbable at the present time.

4.4. *Models Involving Pipe Diffusion*

Recently, electron microscope observations of annealing in Zn (Price 1960, Kroupa and Price 1961), MgO (Groves and Kelly, unpublished) and fatigued Cu and Ni (Segall *et al.* 1961) have shown that prismatic dislocation loops can change their shape or climb 'conservatively' (i.e. without change of area) by pipe diffusion, with an activation energy, U_P, somewhat less than that of self-diffusion, U_D. (U_P is estimated to be about 25% smaller than U_D in Cu and Ni.) However, the term outside the exponential is so small that change of shape by pipe diffusion and annealing by self-diffusion take place in the same temperature range, in Cu and Ni. Nevertheless, since $U_P < U_D$, pipe diffusion might have an effect on the temperature dependence of R. A number of models are possible; for example vacancies emitted by sessile jogs could diffuse along the dislocations; or prismatic loops may be forced to climb away by pipe diffusion in the stress field of a moving dislocation, as observed by Kroupa and Price (1961). The former process is essentially similar to that of climb by self-diffusion of sessile jogs in screw dislocations, except that the vacancies move differently. Although this pipe diffusion process may take place to some extent, it is not sufficiently distinct to be considered in detail here, and in any case it is doubtful if it is very important since measurements of activation energy of creep at high temperatures always give values of the order of U_D (see § 4.5). The process of 'conservative' climb of prismatic

loops suffers from the same disadvantage as ordinary climb of edge dislocations, in that the activation volume is very small, $\sim b^3$. Hence, unless again large stress concentrations are present, this model could not account for the results. In any case prismatic loops are not stable at the high temperatures.

4.5. *Comparison with High Temperature Creep Data*

Sherby *et al.* (1957) have measured the activation energy for creep of polycrystalline Al as a function of temperature, by measuring the change in creep rate with change in temperature, at constant stress. These data should also be interpretable in terms of the theories discussed in this paper.

Fig. 12

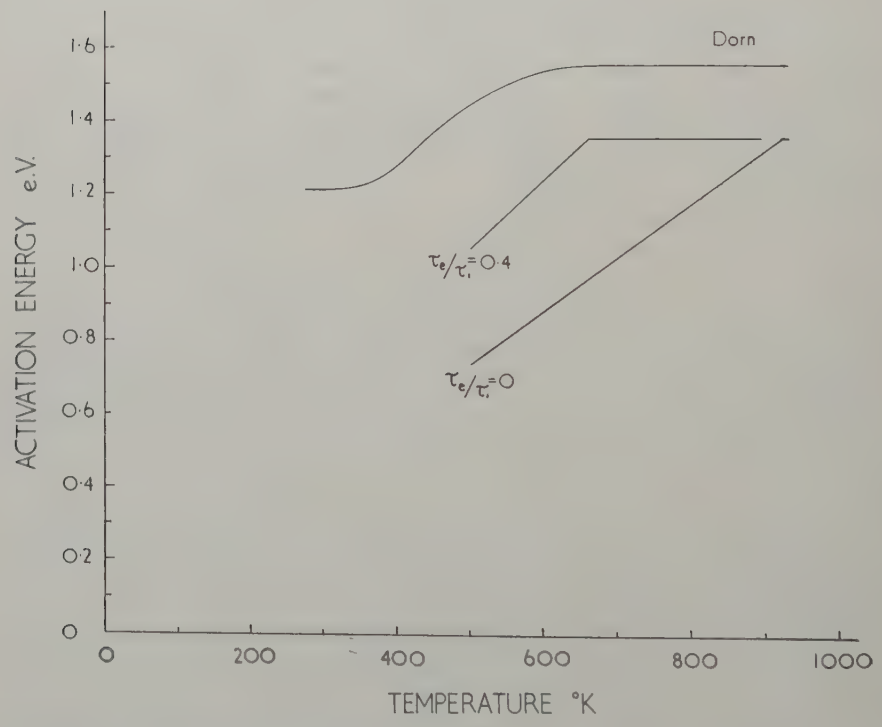

Curves of activation energy versus temperature, obtained respectively by Dorn and his colleagues from creep data (Sherby *et al.* 1957), and from the present data.

Basinski (1957) and Conrad and Wiedersich (1960) had criticized the method adopted by the above workers on the grounds that they failed to correct their results for the temperature dependence of the activation

energy H (enthalpy), the latter depending on the shear modulus. As Zener (1952) has pointed out, however, if a creep relation of the type

$$\dot{\epsilon} = A_0 \exp(s/k) \exp(-H/kT) \quad . \quad . \quad . \quad . \quad . \quad (26)$$

is assumed, where A_0 is a constant, H the enthalpy of activation and S the entropy of activation,

$$\left(\frac{\partial \log \dot{\epsilon}}{\partial T}\right)_\tau = H/kT^2 - (1/kT)(\partial H/\partial T)_\tau + (1/k)(\partial S/\partial T)_\tau$$
$$= H/kT^2, \quad (27)$$

since the other two terms cancel out. Equation (27) is that used by Sherby *et al.* (1957), and it appears that this procedure gives directly the value H at the particular mean temperature of the test. Therefore the values of H deduced by this method should be equivalent to the values of $(U_D - v\tau_2)$ derived from our data.

Our interpretation of the data of the temperature dependence of the flow stress in terms of dragging of jogs in screw dislocations predicts that $H = (U_D - v\tau_2) = kT \log(f N l_j b^2 v z A/\dot{\epsilon})$ above a critical temperature T_c, reaching a constant limiting value of U_D when $\tau_2 = 0$. Figure 12 shows the two curves of H derived from our data, one for $\tau_e/\tau_1 = 0$ and therefore $H = (U_D - v\tau_e)$, and the other for $\tau_e/\tau_1 = 0{\cdot}4$, when $H = [U_D - v(\tau - \tau_e)]$. These two curves may be compared with the experimental curves of Sherby *et al.* (1957) also shown on fig. 12. The curve for $\tau_e/\tau_1 = 0{\cdot}4$ agrees rather better with the creep data than that for $\tau_e/\tau_1 = 0$. It should also be noted that in the creep experiments the strain rates are generally $\sim 10^{-6}\,\mathrm{sec}^{-1}$ compared to $\sim 10^{-4}\,\mathrm{sec}^{-1}$ in the present experiments. Correction for strain rates would have the effect of bringing the two sets of data closer together. However, the general level of the curve derived from creep is rather higher than that deduced from our results. In particular the asymptotic value of H at high temperatures (1·55 ev) seems anomalously high for U_D for Al. The reason for this discrepancy is not understood.

The variation of H with T was interpreted by Sherby *et al.* as a transition region between two regions of constant activation energy. The essential difference in the present analysis is that it predicts a real continuous variation of H with T for a single process.

We conclude that on the whole there is reasonable qualitative agreement between the variations of H with T deduced from the two sets of data, and that best agreement is obtained on assuming a contribution to the flow stress due to elastic interaction.

§ 5. Conclusions

The experimental data presented in this paper show that a considerable part of the flow stress of Al and Cu is strongly temperature dependent at high temperatures. The results are discussed in terms of dragging sessile jogs in screw dislocations, and of climb of edge dislocations. The interpretation in terms of sessile jogs in screws seems the more plausible, and

these results are considered to provide support for the existence of such sessile jogs. This interpretation is strengthened by the fact that theoretical models of dissociated jogs in screw dislocations in face-centred cubic metals (Hirsch, unpublished) suggest that some types of vacancy jogs may indeed be sessile at the temperatures of the experiments, and that in Al the smaller vacancy jogs would be mobile along the screw dislocations, whereas in Cu they would be sessile, in agreement with experiment. The mobility of jogs along the dislocations will also give rise to a temperature-dependent contribution to the flow stress. This problem and the nature of dissociated jogs will be discussed elsewhere.

The effective vacancy jog length in the experiments is found to be rather small (2–5 Burgers vectors for Al, and 1–2 for Cu; if stress concentrations are present the jogs may perhaps be twice as long; see § 4.2.4. Elongated loops from much larger sessile jogs have been observed by transmission electron microscopy in many crystals (for references see § 4.1). Loops from such small jogs would not be directly observable, although their presence may be inferred from cusps in the dislocations. No systematic search for such cusps has yet been carried out. Non-conservative motion of single vacancy jogs at low temperatures would, of course, explain the production of vacancies during deformation (for reviews see Cottrell 1958, Broom and Ham 1958).

If the interpretation in terms of sessile jogs is accepted, jog hardening must be considered as a major contribution to work hardening.

At sufficiently low temperatures elementary, single, vacancy jogs would be sessile. A tentative theory of linear strain hardening (stage II) in face-centred cubic metals, in which linear hardening is ascribed to single vacancy jogs produced by dislocation intersection, has been proposed by Hirsch (1960) and is described by Mott (1960). Stage III hardening is considered to be at least partly due to multiple jogs. It should be noted that the present experiments on Al and Cu have been carried out at temperatures and stresses at which Al stage III conditions apply at all temperatures and for Cu stage II conditions below about 350°c and stage III conditions above this temperature.

From the experimental results obtained so far it is not possible to decide unambiguously whether elastic stresses also make an appreciable contribution to the flow stress. Experiments are now in progress to study this and other points, and the measurements are being extended to other metals.

Acknowledgments

Our thanks are due to Professor N. F. Mott, F.R.S., and Dr. W. H. Taylor for their interest and encouragement, and to Professors Mott, Friedel, Cottrell and Nabarro, Dr. Basinski and Dr. Christian, and many other colleagues for helpful discussions. One of us (D.H.W.) acknowledges financial support from the Ministry of Aviation and the Department of Scientific and Industrial Research.

APPENDIX A

Extent of Sub-grain Boundary Migration

99·99% Al specimens were deformed 30% at $0{\cdot}8 \times 10^{-4}$/sec at 350°C and 510°C. They were cooled, electropolished until clear of surface markings and pulled a further 3% at the respective temperatures when the sub-grain boundaries were made visible by their migration traces on the surface.

If t = sub-grain size, α = the average boundary angle and d the average distance migrated by each sub-boundary in a direction to give a positive specimen elongation, the average tensile deformation of the specimen is $3\alpha d/2t$.

The measured value of d/t for both specimens was $\sim 0{\cdot}08 \pm 0{\cdot}01$. The results of recent microbeam experiments indicate that the average sub-boundary angle for both these specimens is $\sim 1°$. Hence it is clear that extension due to sub-boundary migration at the two temperatures is about the same, and equal to only $100/3(3\alpha d/2t) \sim 6\%$ of the total extension of the specimen. It should be emphasized that x-ray microbeam studies of individual sub-boundary angles show that these are small, and do not support McLean's (1952) much larger estimates using an optical method.

APPENDIX B

Effect of Supersaturation of Vacancies

For a strain rate $\dot{\epsilon}$ the rate of production of vacancies from vacancy jogs (in terms of number per atom) is given by

$$\dot{n} = p\dot{\epsilon}\Omega/l_j b^2 \qquad . \; . \; . \; . \; . \; (28)$$

where Ω is the atomic volume. It will be assumed now that the rate of production of vacancies is uniform and that the vacancies diffuse to sub-grain boundaries. Assuming also spherical symmetry, it is easy to show that the concentration of vacancies at a distance r from the centre of a sub-grain is given by

$$c = c^* + \dot{n}/6D(R^2 - r^2) \qquad . \; . \; . \; . \; . \; . \; (29)$$

where c^* is the concentration of vacancies at the sinks, D the diffusion coefficient and R the radius of sub-grain. Also

$$D = (b^2 z \nu A_m/6) \exp(-U_m/kT) \qquad . \; . \; . \; . \; . \; (30)$$

where U_m is the activation energy for movement of a vacancy and $A_m = \exp(S_m/k)$, where S_m is the entropy of activation for movement of a vacancy.

Now in the steady state the rate at which vacancies are absorbed by sinks must be equal to the rate at which vacancies are emitted by the sources. Hence

$$\dot{n} = c^* N^* \Omega \nu z A_m \exp(-U_m/kT) \qquad . \; . \; . \; . \; (31)$$

where N^* is the concentration of sinks per unit volume.

Equation (29) then becomes

$$c=(\dot{n}b^2/6D)[1/N^*\Omega+(R^2-r^2)/b^2]. \quad . \quad . \quad . \quad . \quad (32)$$

The maximum vacancy concentration is given by

$$c_{\max}=(\dot{n}b^2/6D)[1/N^*\Omega+(R/b)^2]. \quad . \quad . \quad . \quad . \quad (33)$$

Now the equilibrium concentration is given by

$$c_0=A_{\mathrm{f}}\exp(-U_{\mathrm{f}}/kT) \quad . \quad . \quad . \quad . \quad . \quad (34)$$

where U_{f} is the energy of formation of a vacancy, and $A_{\mathrm{f}}=\exp(S_{\mathrm{f}}/k)$, where S_{f} is the entropy of formation of a vacancy.

Hence the maximum supersaturation is given by

$$c_{\max}/c_0=\{\dot{n}/[zvA\exp(-U_{\mathrm{D}}/kT)]\}[1/(N^*\Omega)+(R/b)^2] \quad (35)$$

where $A=A_{\mathrm{m}}A_{\mathrm{f}}=\exp(S/k)$, where $S=$entropy of activation for diffusion.

There are now several cases to be considered:

(*a*) Suppose the strain rate is emission controlled. Then the chemical term is small compared with the first term in eqn. (3), and hence

$$\dot{n}=N\Omega vzA\exp[-(U_{\mathrm{D}}-v\tau_2)/kT]. \quad . \quad . \quad . \quad . \quad (36)$$

The condition for emission control is from (3)

$$(c_{\max}/c_0)\exp(-v\tau_2/kT)<1 \quad . \quad . \quad . \quad . \quad . \quad . \quad (37)$$

and therefore from (35) and (36)

$$[N/N^*+N\Omega(R/b)^2]<1. \quad . \quad . \quad . \quad . \quad . \quad . \quad (38)$$

It follows that

$$N/N^*<1 \quad . \quad . \quad . \quad . \quad . \quad . \quad . \quad . \quad (39)$$

and

$$N\Omega(R/b)^2<1. \quad . \quad . \quad . \quad . \quad . \quad . \quad . \quad (40)$$

If these conditions are satisfied the strain rate is emission controlled and given by the expression

$$\dot{\epsilon}=Nl_{\mathrm{j}}b^2vzA\exp[-(U_{\mathrm{D}}-v\tau_2)/kT] \quad . \quad . \quad . \quad (41)$$

and τ_2 is given by

$$\tau_2=U_{\mathrm{D}}/v-(kT/v)\log(Nl_{\mathrm{j}}b^2vzA/\dot{\epsilon}). \quad . \quad . \quad . \quad . \quad (42)$$

(*b*) Suppose now that the strain rate is diffusion controlled. In that case

$$[N/N^*+N\Omega(R/b)^2]\geqslant 1 \quad . \quad . \quad . \quad . \quad . \quad . \quad (43)$$

and

$$c_{\max}/c_0=\exp(v\tau_2/kT). \quad . \quad . \quad . \quad . \quad . \quad (44)$$

Using (35) and (44) we obtain

$$\dot{n}=zvA[1/N^*\Omega+(R/b)^2]^{-1}\exp[-(U_{\mathrm{D}}-v\tau_2)/kT] \quad . \quad . \quad (45)$$

and therefore from (28)

$$\dot{\epsilon}=Nl_{\mathrm{j}}b^2vzAp^{-1}[N/N^*+N\Omega(R/b)^2]^{-1}\exp[-(U_{\mathrm{D}}-v\tau_2)/kT]. \quad (46)$$

It is clear that the form of the expression for the strain rate is similar to that in eqn. (41), but that the factor outside the exponential is smaller in eqn. (46). The flow stress under diffusion-controlled conditions is

$$\tau_2 = U_D/v - (kT/v)\log\left(\frac{Nl_j b^2 vzA}{p[N/N^* + N\Omega(R/b)^2]\dot{\epsilon}}\right) \quad . \quad . \quad (47)$$

the log term being smaller in this case.

The conditions for emission or diffusion controlled climb are given by (38), (39), (40) and (41). In general it is likely that $N < N^*$, since not only interstitial jogs in screws but jogs in edge dislocations can act as sinks. The controlling condition is therefore likely to be (40). Unfortunately the parameter N is not sufficiently well known to determine whether (40) will be satisfied or not. In both cases, however, the expressions for the flow stress are similar. We shall use therefore the expression

$$\tau_2 = U_D/v - (kT/v)\log(fNl_j b^2 vzA/\dot{\epsilon}) \quad . \quad . \quad . \quad (48)$$

where $f = 1$ in the emission controlled case, and $f = p^{-1}[N/N^* + N\Omega(R/b)^2]^{-1}$ in the diffusion controlled case. This is the equation already quoted in § 4.2.

References

Adams, M. A., and Cottrell, A. H., 1955, *Phil. Mag.*, **46,** 1187.

Bailey, J., and Hirsch, P. B., 1960, *Phil. Mag.*, **5,** 485.

Ball, C. J., 1957, *Phil. Mag.*, **2,** 1011; 1959, *J. Iron St. Inst.*, **191,** 232.

Basinski, Z. S., 1957, *Acta Met.*, **5,** 684; 1959, *Phil. Mag.*, **4,** 393.

Bradshaw, F. J., and Pearson, S., *Phil. Mag.*, **8,** 570.

Broom, T., and Ham, R. K., 1958, *Symposium on Vacancies and Other Point Defects in Metals and Alloys* (London: Institute of Metals), p. 41.

Carrington, W., Hale, K. F., and McLean, D., 1960, *Proc. roy. Soc.* A, **259,** 203.

Conrad, H., and Wiedersich, H., 1960, *Acta Met.*, **8,** 128.

Cottrell, A. H., 1958, *Symposium on Vacancies and Other Point Defects in Metals and Alloys* (London: Institute of Metals), p. 1.

Cottrell, A. H., and Stokes, R. J., 1955, *Proc. roy. Soc.* A, **233,** 17.

De Sorbo, W., and Turnbull, D., 1959, *Acta Met.*, **7,** 83.

Diehl, J., 1956, *Z. Metallk.*, **47,** 331.

Eshelby, J. D., Frank, F. C., and Nabarro, F. R. N., 1951, *Phil. Mag.*, **42,** 351.

Federighi, J., 1959, *Phil. Mag.*, **4,** 502.

Friedel, J., 1955, *Phil. Mag.*, **46,** 1169; 1956, *Les Dislocations* (Paris: Gauthier-Villars).

Fourie, J. T., and Wilsdorf, H. G. F., 1960, *J. appl. Phys.*, **31,** 2219.

Gay, P., Hirsch, P. B., and Kelly, A., 1954, *Acta cryst., Camb.*, **7,** 41.

Haasen, P., 1958, *Phil. Mag.*, **3,** 304.

Herring, C., 1950, *J. appl. Phys.*, **21,** 437.

Hirsch, P. B., 1958, *Report on Symposium on Internal Stresses and Fatigue in Metals* (Detroit: General Motors); 1960, Crystallographic Congress Cambridge Symposium.

Howie, A., 1960, *Ph. D. Thesis*, Cambridge University.

Koster, W., 1948, *Z. Metallk.*, **39,** 1.

Kroupa, F., and Price, P. B., 1961, *Phil. Mag.*, **6,** 243.
Kuper, A., Letaw, H., Slifkin, L., Sonder, E., and Tomizuka, C. T., 1954, *Phys. Rev.*, **96,** 1224.
McClean, D., 1952, *J. Inst., Met,* **81,** 287.
Mott, N. F., 1952, *Phil. Mag.*, **43,** 1151; 1953, *Ibid.*, **44,** 741; 1960, *Trans. Amer. Inst. min. (metall.) Engrs.*, **218,** 962.
Nabarro, F. R. N., 1947, *Report Conf. Strength of Solids* (London: Physical Society), p. 47.
Price, P. B., 1960, *Phil. Mag.*, **5,** 873.
Rebstock, H., 1957, *Z. Metallk.*, **48,** 206.
Saada, G., 1960 a, *Acta Met.*, **8,** 200; 1960 b, *Ibid.*, **8,** 841.
Seeger, A., 1955, *Phil. Mag.*, **46,** 1194.
Seeger, A., Berner, R., and Wolf, H., 1959, *Z. Phys.*, **155,** 247.
Seeger, A., Diehl, J., Mader, S., and Rebstock, H., 1957, *Phil. Mag.*, **2,** 1.
Segall, R. L., 1960, Ph.D. Thesis, Cambridge University.
Segall, R. L., Partridge, P. G., and Hirsch, P. B., 1961, *Phil. Mag.* (in the press).
Sherby, O. D., Lytton, J. L., and Dorn, J. E., 1957, *Acta Met.*, **5,** 219.
Silcox, J., and Whelan, M. J., 1960, *Phil. Mag.*, **5,** 1.
Simmons, R. O., and Balluffi, R. W., 1960, *Phys. Rev.*, **117,** 52.
Thompson, N., 1953, *Proc. Phys. Soc. Lond.*, B, **66,** 481.
Thornton, P. R., 1958, Ph.D. Thesis, University of Cambridge.
Thornton, P. R., and Hirsch, P. B., 1958, *Phil. Mag.*, **3,** 738.
Van Bueren, H. G., 1957, *Acta Met.*, **3,** 519.
Warrington, D. H., 1960, Proceedings of European Conference on Electron Microscopy, Delft, 1960.
Warrington, D. H., 1961, Ph.D. Thesis, University of Cambridge.
Washburn, J., Groves, G. N., Kelly, A., and Williamson, G. K., 1960, *Phil. Mag.*, **5,** 991.
Weertman, J., 1955, *J. appl. Phys.*, **26,** 1213.
Zener, C., 1952, *Imperfections in Nearly Perfect Crystals* (Pocono Manor Symposium 1950) (London: Chapman and Hall), p. 289.

The Face-centred Cubic Solid Solutions in Transition Metal Alloys of the First Long Period†

By W. Hume-Rothery
Department of Metallurgy, University of Oxford

[Received December 13, 1960]

Abstract

The limits of composition of the face-centred cubic solid solutions in binary alloys of the elements V, Cr, Fe, Co and Ni are discussed. The term group number (G.N.) is used to denote the position of the transition metal in the First Long Period (i.e. G.N.=4 for Ti). It is shown that if the binary equilibrium diagrams are drawn in terms of the average G.N. values of the alloy, and if manganese is omitted as an abnormal element, the face-centred cubic solid solutions are stable from G.N. 10 (pure Ni) to a value of about 7·7, in cases where the size-factors are favourable. The limits of the face-centred cubic solid solution occurs at an approximately constant G.N. value, in very much the same way that the limits of the α-solid solutions in copper and silver alloys occur at an approximately constant electron : atom ratio. It is also shown that, when plotted in terms of average G.N. value, the liquidus and solidus curves for the γ-phases in the systems Fe–Co and Fe–Ni are almost superposed, this behaviour being analogous to that shown by the α-liquidus and solidus curves in the systems Cu–Zn and Cu–Ga.

§ 1. Introduction

Copper, in Group IB of the Periodic Table, crystallizes in the face-centred cubic structure. When alloyed with the succeeding elements, Zn, Ga, Ge and As, primary or α solid solutions are formed in copper whose extent diminishes with the valency of the solute. In these alloys, the size-factor is favourable. The electrochemical factor is small in the systems Cu–Zn and Cu–Ga, but is appreciable in the system Cu–As where the liquidus curve shows a pronounced maximum in the region of 26 atomic % As ('Cu_3As' phase). The system Cu–Ge is a borderline case in which the electrochemical factor is beginning to exert its influence, as is shown by the presence of a slight maximum in the liquidus curve at the composition 23·5 atomic % Ge (ϵ_1 phase).

It is well known that in the systems Cu–Zn, Cu–Ga and Cu–Ge the maximum solubility limit of the α-solid solution occurs at an electron concentration of approximately 1·4; the exact values are Cu–Zn, 1·38; Cu–Ga, 1·40; Cu–Ge, 1·36. Where the α-solid solution is in equilibrium with a random body-centred cubic β-phase (Cu–Zn and Cu–Ga) the $\alpha/\alpha+\beta$ solid solubility curves are approximately superposed if the equilibrium diagrams are drawn in terms of electron concentration. To a higher degree of accuracy the Cu–Ga curve $\alpha/\alpha+\beta$ solid solubility curve lies at slightly higher electron concentrations than that for Cu–Zn,

† Communicated by the Author.

in agreement with the fact that *for a given electron concentration*, the lattice distortion is greater for the system Cu–Zn. In a recent paper Hume-Rothery and Burns (1957) have shown how the liquidus curves of the above alloys may be interpreted in terms of an electron concentration principle modified by lattice distortions and electrochemical factors, the lattice distortion again being compared at equal electron concentrations.

On proceeding backwards in the Periodic Table from Fe←Co←Ni←Cu, the face-centred cubic structure persists as the only allotropic modification of nickel. In cobalt, the face-centred cubic structure is stable from 400°c. to the melting point. In iron the face-centred cubic structure becomes relatively less stable and exists only between 910°c and 1370°c, with the body-centred cubic structure stable at both low and high temperatures. In spite of extremely favourable size-factors, and of the absence of intermediate phases, no wide solid solutions exist in the systems Cu–Co and Cu–Fe. In these systems the maximum solubilities of cobalt and iron in solid copper are about 4·5 atomic %, whilst about 12 atomic % of copper dissolves in α(face-centred cubic) cobalt, as compared with only 8 atomic % of copper in iron. It is well known that the temperatures of the b.c.c.⇌f.c.c. transformations in iron are greatly affected by the presence of other metals in solid solution.

It appears, therefore, that on passing backwards in the Periodic Table from Fe←Co←Ni←Cu, the face-centred cubic structure is becoming increasingly less stable, and would be expected to disappear between iron and manganese. Actually, a face-centred modification of manganese (γ-Mn) exists over a very small temperature range (1295°–1325°c), but the alloy chemistry of this phase is abnormal, and it does not seem to continue the sequence of the elements from iron to copper. It is the object of the present paper to show that, *if manganese is omitted as an abnormal element*, and if attention is confined to systems where the size-factor is favourable, the face-centred cubic solid solutions of the transition elements of the First Long Period show Group Number relations very much like those of the solid solutions of Zn, Ga and Ge in copper.

§ 2. The Face-centred Cubic Phases

The equilibrium diagrams of the systems Ni–Co, Ni–Fe and Ni–V are known accurately for the f.c.c. regions. In the system Ni–Cr the limit of the f.c.c. solid solution is well established, but the liquidus and solidus curves are less certain. In the system Co–Fe, the diagram is well established. For the systems Co–Cr and Co–V the liquidus and solid solubility curves for the f.c.c. solid solutions have been determined approximately, but the solidus curves have only been estimated†.

† In the textbook by Hansen (1958), the Co–Cr and Co–V solidus curves are shown by dotted lines. For the system Co–V, Hansen gives liquidus and solidus curves joining up to a melting point of 1445° for pure cobalt, instead of to the accepted value of 1495°c. This is based on the work of Köster and Schmid (1955), and correspondence with Professor Köster has shown that the diagram was incorrectly reproduced. The figure in the present paper gives the correct values.

In the systems Ni–Co, Ni–Fe and Co–Fe the face-centred cubic structure exists for the whole of the way across the equilibrium diagram. If we use the abbreviation G.N. for Group Number, we may say that in these systems the face-centred cubic structures persist over the G.N. ranges 10 to 9, 10 to 8 and 9 to 8 respectively. The G.N. value is of course equal to the total mean number of electrons per atom outside the argon shell, but it seems better to speak of a G.N. value, because the relations which follow may be interpreted in several ways.

Fig. 1

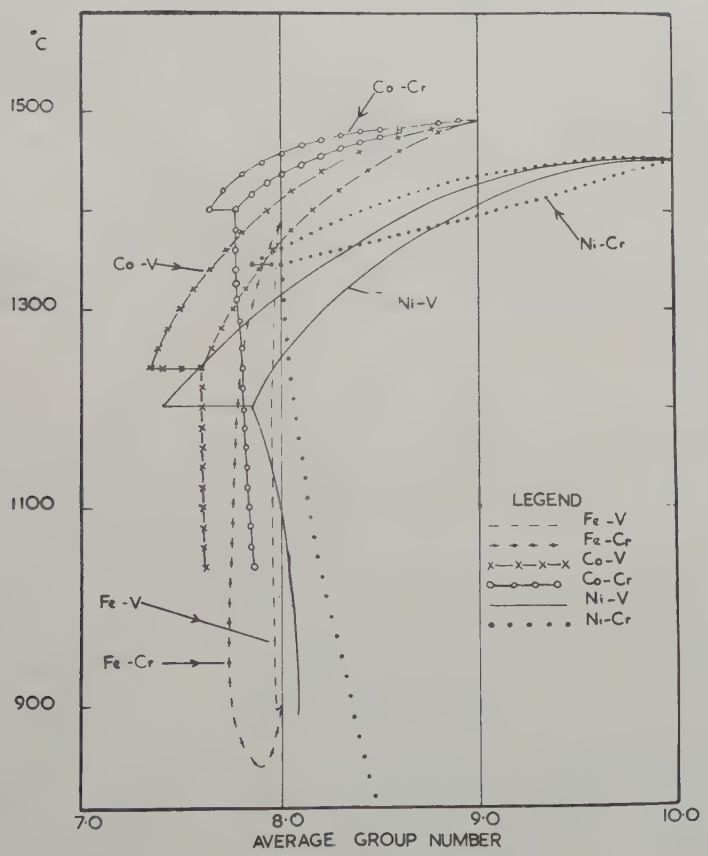

Figure 1 shows the limits of the face-centred cubic phases in the systems Ni–V, Ni–Cr, Co–V, Co–Cr, Fe–V and Fe–Cr, plotted in terms of the mean G.N. values of the alloys, in place of the usual atomic percentages. This method of plotting means that in alloys of nickel, the curves start from G.N. 10·0 (pure Ni) and that 1 atom of Co is equivalent to $\frac{1}{2}$ atoms of Fe, $\frac{1}{4}$ atoms of Cr, and $\frac{1}{5}$ atoms of V. For the cobalt alloys, the curves

start from G.N. 9·0 (pure Co) and 1 atom of Fe is equivalent to $\frac{1}{3}$ atoms of Cr, and $\frac{1}{4}$ atoms of V.

In the systems Ni–Co, Ni–Fe and Co–Fe there are continuous ranges of face-centred cubic solid solutions, and for clarity in drawing these are not shown in fig. 1.

In the systems Ni–V, Ni–Cr, Co–V, Co–Cr, Fe–V and Fe–Cr the face-centred cubic solid solutions extend backwards from the values 10, 9 and 8 for Ni, Co and Fe, to 7·85, 8·0, 7·6, 7·76, 7·95 and 7·74 respectively. The approximate constancy of these values is almost as great as that of the electron : atom ratios for the limits of the α-solid solutions in copper and silver alloys, and is even more remarkable when it is remembered that nickel and vanadium differ by five places in the Periodic Table, whereas the relations for copper and silver alloys extend only over a difference of three places†. The results suggest clearly that this kind of face-centred cubic phase cannot exist with a mean G.N. less than about 7·7. In the above systems the size-factors are favourable, but in the alloys of titanium with iron, cobalt and nickel the size-factor is on the borderline of the favourable zone (if the latter is taken to be limited by a difference of 15% between the atomic diameter of solvent and solute) and the solid solutions in the face-centred cubic metals are more restricted than would be expected from fig. 1. As with the α solid solution in copper and silver, the G.N. relations hold only when the size-factors are favourable.

§ 3. Liquidus and Solidus Relations

For the equilibrium between the liquid and f.c.c. phases (γ-phases) in iron alloys, accurate data are available for iron-rich Fe–Ni and Fe–Co alloys. Figure 2 shows the liquidus and solidus points for these systems plotted in terms of average G.N. values. The ends of the horizontal line at 1512°C show the compositions of the liquid and γ-phases at the (Liq. $+\gamma \rightleftharpoons \delta$) peritectic in the system Fe–Ni . The points marked ⊹ indicate the liquidus and solidus points determined by Hellawell and Hume-Rothery (1957), whilst the ○ points are the liquidus values‡ of Hanson and Freeman (1923) who did not determine the solidus curve. The points marked ● indicate the liquidus and solidus determinations of Harris and Hume-Rothery (1953) for the system Fe–Co, and the ends of the horizontal line at 1499°C give the compositions of the liquid and γ-phases at the peritectic horizontal.

Figure 2 shows clearly that the Fe–Co and Fe–Ni liquidus and solidus curves are very nearly superposed when drawn in terms of average G.N. The freezing range is greater for Fe–Ni alloys than for Fe–Co alloys of the

† In the systems Cu–As and Ag–Sb the limit of the α solid solutions is at an electron concentration of 1·28 instead of the value 1·4 required by a constant electron : atom ratio.

‡ The liquidus points of Hanson and Freeman have been raised by 3°C because their iron melted at 1530°C as compared with the value 1533°C for the purer iron used by Hume-Rothery and his co-workers.

same G.N. value, and these relations are like those found for the Cu–Zn, Cu–Ga and Ag–Cd, Ag–In liquidus and solidus curves discussed by Hume-Rothery and Burns (1957). Unfortunately lattice spacing measurements are not available for these dilute γ-solid solutions, and the effect of lattice distortion cannot be discussed.

For the Co–Cr and Co–V alloys the liquidus and solidus curves are not yet known with sufficient accuracy to justify detailed comparison. It is almost certain that the Co–V liquidus curve in fig. 1 falls more steeply than the Co–Cr curve. This is what would be expected from lattice distortion effects. A pure G.N. effect would mean that three atoms of vanadium were equivalent to four of chromium. Although lattice spacing measurements are not available, the atomic diameters make it very probable that three atoms of vanadium produce a greater lattice expansion of cobalt than four of chromium.

Fig. 2

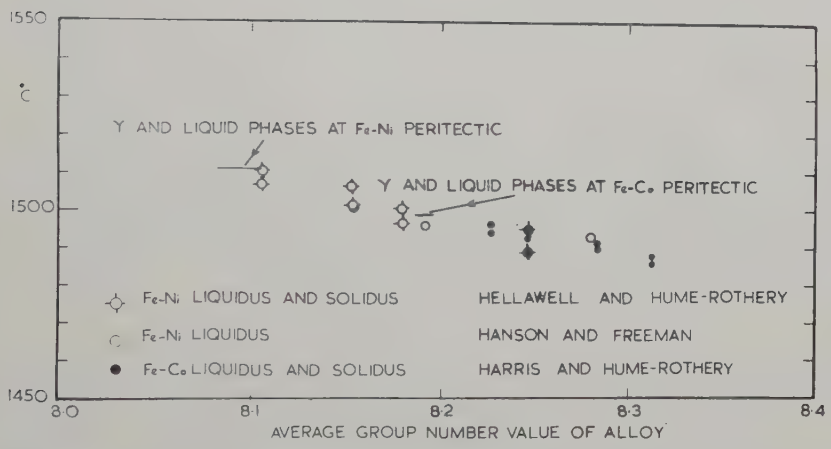

When plotted in terms of G.N. values, the cobalt-rich Co–Fe liquidus curve† is nearly the same as that for Co–Cr, but it is not possible to predict whether three atoms of iron would produce a greater or smaller lattice distortion than one atom of chromium.

For the nickel-rich alloys the freezing range of the Ni–Cr alloys shown in fig. 1 is almost certainly too great, and a redetermination is necessary. When plotted in terms of G.N. values, the Ni–V liquidus curve is lower than that for Ni–Cr. This is what would be expected from lattice distortion effects, since four atoms of vanadium produce a greater lattice expansion than five of chromium. In the system Ni–Fe, the liquidus curve passes through a minimum. In the nickel-rich alloys the Ni–Fe liquidus in terms of G.N. values falls more steeply than that for Ni–V, in agreement with what would be expected for lattice distortion effects, since five atoms of iron expand the lattice of nickel more than two atoms of vanadium.

† The solidus curve has not yet been determined.

§ 4. Conclusion

The above facts indicate that the composition limits of the face-centred cubic phases concerned are controlled by relations closely resembling those for the α-solid solutions of copper and silver alloys. They suggest an interpretation in terms of the total number of electrons per atom outside the argon shell, but they could also be interpreted in terms of any scheme in which a constant number of electrons per atom occupied atomic orbitals.

In view of the acute controversy regarding the numbers of 'free electrons', 'bonding electrons', and 'conduction electrons' in the transition elements of the First Long Period, it seems best to present the above relations as an empirical principle underlying the constitution of the alloys concerned, and to leave a theoretical interpretation until later.

Acknowledgment

The author must express his thanks to Dr. S. L. Altmann for much valuable discussion on this matter.

References

Hansen, M., 1958, *Constitution of Binary Alloys* (New York: McGraw-Hill).
Hanson, D., and Freeman, J. R., 1923, *J. Iron St. Inst.*, **107,** 301.
Harris, G. B., and Hume-Rothery, W., 1953, *J. Iron St. Inst.*, **174,** 212.
Hellawell, A., and Hume-Rothery, W., 1957, *Phil. Trans.*, **249,** 417.
Hume-Rothery, W., and Burns, J., 1957, *Phil. Mag.*, **2,** 1177.
Köster, W., and Schmid, H., 1955, *Z. Metallkde.*, **46,** 195.

Heat Conduction by Liquid Helium II in Capilliary Tubes I: Transition to Supercritical Conduction†

By D. F. Brewer and D. O. Edwards‡
The Clarendon Laboratory, Oxford

[Received December 13, 1960]

Abstract

Measurements have been made of the heat conduction by liquid helium II in capillary tubes of diameter 52·0 microns, 107·6 microns and 366 microns. The results on subcritical flow have been described previously, and the present paper is concerned with observations in the transition region to supercritical conduction. Outstanding features of the transition are (i) spontaneous fluctuations in the thermal resistance; (ii) very large hysteresis effects in the resistance at low temperatures in the wide tubes, which decrease as the lambda point is approached, and which depend on the previous history of the helium; and (iii) sensitivity of the thermal resistance to mechanical shock or vibration, including permanent changes from one branch of the hysteresis loop to the other.

The observations, which include measurements of the critical velocity as a function of tube size and temperature, are discussed in terms of the vortex line theory of Feynman and its development by Vinen, which are found to give good agreement with the experiments.

§ 1. Introduction

In a previous paper (Brewer and Edwards 1959, referred to here as B & E) we have described accurate determinations of the normal viscosity of liquid helium II by measurement of its subcritical heat conduction in glass capillary tubes of 52·0 microns and 107·6 microns bore. It was shown that at low heat current densities, the thermal resistance is limited only by the normal component viscosity, and can be described by a simple linear equation of the two-fluid model (see also Keller and Hammel 1960). At certain critical heat currents, which depend on temperature, tube size and liquid density, the thermal resistance rises sharply above the subcritical value and becomes strongly current-dependent, as mentioned briefly in B & E. The present paper gives details of our measurements of critical velocities and of other phenomena associated with the transition to supercritical flow, and in a later paper we shall analyse the thermal resistance data obtained in the stable supercritical region. Preliminary reports of part of this work have already been published (Brewer *et al.* 1956, Brewer and Edwards 1958).

† Communicated by the Authors.

‡ Present address: Department of Physics, Ohio State University, Columbus, Ohio.

§ 2. Experimental

All the apparatus is identical with that used in B & E except that in addition to the tubes of 52·0 micron and 107·6 micron bore used there, we have made measurements on a 366 micron diameter tube of similar length (about 10 cm) and a 107·6 micron diameter tube of much shorter length (about 1 cm). We summarize in the table the geometrical constants of the four tubes.

Geometrical constants of the capillary tubes

Capillary	Poiseuille constant (c.g.s. units)	Length (cm)	Average diameter (mm)
1	$1{\cdot}57\times10^{-12}$	10·2	0·0520
2	$3{\cdot}23\times10^{-11}$	10·2	0·1076
2a†	$2{\cdot}89\times10^{-11}$	—	—
3	$3{\cdot}60\times10^{-10}$	0·92	0·1076
4	$4{\cdot}88\times10^{-9}$	9·1	0·3656

† Capillary 2a is capillary 2 with the ends obstructed by short lengths of thin tungsten wire (see text).

Essentially, the experiments consist in measurement of the temperature difference ΔT across the glass capillary tubes as a function of heat flow, the temperature at one end being kept accurately constant (within less than 2×10^{-5} °K during a single experiment). Hence the average thermal resistance, $\Delta T/W$, is calculated, where W is the heat current. Complete details of the apparatus, auxiliary equipment, and measurement of the tube sizes, are given in B & E. The measurements have been carried out between 1·2°K and the lambda point at the saturated vapour pressure, with a few experiments at higher pressures.

§ 3. Results

3.1. *Instability in the Thermal Resistance*

Two graphs of the thermal resistance $\Delta T/W$ against total heat flow W for the 52·0 micron capillary (No. 1) are shown in fig. 1 (*a*) and (*b*) for two different temperatures. For small heat currents the thermal resistance remains constant or decreases slightly, as explained in detail in B & E. At a well-defined heat current the resistance increases rapidly, and there is a fairly narrow transition to supercritical behaviour, shown in fig. 1 (*a*) and (*b*) as the regions between the two broken lines. For supercritical currents the resistance appears to have two additive components, the viscous contribution, and another which depends on the current. The second contribution extrapolates back to zero at zero heat current, as was discussed by Brewer *et al.* (1956), and by Mendelssohn (1958 a, b) who suggested that the sharp transition shown in the graphs indicates the existence of two distinct states of flow.

Fig. 1

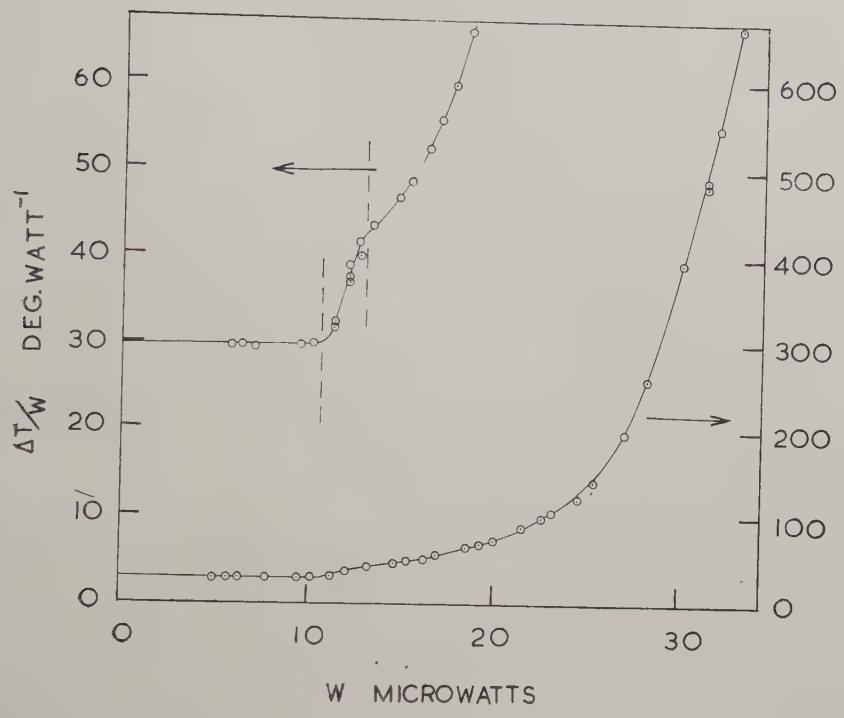

(*a*)

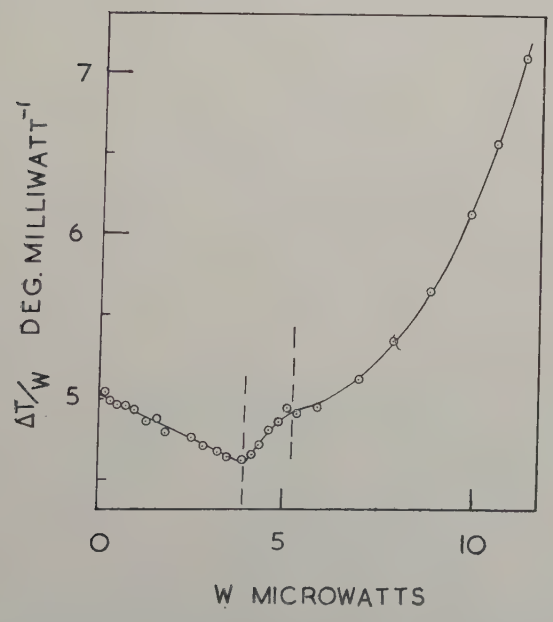

(*b*)

Average thermal resistance $\Delta T/W$ as a function of heat current W for capillary 1 (52 micron diameter). (*a*) $T = 1{\cdot}963°\text{K}$, showing $\Delta T/W$ over a wide range, and also details of the transition region. (*b*) A low temperature graph at $T = 1{\cdot}304°\text{K}$. The transition region for this capillary tube lies between the two broken lines.

Experiments carried out in the transition region show some interesting features which cannot be represented on the graph. Spontaneous fluctuations in the resistance occurred around the mean values shown, decaying with a time constant of a few seconds, and sometimes the resistance increased or decreased by a small amount and remained constant at its new value for 10 or 20 sec. The amplitude of the fluctuations was occasionally comparable with the 'step' in the graph at the critical heat current. No fluctuations were observed in the lower part of the subcritical region or in the upper part of the supercritical region. Similar fluctuations in flow resistance were observed by Winkel, Delsing and Poll (1955). In addition, the thermal resistance in the transition region was found to be susceptible to mechanical shock and vibration, and special precautions were therefore taken to reduce the level of background vibration. All mechanical and diffusion pumps in the room were turned off, and the helium vessel was braced against the vacuum jacket and hydrogen dewar by plastic spacers to make the cryostat more rigid.

A mechanical shock applied to the cryostat increased the apparent thermal resistance in the transition region for a short time. The additional resistance decayed with a period of several seconds, although this time may well be determined by the damping of some solid part of the apparatus. Continuous vibration increased the resistance permanently and in a rather irregular way. To produce an appreciable change, the amount of vibration had to be quite large, and we can therefore assume that the spontaneous fluctuations were not due to the vibration normally present. Moreover the resistance–current curves for a particular tube at a given temperature were found to be reproducible from day to day. Mechanical disturbance had little effect except near the transitional region.

3.2. *Hysteresis*

The existence of two states of flow in helium II is confirmed in a striking way by observations on the wider tubes (capillaries 2, 3 and 4). Figure 2 shows two graphs of thermal resistance versus heat flow which are typical of the results at low temperatures in these tubes. Here the heat flow can be increased to very large values without the appearance of any current-dependent resistance (lower set of points). When at length friction does occur it is extremely large, and the heat current may be reduced step by step to produce the upper curve of a broad hysteresis loop. Thus either of two distinct states of flow may be found at a given heat current density. At low temperatures, the thermal resistance in the entire lower branch is, to a good approximation, due only to the normal component viscosity, and the flow is determined by the linear equations of the two-fluid model. In this paper we shall refer to this as the *linear* state, although at higher temperatures, as we shall show later, some additional friction may be found. The upper branch, where strongly non-linear friction terms appear, will be referred to as the supercritical or current-dependent state.

The additional current-dependent resistance in the supercritical state does not spontaneously disappear until the heat current is reduced to only

Fig. 2

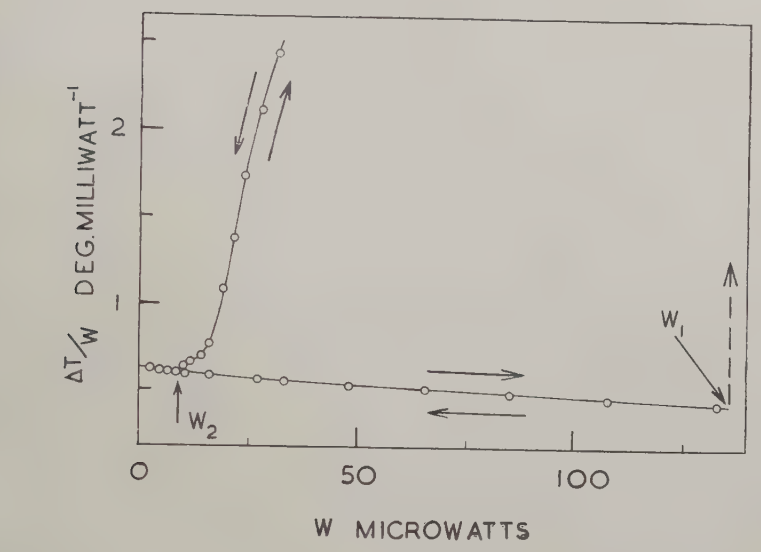

(*a*)

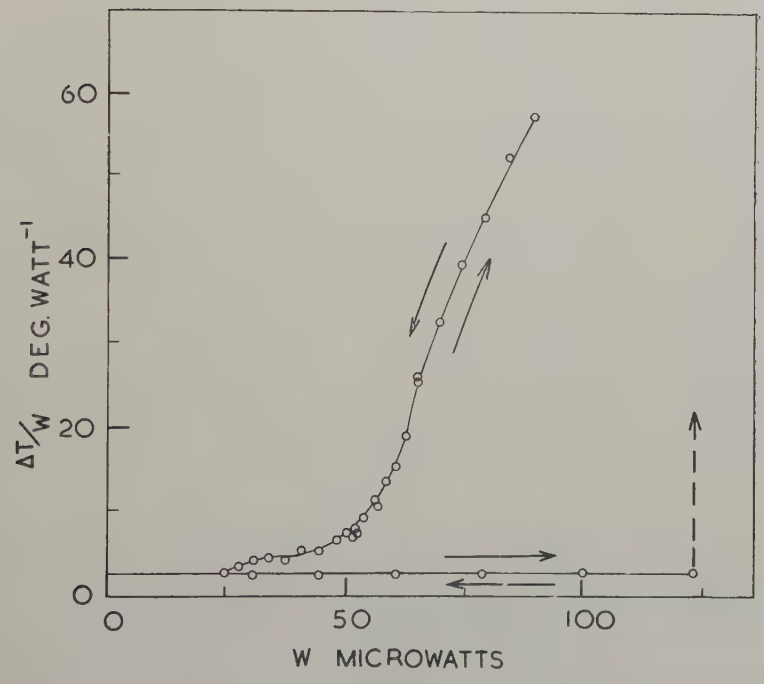

(*b*)

Average thermal resistance $\Delta T/W$ as a function of heat current W showing broad hysteresis loops for the 107·6 micron tubes. (*a*) $T=1{\cdot}212°$K, long tube (capillary 2). (*b*) $T=1{\cdot}563°$K, short tube (capillary 3).

a fraction of the value which first produces friction. If we call these two heat currents W_1 and W_2 respectively (see fig. 2 (*a*)), it is found that the value of W_1 (the heat current at which friction first appears) very much depends on the previous history of the helium. It has its maximum value if the helium has been left undisturbed for a considerable time (half an hour or more) before switching on the heat current. On the other hand, if the helium is in a supercritical state and the heat current is switched off for a few seconds only, the subsequent value of W_1 will be very small, perhaps only slightly larger than W_2.

Helium in the linear state but carrying a heat current near the maximum value of W_1 is extremely sensitive to mechanical shock and vibration. For a sufficiently large current, a very light tap on the cryostat will change the flow rapidly to the stable supercritical state. At smaller currents tapping may produce only a temporary rise in the thermal resistance, which then falls back to the linear value in a time of 1 sec or more, depending on how much the resistance increased. At the smallest currents, well below W_2, light tapping produces no change at all of the thermal resistance. The supercritical state at *large* currents is also insensitive to shock, but at currents just above W_2, tapping brings about a temporary *decrease* in the thermal resistance, and sometimes a permanent transition to the linear state. In the supercritical state close to W_2 we again observed spontaneous fluctuations in the thermal resistance.

The value of W_2 seemed reproducible to within 10 or 20%, although its determination was complicated by the spontaneous fluctuations and the difficulty of measuring the small temperature differences with sufficient accuracy to distinguish between linear and supercritical states. Measurements of W_2 are dealt with in the next section, where we discuss the critical velocities.

The size of the hysteresis loops, that is the ratio W_1/W_2, became in general smaller as the temperature increased. For example, hysteresis in capillary 2, which was very large at low temperatures, had completely disappeared at 1·806°K, as shown in fig. 3 (*a*). Capillaries 3 and 4 showed a similar, but smaller, temperature dependence, and small hysteresis loops could still be seen at 2°K or higher (see, for example, fig. 3 (*b*)). The variation with diameter was irregular, hysteresis being in general larger in the 107·6 micron tubes and smaller in the other two.

3.3. *Critical Velocities*

For the narrowest tube (52·0 microns) at temperatures not too close to the lambda point, it is possible to define one critical heat current for the appearance or disappearance of friction. Typical graphs of thermal resistance versus heat current have been shown in fig. 1 for this tube. The thermal resistance was found to be reproducible and not to show any hysteresis effects, so that there was always a single, well-defined transition curve. We may, therefore, define the critical heat current as that at the

Fig. 3

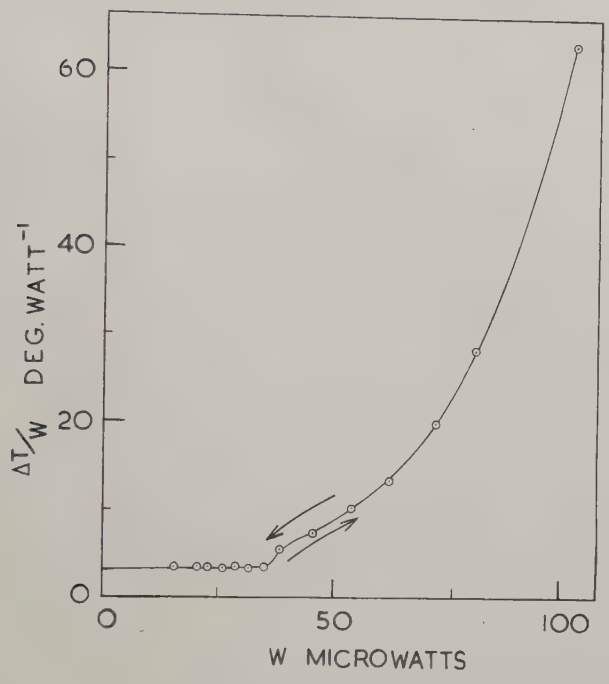

(*a*)

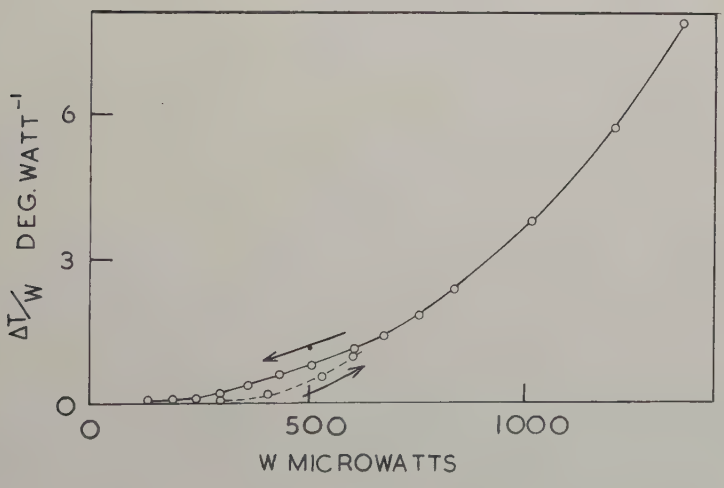

(*b*)

Average thermal resistance $\Delta T/W$ as a function of heat current W. (*a*) Capillary 2 (107·6 micron diameter, 10 cm long), showing no hysteresis at 1·806°K. (*b*) Capillary 4 (366 micron diameter, 10 cm long) showing hysteresis loops still remaining at 1·99°K.

centre of the transition from linear to supercritical resistance. From the critical heat current one may calculate the critical superfluid velocity v_s^{crit} from the equation

$$v_s^{\text{crit}} = \frac{x W_{\text{crit}}}{(1-x)\rho S T \pi a^2} \qquad \ldots\ldots (1)$$

where x and ρ are the normal fluid fraction and the total densities respectively, S is the entropy per gram at temperature T, and a is the radius of the tube. The value of v_s^{crit} therefore represents the critical velocity of the superfluid averaged over the cross section of the tube. It has been shown by Winkel, van Groenou and Gorter (1955) that it is this *superfluid* velocity with respect to the channel wall, rather than the relative velocity of superfluid and normal fluid, which determines the point of onset of friction, at least in the narrow channels. We therefore restrict our discussion of critical velocities to v_s^{crit} as defined by eqn. (1).

In fig. 4 we plot critical superfluid velocities for the 52·0 micron tube (full circles) as a function of temperature. At higher temperatures the measured temperature differences are very small, and the percentage error in the thermal resistance correspondingly greater. The form and position of the transition were thus well defined, and the errors in the critical velocities (shown in fig. 4 by vertical lines through the points) are larger.

Fig. 4

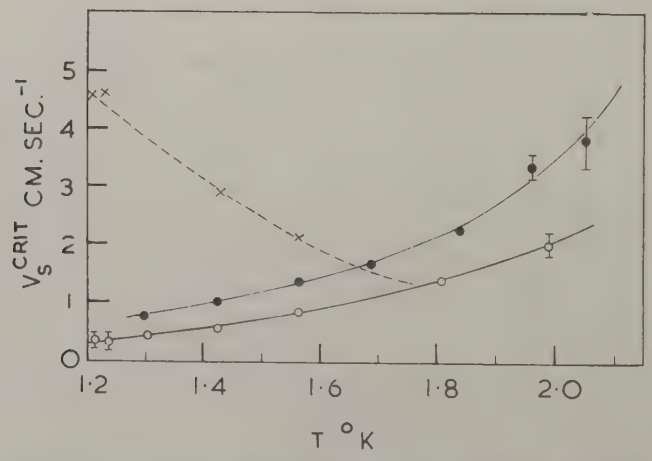

Critical superfluid velocities in capillaries 1 (52·0 micron diameter, shown by symbols ●) and 2 (107·6 micron diameter, shown by symbols ○) as a function of temperature calculated from W_2. Crosses show critical velocities calculated from W_1 (see text) for capillary 2.

For the wider tubes the critical velocity is not so unambiguously defined, because of the occurrence of hysteresis. As fig. 2 shows, there are two separate heat currents for transition between linear and supercritical flow. However, as we have said in the previous section, the larger heat

current (W_1) depends strongly on vibration and on the previous history of the helium, while the smaller one (W_2) was fairly reproducible. We show in fig. 4 as open circles the critical velocities for capillary 2 calculated from the smaller values of critical heat current (W_2). The temperature dependence is similar to that for capillary 1, supporting the supposition that the lower critical velocity is the significant one. For comparison, we also include as crosses in fig. 4 the critical velocities for capillary 2 calculated from the higher critical heat currents (W_1) as found starting from an initially undisturbed state of the liquid; the temperature dependence in this case is quite different from those calculated from the smaller critical heat currents with this tube, and from the unambiguously defined critical values in tube No. 1.

Fig. 5

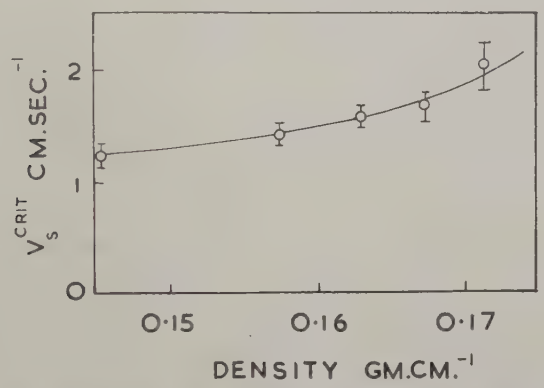

Critical superfluid velocities in capillary 1 (52·0 micron diameter) as a function of density at temperature 1·563°K.

The effect of increasing pressure on the critical velocity has been investigated only in detail in the case of the 52·0 micron tube. It was found that the transition region continued to be well defined at pressures up to the melting pressure, without any hysteresis. Critical velocities, defined in the same way as those at the vapour pressure, are shown in fig. 5 plotted as a function of density at the temperature 1·564°K. For other temperatures, the variation with density was found to be similar but has not been measured in such detail. The values of x used in these computations were calculated from second sound measurements. Qualitatively, one expects an increase of density at constant temperature to increase the number of excitations in the liquid, which would correspond to an increase of temperature at the saturated vapour pressure. Thus, by comparison with the temperature dependence shown in fig. 4 we may anticipate that the critical velocity would increase with pressure. Such an effect is indeed shown to occur in fig. 5.

The effect of the channel length on critical velocity was investigated in the two 107·6 micron tubes, which differed in length by a factor of ten

(about 1 cm and 10 cm, see table). In both of these tubes, as already mentioned, hysteresis effects occurred, so that two separate values of critical velocity could be derived. It was found that the *lower* critical velocity, calculated from W_2, which we have suggested is the more significant one, is not appreciably affected by length. The *higher* critical velocity, where friction first appears in the initially undisturbed liquid, seemed to be somewhat larger with the shorter tube.

§ 4. Discussion

4.1. *Hysteresis and Friction in the Linear Region*

The features of the transition that we have observed are analogous to those in the transition from laminar to turbulent flow in ordinary liquids. For a viscous liquid flowing in a pipe, turbulence occurs at a certain critical velocity which is determined by the shape and size of the pipe and the density and viscosity of the liquid. As the flow rate is increased to the critical value, fluctuations are observed in the pressure head as eddies are formed near the outlet of the pipe. If the velocity is increased above the critical value the pressure head rises rapidly and irregularly with increasing flow velocity.

When turbulence is fully developed, the pressure difference necessary to maintain the flow is steady. If the flow rate is reduced from a high value, i.e. a turbulent state, the velocity at which the eddies die out is lower than the one at which they were first produced when the flow was increased. This lower critical velocity is more reproducible than the higher critical velocity, which is very sensitive to any disturbance. In the range between the two critical velocities, the liquid, if in streamline flow, is in an essentially unstable state and mechanical shock may cause it to break into turbulent motion.

This description of the appearance of turbulence in an ordinary liquid is so close to our observations of the onset of friction that it provides evidence of some form of turbulence in helium II. An obvious explanation would be that the laminar flow of the normal component becomes turbulent at the critical velocity, but calculation of the corresponding Reynolds numbers shows these are much too low. Moreover a fixed critical Reynolds number for the normal component would lead to quite wrong temperature dependence for the critical value of the normal component velocity. The turbulence is therefore connected with the motion of the superfluid, and the experiments give further support to the vortex line theory proposed by Feynman (1955, see also Onsager 1949) who predicted the occurrence of just such effects as we have observed near the critical velocity. According to Feynman, supercritical friction in helium II arises from the creation of vortex lines of quantized circulation in the superfluid, and the critical flow velocity is that at which the kinetic energy of the liquid is just sufficient to create a vortex line. Near the critical velocity, vortex lines

or rings may be created and decay in an irregular manner, producing the spontaneous fluctuations of the thermal resistance.

Extensions of the vortex line theory have been made by Hall and Vinen (1957) and by Vinen (1957 a, b). The latter has made extensive experiments on heat conduction in tubes much larger than ours and he has developed a theory which explains his observations rather well. The theory indicates that, in a heat conduction experiment which involves counterflow of normal fluid and superfluid, the principal contribution to the current-dependent resistance is due to collisions between vortex lines and normal fluid excitations. Detailed comparison between the theory and our values of stable supercritical friction will be made in a later paper. The theory also leads to a critical velocity, and to hysteresis effects which increase with decreasing temperature and decreasing size of the flow channel. Qualitatively, the observed variation in size of the hysteresis loops with temperature in tubes 2, 3 and 4 is therefore in agreement with the theory (see for example, figs. 2 (*a*) and 3 (*a*)). The variation with tube diameter is not, apparently, in agreement since we find the largest hysteresis loops with the 107·6 micron tube, smaller loops with the 366 micron tube, and no hysteresis in the 52·0 micron tube. However, it is difficult to assess with any accuracy the way in which the hysteresis effects differ in various tubes, since they probably depend to a large extent on the mounting of the tube, on the surface roughness, and on the shape of the exit and entrance.

The effect of the exit and entrance was investigated in some experiments with capillary 2 obstructed at both ends with short pieces of 70 micron diameter tungsten wire. The values of the thermal resistance in both the linear and supercritical regions were not greatly changed except that the hysteresis loops were very much reduced in size, and were detectable only at the lowest temperatures. Earlier experiments on a 10 cm long, 52·0 micron diameter tube (not included in the table) had already suggested that obstructions might strongly influence the results. A graph of the thermal resistance versus heat current for this capillary at 1·563°K is given in fig. 6. It showed not only an appreciable hysteresis which was absent in capillary 1 (whose nominal diameter was the same) but also a large amount of friction in the 'linear' region. This tube was subsequently found to be partly blocked with dirt at a point about 3 cm from one end, and the normal component viscosity determined from the intercept on the $\Delta T/W$ axis (see B & E) was too large by a factor of about two.

The existence of frictional forces additional to the normal viscosity in the linear region was also predicted by Vinen. The magnitude of the theoretical effect increases with temperature and tube diameter, but a calculation from Vinen's theory shows that it would be of the same order as our experimental error, and could probably not be detected. We *do* however observe appreciable friction in the lower branches of the hysteresis loops at higher temperatures with the short 107·6 micron tube and with the 366 micron tube. An example of this has been given in fig. 3 (*b*). Both in

this tube (No. 4) and in the short tube, the observed friction greatly exceeds theoretical expectation. For example in fig. 3 (*b*), Vinen's subcritical friction would give a thermal resistance of about 0·006 deg. watt^{-1} at $W = 500\,\mu$watt, which is 50 times smaller than observed. However, it is believed that this friction in the lower branch of the hysteresis loop is not of the same nature as the theoretical effect, but is connected rather with effects at the ends of the tubes or at obstructions. We believe this

Fig. 6

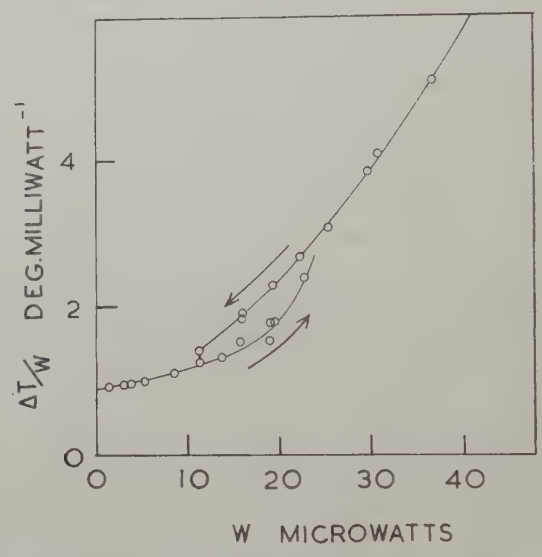

Average thermal resistance $\Delta T/W$ versus heat flow W at 1·563°K for an accidentally obstructed tube of diameter 52·0 microns.

because (*a*) the observed effect was increased when the ends of capillary 2 were obstructed with tungsten wire; (*b*) this friction was relatively larger in the short 107·6 micron tube (No. 3) than in the long 107·6 micron tube (No. 2); and (*c*) a large friction of this type was observed in the accidentally obstructed 52 micron tube, whereas it was completely absent in capillary 1. Quantitative comparison with Vinen's theory is not, in any case, valid in the linear region of flow. The theory assumes that the average spacing between vortex lines is very small compared with the channel width, whereas, as we shall show in paper II, the average spacing between lines in the linear region discussed above is of the same order as the tube diameters.

While comparing the present experiments with Vinen's work, it should be mentioned that he observed experimentally a delay time in the build-up and decay of supercritical friction. The time constant was found to be independent of tube width and given by a relation $t = kw^{-3/2}$ where w is the

heat current density and the constant k is about 4×10^{-2} sec (watt-cm^{-2})$^{3/2}$. If this equation is also valid for channel sizes as small as ours, the delay times would be less than a second for all the experiments, except for heat currents close to the critical values. Our experimental arrangement is not suitable for measurements of such short time effects which must have been completely masked by the thermal time constant of the system. For velocities close to the critical value Vinen's delay time increased rapidly, tending to infinity at the critical value. Although delays in the appearance of friction were certainly observed in our experiments, they were not reproducible and no systematic measurements could be made. As was stated before, the behaviour depended critically on the previous history of the helium and on the amount of vibration present. Variations in the delay time were also observed by Vinen but they do not appear to have been so serious. The hysteresis is definitely not a time effect, as even at very large heat currents the resistance was observed to stay in the linear region without any change for up to half an hour. If the metastable linear state was deliberately disturbed, the thermal resistance increased rapidly to the supercritical value.

Using the same experimental arrangement as ours, Mendelssohn and Steele (1959) have since continued these measurements in tubes of similar diameter but fifteen times longer, and have observed both hysteresis and time delays. The latter were shown to be due to a steady propagation of turbulence along the tube and have been further investigated by Critchlow (1960). In our experiments with tubes only 10 cm long these effects would again be difficult to separate from those due to the thermal time constant.

The large hysteresis effects described in the present paper were first observed and reported by us some time ago (Brewer and Edwards 1958) and some hysteresis was also found in a different experimental arrangement by Rorschach and Romberg (1958). We have shown that they are strongly influenced by vibration and may be inhibited by obstructions in the channel. As already mentioned, we took special precautions in the present experiments to avoid extraneous mechanical vibration, and also to ensure constancy of the bath temperature. In addition, the entrances and exits of the tubes were made as smooth and rounded as possible. However, control of all the factors affecting the appearance of hysteresis seems to be difficult, since capillary 1, in which there was no evidence of any obstruction (see B & E) showed no hysteresis, whereas a tube of the same nominal diameter which was known to be blocked, did (see fig. 6). These considerations may explain why the effects have not been generally observed before.

4.2. *Critical Velocities*

The temperature dependence of the critical superfluid velocity shown in fig. 4 may be compared with that found by Winkel, Delsing and Poll (1955) for thermomechanical flow in much narrower channels (1 to

6 microns in width). Both sets of experiments show an increase of velocity with temperature at the lower temperatures, but the maximum in the results of Winkel *et al.* must, if it occurs at all in the present experiments, be shifted much nearer the lambda point. Such a shift with increasing channel size was found by Winkel *et al.* Most of the published data are consistent if we assume that the temperature dependence of v_s^{crit} has a smooth variation with channel size, from the behaviour in the very narrow helium film where it is independent of temperature or has a very shallow maximum, to the behaviour found by Vinen in channels of a few millimetres, width, and observed in the present experiments, where it increases rapidly with temperature. There is no theoretical explanation of this temperature variation at present. An estimate of the superfluid critical velocity at the absolute zero for a long slit of width d has been made by Feynman (1955) on the basis of his theory of vortex lines, and is given by the equation

$$v_s^{\text{crit}} . d = \frac{\hbar}{m} \ln\left(\frac{d}{a_0}\right) \qquad . . . . . \quad (2)$$

where m is the mass of the ^{4}He atom, and a_0 is the core radius of a vortex line. For channels of different shapes, the quantity corresponding to d in eqn. (2) is twice the ratio of area to perimeter, which for a cylindrical capillary is the radius. The argument in the logarithm is only approximate. The result is obtained by calculating the minimum kinetic energy needed to create quantized vortices at the exit of a channel from which a uniform jet emerges, but the real situation must be very much more complicated.

In fig. 7 we give eqn. (2) in a logarithmic plot for two values of a_0, namely 4 Å and 40 Å. Our experimental results at 1·3°K are also shown, together with those of Winkel *et al.* and of Vinen at about the same temperature. The lower values shown for Vinen's velocities are those where his measured friction apparently disappears completely, a definition of v_s^{crit} which is consistent with our own. All the velocities shown are in extremely good agreement with eqn. (2), despite the fact that it is not supposed to represent a precise calculation. Vinen observed and quoted another critical velocity, shown by the higher points in fig. 7, where the supercritical friction dropped sharply from a high to a low value. We also observed such an effect, to be described in a later paper, and our measurements of it are in fairly good agreement with Vinen's experiments and with his theory. However, since friction and therefore vorticity are still present below this critical velocity it has no direct connection with the velocity discussed by Feynman, and indeed the values shown in fig. 7 do not agree so well with the equation. Although Winkel *et al.* also observed some 'subcritical friction' and applied the same criterion as Vinen, their critical velocities lie very close to Feynman's curves. All results shown in fig. 7 were obtained in experiments on thermomechanical flow. Atkins (1959) has shown that critical velocities deduced from several other types of experiments, although not so accurate, also fit in with eqn. (2) provided that the flow channel is not too small.

There are at present wide variations in the experimentally estimated values of the vortex core radius a_0. The critical velocity $v_s = 54{\cdot}1$ cm sec^{-1} for a helium II film of thickness 302 Å at 1·60°K (Jackson and Grimes 1958) would lead to a much larger value of a_0 in eqn. (2) than those used in fig. 7. A recent tentative estimate of $a_0 \approx 10^{-4}$ cm for a free vortex (Vinen 1961) is however too large to use in the equation, since it would give negative critical velocities in channels smaller than this size.

Fig. 7

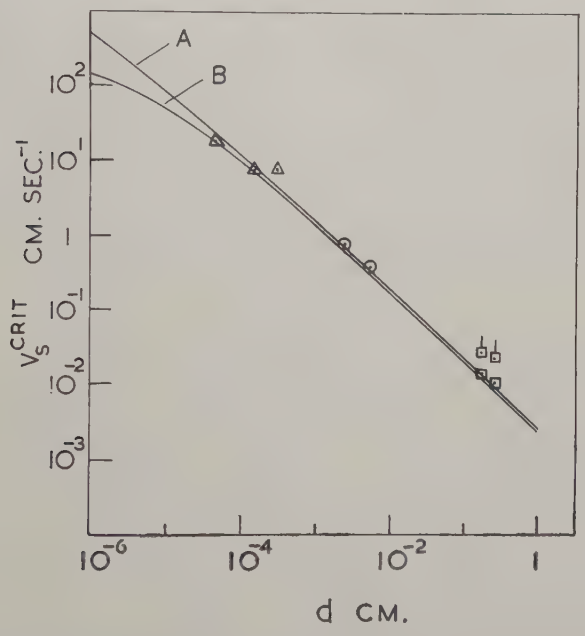

Critical superfluid velocities as a function of channel size d (see text) at about 1·3°K. ○ Present results; □ Vinen's results (1957 (*b*)); ⊡ Vinen's quoted results; △ Winkel, Delsing and Poll (1955). Curve A, eqn. (2) with $a_0 = 4$ Å; curve B, eqn. (2) with $a_0 = 40$ Å.

Acknowledgments

We wish to thank Dr. K. Mendelssohn for his interest in this work and Dr. W. F. Vinen for some useful discussions. We are grateful to the Nuffield Foundation for a Research Fellowship held by D. F. B., and Brasenose College for a Senior Hulme Scholarship held by D. O. E.

References

Atkins, K. R., 1959, *Liquid Helium* (Cambridge: University Press).

Brewer, D. F., and Edwards, D. O., 1958, *Low Temperature Physics and Chemistry* (Madison: University of Wisconsin Press), p. 12; 1959, *Proc. roy. Soc.* A, **251**, 247 (referred to in the present paper as B & E).

Brewer, D. F., Edwards, D. O., and Mendelssohn, K., 1956, *Phil. Mag.*, **1,** 1130.

Critchlow, P. R., 1960, *Thesis*, Oxford.

Feynman, R. P., 1955, *Progress in Low Temperature Physics*, Vol. 1 (Amsterdam: North-Holland Publishing Company), Chap. 2.

Hall, H. E., and Vinen, W. F., 1957, *Proc. roy. Soc.* A, **238,** 215.

Jackson, L. C., and Grimes, L. G., 1958, *Advanc. Phys.*, **7,** 435.

Keller, W. E., and Hammel, E. F., 1960, *Ann. Phys.*, **10,** 202.

Mendelssohn, K., 1958 a, *Nuovo Cim.*, Suppl., **9,** 228; 1958 b, *Z. phys. Chem.*, **16,** 332.

Mendelssohn, K., and Steele, W. A., 1959, *Proc. Phys. Soc. Lond.* A, **73,** 144.

Onsager, L., 1949, *Nuovo Cim.*, Suppl., **6,** 249.

Rorschach, H. E., and Romberg, F. A., 1958, *Low Temperature Physics and Chemistry* (Madison: University of Wisconsin Press), p. 35.

Vinen, W. F., 1957 a, *Proc. roy. Soc.* A, **242,** 493; 1957 b, *Ibid.*, **243,** 400; 1961, *Proceedings of VIIth International Conference on Low Temperature Physics* (University of Toronto Press) (to be published).

Winkel, P., Broese van Groenou, A., and Gorter, C. J., 1955, *Physica*, **21,** 345.

Winkel, P., Delsing, A. M. G., and Poll, J. D., 1955, *Physica*, **21,** 331.

Etch Figures on Alum and the Diamond Pattern†

By M. Omar and T. H. Youssef
National Research Centre, Cairo, Egpyt

[Received October 5, 1960]

Abstract

Potash alum crystals grown from solution had fine octahedron faces. They were etched by a quick dip in water. The etch figures obtained were not only similar in orientation and appearance to ' natural growth ' figures on diamond, but were identical with them in every respect.

Due attention is paid to ' growth ' hillocks on one crystal and the etch hillocks on the other crystal. Interfacial angles as well as other characterizing marks of both kinds of pits are compared. It is concluded that diamond is not characterized by a special growth pattern and that in fact all figures naturally obtained on diamond are a result of natural dissolution.

§ 1. Introduction

It is well known that diamond octahedral faces are possessed with triangular depressions of a pyramidial nature called 'trigons'. These trigons are characteristic of nearly all diamond octahedral faces.

The controversy whether these are to be attributed to growth or to etch phenomena, has been discussed by nearly all workers on diamond, see, for example, Fersmann and Goldschmidt (1911), Sutton (1928), Williams (1932), Tolansky and Wilcock (1947), Omar and Kenawi (1957), Frank *et al.* (1958). Even books on crystallography shared in the controversy, as can be checked by reviewing old and recent editions of these books. In the last few years the tide is that trigons are mostly due to the etching effect of an agent which is not oxygen (oxygen etch pits are inverted with respect to the trigons). The problem lies in the fact that if trigons are due to growth then a special theory for the growth of diamond must be made. There is no evidence that diamond should be singled out of all crystals by a special mode of growth.

The observation made by Omar and Kenawi (1957) that the oxygen etch patterns of diamond in vacuum are exactly similar (except in orientation) to the natural diamond pattern and that the natural pattern must therefore be due to an unknown etchant in the history of diamond, has been fairly established by Frank *et al.* (1958). In these two papers Frank has not only analysed the whole problem but succeeded in etching diamond in the natural orientation of trigons.

We here produce further evidence that the trigons are due to an etching mechanism. For this purpose a crystal from the cubic system that crystallizes in the octahedron form has been chosen. The crystal is

† Communicated by the Authors.

potash alum, which has been lightly etched with pure water. The results we expected occurred, i.e. the etch pattern obtained was exactly identical in every detail with the 'natural growth' pattern on diamond. Such an observation has not been analysed before, and we proceed to show that complete identity exists. In recent times alum has been etched by Bauhans (1913) and by Friedel (1924) but no such complete analysis has been made.

§ 2. Experimental Procedure

A small nucleus of potash alum crystal is suspended in a saturated hot alum solution (80°C), then the whole is left at laboratory temperature (25°C) for about 30 hours, after which a nice well-developed crystal is formed. The crystal usually has very neat octahedral surfaces without any characterizing marks. Some crystals grew at the bottom of the containing vessel; these were also examined. The crystals were then dipped in cold (laboratory temperature) distilled water for a very short time (1 to 2 sec), after which the etch figures were observed.

§ 3. Observations

Figures 1 and 2† are samples chosen from hundreds of photomicrographs taken on our many etched alum crystals. Any worker, familiar with diamond octahedral faces, will realize the complete similarity of these figures to those naturally observed on diamond. The triangles are depressions imitating the trigons on diamond. The parts marked H are areas between the 'triangles' which are actually etch hillocks, similar to the 'growth hillocks' observed on diamond. Overlapping triangles can be observed on all the photomicrographs, in conformity with the observation made by Frank *et al.* on natural diamond, an observation which they analysed and attributed to etch. The fact that the overlapping exists as a result of etching is a direct proof of Frank's view, that the natural pattern on diamond can only have been the result of surface dissolution. The orientation with respect to the crystal edge is clear from fig. 3.

Figure 4 is the natural pattern on diamond and fig. 3 (as well as figs. 1 and 2) the etched pattern of alum. The natural 'growth' hillocks on diamond have curved edges; this is clear in fig. 4. Figure 5 shows a similar curvature on the etch hillocks of alum. We call this curvature horizontal curvature, which is marked C on both photomicrographs. This has been measured carefully on both crystals and an average value for the radius of curvature of 0·5 mm seems to exist on both types of hillocks. It should be noted that the natural trigons on diamond, as well as the pits produced by etching octahedral faces of alum, have exact straight edges; the sloping walls of these triangular depressions are not however straight: they have what is called cylindrical curvature, i.e. curvature perpendicular to the layer edges. This is deduced by using interferometry: fig. 6 is an

† All figures are shown as plates.

interferogram taken for an etch pit on alum using thin film interferometric techniques (see Tolansky and Omar 1952).

On account of the small etch pits obtained and the existence of small local irregularities in the crystal surface we have not yet succeeded in obtaining interferograms by using optical flats. However, both interferograms show that the fringes are not equidistant (a sign of cylindrical curvature).

From the fringes, both crystals have an approximate radius of curvature for the sloping sides of the 'triangles' in the order of (1000–1500 μ).

The fringes also enable us to measure interfacial angles between the sloping sides of the triangles which are actually pyramidal depressions on both crystals; these angles were found to be in the order of 1·5 degrees. Another characteristic feature of the diamond trigons is an extension to the sides of some trigons called 'basal extension'. This was attributed by Tolansky and Wilcock (1947) to a growth phenomenon. In our etched alum crystals basal extension was also found and exists on some figures, as a result of dissolution. An example on etched alum is shown as CD (fig. 7).

§ 4. Conclusion

It is thus clear that every characteristic feature of the supposed diamond growth pattern has its prototype in the etched face of a similar cubic crystal; these figures are also similarly oriented. Apart from orientation, the important similar features may be summarized in the following remarks.

1. Both features are characterized by similar hillocks, of the same shape and of the same order of horizontal curvature.

2. The interfacial angles of the pyramidal depressions in both cases are of the same order.

3. Both depressions are characterized by what we call cylindrical curvature (curvature perpendicular to the sides of the depressions); this curvature, whether positive or negative, is of the same order in both patterns.

4. Both patterns of triangles have sometimes 'basal extension', i.e. extension to the sides of the triangles.

5. In the pattern of natural diamonds we sometimes see two trigons partly overlapping. This has been analysed (see Frank *et al.* 1958) to be a sign of natural dissolution; this partial overlapping also exists in our photomicrographs of the etched octahedral faces of alum. Since this had occurred as a result of surface dissolution, it may be taken as a partial confirmation to Frank's view.

6. Large triangles rarely occur in both patterns, which in our view is due to the fact that when dissolution proceeds further the whole face is wiped out completely and a new face appears with new small triangles which become larger to a certain extent, after which they are removed completely, and new triangles formed.

We conclude this article by supporting the view that trigons and other supposed growth patterns, naturally existing on diamond, are actually etch patterns, obtained as a result of natural surface dissolution in the fluid magma in which diamond existed after it had been formed in geological times.

References

Bauhans, 1913, *Verh. naturh.-med. Ver. Heidelb.*, **12,** 319.
Fersmann, A., and Goldschmidt, V., 1911, *Der Diamant* (Heidelberg: Winter).
Friedel, 1924, *C. R. Acad. Sci., Paris,* **179,** 796.
Frank, F. C., Puttick, K. E., and Wilks, E. M., 1958, *Phil. Mag.*, **3,** 1262.
Frank, F. C., and Puttick, K. E., 1958, *Phil. Mag.*, **3,** 1273.
Omar, M., and Kenawi, M., 1957, *Phil. Mag.*, **2,** 859.
Sutton, M. J. R., 1928, *Diamond* (New York: Van Nostrand).
Tolansky, S., and Wilcock, W. L., 1947, *Proc. roy. Soc.* A, **191,** 182.
Tolansky, S., and Omar, M., 1952, *Nature, Lond.*, **170,** 758.
Williams, A. F., 1932, *The Genesis of Diamond* (London: Benn).

The Ledge Theory of Recrystallization in Polycrystalline Metals

By P. W. Davies, A. P. Greenough and B. Wilshire
Metallurgy Department, University College of Swansea

[Received January 12, 1961]

Abstract

When a polycrystalline metal specimen is deformed, ledges must be produced on grain boundaries in the interior of the specimen, corresponding to slip lines on the external surface, but much less pronounced. During recrystallization, grain boundary migration occurs and a ledge would tend to straighten out so as to reduce the total energy by decreasing the area of grain boundary. If the volume swept by the migrating boundary remains stress free, and the height of the ledge is greater than a critical value dependent on the energy density in the deformed material, it is shown that the grain boundary will continue to migrate until the nucleus of a new grain capable of indefinite growth has been produced. The critical height h is given by $h=0{\cdot}1r=0{\cdot}1\ \gamma/E$, where E is the energy density of the deformed material, γ is the grain boundary energy per unit area, and r is the equilibrium radius of curvature of the grain boundary between a recrystallized grain and the deformed matrix. On this basis it is shown that when a metal is cold-worked to a given strain, the temperature at which the metal is strained could have an effect on the grain size of the recrystallized specimen.

The generally accepted theory of recrystallization is that proposed by Cahn (1950) and Cottrell (1953) who suggested that the dislocations in a cold-worked metal polygonize to form sub-grains. Certain sub-grains then grow at the expense of others, so acting as recrystallization nuclei.

The theory has been criticized (Kennedy 1955) on the ground that sub-grain growth requires the movement of low-angle boundaries and decreases in rate as these angles increase, whereas high-angle boundaries appear to be necessary for the high mobility observed in the growth process. Rutter and Aust (1960) observed that the rate of migration of a medium angle (10°) boundary in high purity lead with very small additions (less than 10^{-4} atomic %) of silver and gold was an order of magnitude slower than a random high-angle boundary under the same conditions.

Electron microscopic observations (Bollmann 1959) on the recrystallization of nickel have shown that nucleation does not take place in exactly the way predicted by Cahn. Recrystallization starts before distinct sub-grains are formed and develops independently of polygonization over a certain period, until the whole volume is consumed by the more rapidly growing crystal grains.

The marked difference in recrystallization properties of single crystals and polycrystalline materials emphasizes the importance of grain boundaries. Single crystals of aluminium deformed 99·6% by rolling did not

recrystallize after annealing for five minutes at 300°c, whilst a polycrystalline specimen given the same treatment would have recrystallized completely (Liu and Hibbard 1955). A similar effect has been observed with pure copper (Liu and Hibbard 1953).

Recovery and recrystallization have been extensively studied in cold-worked silver (Bailey and Hirsch 1960, Bailey 1960) and it has been shown that recrystallization is initiated by the migration of high-angle boundaries which were present in the metal before deformation. Bailey considers that this migration may start at an area of grain boundary across which there is a fairly large difference in dislocation density. As soon as the boundary has moved, a dislocation free region is generated on one side so that the driving force is then governed by the average value of the stored energy. No conclusive experimental evidence has been presented for the existence of such areas of high-angle grain boundary across which there is a large difference in dislocation density, and indeed it is not necessary to postulate such a difference.

In a plastically deformed metal, ledges will be formed at grain boundaries, corresponding to slip lines on the external surface. The displacement on any slip plane will be considerably reduced in the interior of a metal because of the non-conformity of the slip systems in the adjoining grains. Such ledges play an important part in some theories of creep fracture (Gifkins 1956, Chen and Machlin 1956). We suggest that recrystallization nuclei form at these ledges in the following way. At the temperature at which grain boundary migration can occur, the ledge would tend to straighten out, and so reduce the total energy by decreasing the area of grain boundary (figure (*a*) and (*b*)). Provided the internal stress in the specimen is released before this temperature is reached, and Bailey and Hirsch (1960) have shown that in silver this condition is satisfied, no dislocations will run into the volume swept by the migrating boundary. This volume will therefore have the same energy per unit volume as a completely recrystallized specimen. Assuming for the moment that AC remains straight, when the length of AC exceeds 1 μ, boundary migration can continue under the driving force provided by the energy density difference across the boundary, as shown by Bailey (1960).

The orientation of the new grain is clearly related to that of grain X in the figure. However, the region round the ledge is very likely to be a region where the lattice curvature is particularly severe after cold work, because of the non-conformity of the slip systems in the adjoining grains, so that there may well be several degrees orientation difference between the new nucleus and the centre of the grain from which it has formed. Under these circumstances, it is possible that the new nucleus would grow into the grain X, though probably at a considerably slower rate than the rate of growth into grain Y.

It can be shown that the height of a ledge which will produce a recrystallization nucleus capable of unlimited growth must exceed a critical value. In order to calculate this, we must consider a more detailed picture

of the process that produces the nucleus. The figure (*a*) shows the initial situation, assuming for simplicity that angle B is a right angle. The boundary at B starts to move into crystal Y, and as the area swept through initially takes up the orientation of the crystal X at B, no sub-boundary is at first formed.

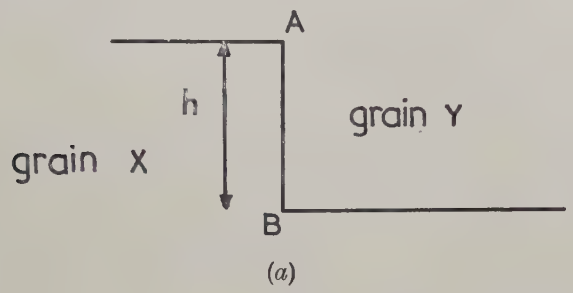

(*a*)

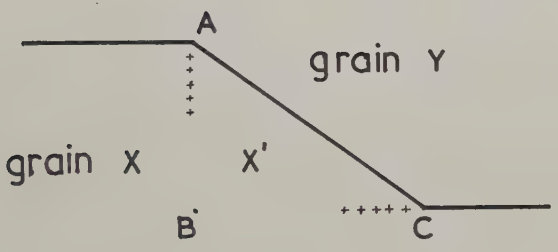

(*b*)

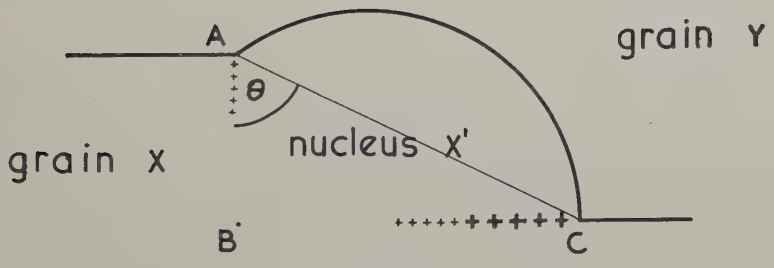

(*c*)

(*a*) AB is a slip step or ledge on the high-angle boundary between plastically deformed grains *X* and *Y*. (*b*) By migrating to AC, the total grain boundary area is reduced and the nucleus of a recrystallized grain X′ having the same orientation as grain X at the point B is formed. Near A and C very low-angle grain boundaries are produced in the plane of the original high-angle boundary. (*c*) AC bulges out with radius of curvature *r* into grain Y, because of the difference in energy density across the grain boundary. Further growth leaves behind a low-angle grain boundary along the plane BC.

Since the height of the ledge h could be several hundred angstroms, the orientation of crystal X may change slightly along BA, and a low-angle boundary may appear between the nucleus and the grain X in the region of A. This orientation difference may be $\sim 0{\cdot}1^\circ$, so that the energy required to create the low-angle boundary will be very small in comparison with the energy obtained from the decreasing area of the high-angle boundary. Similar conditions exist along BC. The nucleus can thus rapidly grow to the shape shown in the figure (*b*). The energy density difference E across the grain boundary AC will cause the boundary to bulge out into grain Y with a constant radius of curvature r, where $r = \gamma/E$. γ being the energy per unit area of the high-angle grain boundary. To produce a nucleus that can give indefinite growth, it is still necessary for the length of the straight line AC to be at least $2r$. In silver deformed 25% in tension at room temperature, on which all our numerical estimates are based, $r \sim \frac{1}{2}\mu$ (Bailey 1960). Under these conditions, the orientation of grain X will have changed appreciably from the orientation of grain X at point B. We assume that the new grain X′ retains essentially the same orientation as it has at B. Thus there is now a low-angle boundary along the plane of the former high angle boundary (figure (*c*)). In silver the misorientation is $\sim 1^\circ$ and the energy of such a boundary is about $0{\cdot}1\gamma$, where γ is the energy of a high-angle boundary (Greenough and King 1951). Further increase in the length of AC can only occur if the area of the low-angle grain boundary along BC is increased. The energy density difference E across the grain boundary AC must also provide the energy required for the increase in the total length of the high angle grain boundary as C moves away from B.

If V is the total energy required for the nucleus to grow to a given stage, then it can be shown that

$$\frac{dV}{d\theta} = \gamma h \sec^2\theta \left\{ -\left(\frac{9}{10} + \frac{h}{2r}\right) + \sqrt{\left(\sin^2\theta - \frac{h^2}{4r^2}\tan^2\theta\right)} \right\}$$

(where θ is the angle BAC (figure (*c*)).

Indefinite growth becomes possible when $AC = 2r$, i.e. when $\theta = \cos^{-1} h/2r$. In order for the nucleus to grow spontaneously to this critical size, $dV/d\theta$ must be negative for all values of θ between $\theta = 0^\circ$ and $\theta = \cos^{-1} h/2r$. It can be shown that this condition is satisfied when $h > 0{\cdot}1r$. With silver it would then be necessary that $h \gtrsim 500$ Å, and these ledges would still be too small to detect experimentally (Bailey 1960).

It is not necessary for BA to be a single slip line normal to the plane of the boundary. A group of closely spaced (~ 100 Å) slip lines would give equally effective nucleation, and if angle BAC were acute, conditions during the early stages of nucleus formation would be even more favourable than in the case we have considered. Under these circumstances, h would be the overall height of the step resolved perpendicular to the plane of the boundary.

We have further assumed in our analysis that the energy density in the cold worked metal prior to recrystallization is uniform. There may be

a high energy density in the region of the ledge which would decrease the equilibrium radius of curvature of the high-angle grain boundary and decrease the critical ledge height.

The requirements that for the production of a nucleus capable of indefinite growth, the ledge height h must exceed a critical value dependent on the energy density E of the metal before recrystallization gives a simple explanation of the decrease in grain size of a recrystallized metal as the pre-strain is increased above the critical value required to give recrystallization. Both E, and the number of ledges of a given height, are increased by increasing pre-strain.

On this basis it is considered that the temperature at which the metal is cold-worked could have an effect on the grain size of the recrystallized specimen. Cottrell (1952) shows that the spacing of slip lines visible in a polycrystalline metal is independent of temperature of deformation and depends only on the stress. For a given amount of pre-strain, the lower the temperature, the greater the stress required. Hence the lower the temperature of pre-straining the larger the number of slip-lines, and the smaller the extent of slip on each line. Thus the number of ledges of a given height should decrease as the temperature of pre-straining is reduced. However, E for a given amount of pre-strain should be increased as the temperature is lowered and the critical height of ledge will be reduced. By measuring E just before recrystallization after deformation to a given strain at different temperatures a quantitative check on the theory may be possible.

Acknowledgment

The authors are indebted to Mr. T. S. Walters for helpful mathematical discussion.

References

Bailey, J. E., 1960, *Phil. Mag.*, **5,** 833.
Bailey, J. E., and Hirsch, P. B., 1960, *Phil. Mag.*, **5,** 483.
Bollmann, W., 1959, *J. Inst. Met.*, **87,** 439.
Cahn, R. W., 1950, *Proc. phys. Soc. Lond.* A, **63,** 323.
Chen, C. W., and Machlin, E. S., 1956, *Acta Met.*, **4,** 655.
Cottrell, A. H., 1952, *Dislocations and Plastic Flow in Crystals*, p. 158; 1953, *Progress in Metal Physics*, edited by Chalmers, B., **4,** 205.
Gifkins, R. C., 1956, *Acta Met.*, **4,** 98.
Greenough, A. P., and King, R., 1951, *J. Inst. Met.*, **79,** 415.
Kennedy, A. J., 1955, *Metallurgia*, **52,** 265.
Liu, Y. C., and Hibbard, W. R. Jr., 1953, *Trans. Amer. Inst. min. (metall.) Engrs*, **197,** 672; 1955, *Ibid.*, **203,** 1249.
Rutter, J. W., and Aust, K. T., 1960, *Trans. Amer. Inst. min. (metall.) Engrs*, **218,** 682.

Soft X-ray Emission Spectrum of Niobium

By J. E. Holliday
Edgar C. Bain Laboratory for Fundamental Research, United States Steel Corporation, Research Center, Monroeville, Pennsylvania

[Received December 1, 1960; in revised form June 26, 1961]

Abstract

The soft x-ray M-emission spectrum of Nb has been measured. The $M_{IV,V}Y_{II}$ peak has been found to be the $M_{IV,V}$ emission band and the $M_{IV,V}Y_{I}$ peak is a satellite of the $M_{IV,V}$ $N_{II,III}$ emission line. The emission spectrum indicates that Nb is similar to vanadium in that the 4d electrons are not localized and are in the conduction band. In addition, the soft x-ray spectrum indicates that some of the electrons in the band have p character.

There is an increasing amount of interest in the second series transition metals, and more experimental data are becoming available on the electronic structure of these metals. Except for Siegbahn and Magnusson's (1934) and Kiessig's (1935) works, however, there has been very little done on the soft x-ray emission spectrum of these metals. It is believed that a great amount of valuable information can be obtained from a study of their soft x-ray emission spectra. Lomer and Marshall (1958) have concluded from neutron diffraction data (Shull and Wilkinson 1953) that the 3d electrons in vanadium are not localized but are in the conduction band. Coles (1958) has shown by electrical resistivity measurements that the second series transition metals have an electronic structure similar to that of the first series. It is the purpose of the present investigation to determine if soft x-rays can give any information regarding the 4d electrons in Nb.

The measurements were carried out on a grazing incidence spectrometer (Holliday 1960) using a flow proportional counter as an x-ray detector. The grating with 600 lines/mm was used at a glancing angle of 2°. The current to the target was 1 ma with a potential of 4000 v. The Nb sample was cleaned by ion bombardment, and the system was pumped to 5×10^{-8} mm of Hg before the spectrum was recorded. In order to improve the signal to noise ratio, a cascade circuit (Wilson 1950) has been added inside the spectrometer chamber next to the counter. The improvement can be seen in the results for the $M_{IV,V}N_{II,III}$ emission line shown in fig. 1. The peak to background is about 50/1 compared to 4/1 that was obtained before the circuit was added. The spectrum of Nb in fig. 1 is a ratemeter trace and no correction has been made. The other emission line indicated in fig. 1 is the $M_{III}M_{IV,V}$ transition which occurs at 78·2 Å. The $M_{IV,V}Y_{I}$ and $M_{IV,V}Y_{II}$ peaks indicated in fig. 1 were first labelled by Siegbahn and Magnusson. They called Y_{I} and Y_{II} unknown external energy levels.

The emission edge of the $M_{IV,V}Y_{II}$ transition occurs at 206 ev and corresponds in energy to (Valence → 3d) transition. In addition, preliminary measurements of the $M_{IV,V}Y_{II}$ emission edges for Zr, Mo and Ru are in very close agreement with the ionization energy of the $M_{IV,V}$ level given by Sandstrom's (1957) table of energy levels. On this basis the $M_{IV,V}Y_{II}$ transition should be called the $M_{IV,V}$ emission band. The $M_{IV,V}Y_{I}$ peak does not correspond to any known transition and is too widely separated from the $M_{IV,V}$ emission band to be a part of the band. This is well

Fig. 1

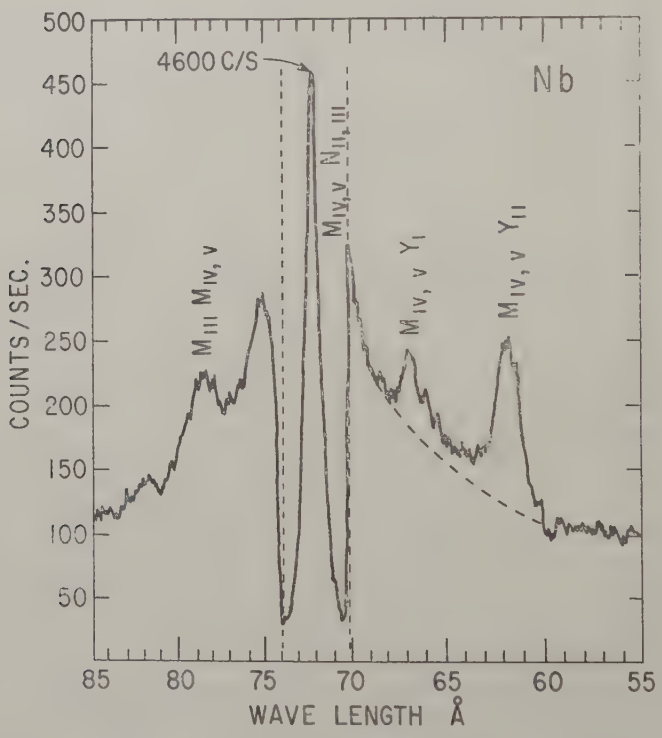

The M emission spectra of Nb showing the M_{III} $M_{IV,V}$ and $M_{IV,V}$ $N_{II,III}$ emission lines, and the $M_{IV,V}Y_{I}$ and $M_{IV,V}Y_{II}$ peaks. The beam current was 1 mA with a potential of 4000 v. The scale between the dotted lines has been increased by a factor of 10.

illustrated for the case of Ru, where the emission edge of the $M_{IV,V}$ emission band and the $M_{IV,V}Y_{I}$ peaks are separated by 31 ev. The separation between $M_{IV,V}Y_{I}$ peak and the $M_{IV,V}N_{II,III}$ peak in going from Zr to Ru was found to increase about 1 ev when the atomic number was increased by one. In addition, there is a sharp intensity drop in going from Nb to Mo in the $M_{IV,V}Y_{I}$ peak. The above experimental results are characteristic of a satellite and it would appear safe to label the $M_{IV,V}Y_{I}$ peak a satellite of the intense $M_{IV,V}N_{II,III}$ line.

In fig. 2 is shown a point by point plot of the $M_{IV,V}$ emission band of Nb and the Mζ satellite corrected for the tail of the $M_{IV,V}N_{II,III}$ emission line. A total of 2000 counts were taken on each point giving a standard deviation of 2·2%. It will be noted from fig. 2 that the $M_{IV,V}$ emission band is strongly asymmetric. An exact determination of the energy width of the band will have to wait till further instrument corrections are made and the M_{IV} and M_V peaks are separated.

The emission peak for the (4d → 3p) transition should occur at approximately 33 Å. Our investigation of this region of the spectrum gave no indication of any transition. It is important to note that Kiessig did not find this transition for pure Nb either.

Fig. 2

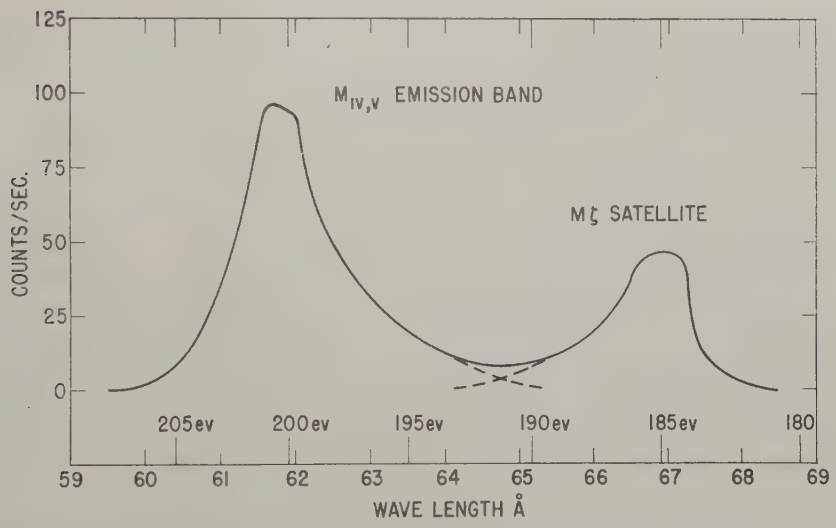

The $M_{IV,V}$ emission band and the Mζ($M_{IV,V}N_{II,III}$) satellite of Nb corrected for the tail of the Mζ emission line. The $M_{IV,V}$ emission edge occurs at approximately 206 ev.

In order to determine the status of the 4d electrons from the above experimental results, it is necessary to determine whether the $M_{IV,V}$ emission band is dipole or quadrupole transition and to determine the significance of the absence of the (4d → 3p) transition. It is possible that the absence of this transition is due to the Auger process. However, the (4d → 3p) transition has been detected by Kiessig for niobium carbide which makes the above explanation unlikely. Another explanation for this anomaly is that there are no localized 4d electrons for pure Nb. By dipole selection rules, the $M_{IV,V}$ emission band is a (conduction p → 3d) transition. If the $M_{IV,V}$ emission band was quadrupole, the transition would be (4d → 3d). Since dipole transitions are much more intense than quadrupole, it is unlikely that we would observe the quadrupole transition (4d → 3d), and not see the dipole transition (4d → 3p). The results are in

favour of the dipole transition (conduction p → 3d). There has been some question as to the validity of applying selection rules to transitions from electrons in the band. However, the justification for this has been given by Tomboulian (1957). Thus, the above experimental results indicate that Nb is similar to vanadium in that the 4d electrons are not localized and are in the conduction band. In addition, the soft x-ray spectrum indicates that some of the electrons in the band have p character.

It is planned to do more work on the second series transition metals, especially with alloys. In addition, the necessary corrections will be made to the spectra in order to obtain an accurate picture of the shape and width of the band. With these corrections, a close correlation to the density of states curve should be obtained.

Acknowledgment

Thanks are due to E. L. Jossem of Ohio State University and S. Arajs of this Laboratory for their helpful comments concerning this work and to W. A. Hester for technical assistance.

References

Coles, B. R., 1958, *Advanc. Phys.*, **7,** 40.
Holliday, J. E., 1960, *Rev. sci. Instrum.*, **31,** 891.
Kiessig, H., 1935, *Z. Phys.*, **95,** 555.
Lomer, W. M., and Marshall, W., 1958, *Phil. Mag.*, **3,** 184.
Sandstrom, A. E., 1957, *Handb. Phys.*, **30,** 226.
Shull, C. G., and Wilkinson, M. K., 1953, *Rev. mod. Phys.*, **25,** 100.
Siegbahn, M., and Magnusson, T., 1934, *Z. Phys.*, **88,** 559.
Tomboulian, D. H., 1957, *Handb. Phys.*, **30,** 261.
Wilson, R., 1950, *Phil. Mag.*, **41,** 66.

CORRESPONDENCE

Observations on the Oxygen Solubility and Magnetic Susceptibility of Body-centred Cubic Transition Metal Alloys

By R. T. Bryant and E. W. Evans
Research Department, Imperial Chemical Industries Ltd.,
Kynoch Works, Witton, Birmingham 6

[Received January 10, 1961]

The solubility of oxygen in body-centred cubic alloys of niobium, with molybdenum, rhenium and ruthenium, has been measured, these alloying elements being members of Groups VIA, VIIA and VIIIA respectively. In each of these three alloy systems, increasing the electron to atom ratio decreases the oxygen solubility, effectively zero solubility being reached with additions to niobium of about 75 at. % molybdenum, 35 at. % rhenium, and 25 at. % ruthenium. In these alloys, therefore, assuming the values 5, 6, 7, 8 for the electron to atom ratios for niobium, molybdenum, rhenium and ruthenium respectively, the point of zero oxygen solubility is reached at an electron to atom ratio of between 5·70 and 5·75.

The striking similarity between the behaviour of hydrogen (Jones *et al.* 1961) and that of oxygen in these alloys indicates that oxygen is probably behaving as an electron donor in solution. The existence of zero solubility at an electron to atom ratio of about 5·75 is evidence for the filling of a sub-band at this electron concentration, the higher sub-band being unable to accept electrons from oxygen atoms.

Electronic changes occurring as electrons are added to the niobium structure have also been observed by measuring the magnetic susceptibility of niobium–molybdenum alloys at 20°C for a range of compositions between niobium and molybdenum. These observations indicate that the susceptibility decreases rapidly as the molybdenum content is increased from zero to about 60 at. % and that there is a minimum in the susceptibility/composition curve beyond this concentration of molybdenum. There remains some uncertainty regarding the position and form of this minimum and there is some evidence for a low maximum at 75% molybdenum with two shallow minima at 60 and 90 at. % molybdenum. A sharp minimum observed in the susceptibility values at about 10 at. % molybdenum has not yet been confirmed.

Reference

Jones, D. W., Pessall, N., and McQuillan, A. D., 1961, *Phil Mag.*, **6**, 455.

Stored Energy and Electrical Resistivity in Deformed Metals

By L. M. Clarebrough, M. E. Hargreaves and M. H. Loretto
Division of Tribophysics, C.S.I.R.O., University of Melbourne, Australia

[Received November 14, 1960]

The purpose of this note is to present results on the energy stored in deformed aluminium and the change in electrical resistivity that occurs on annealing. The results are compared with those obtained previously for copper (Clarebrough *et al.* 1957), nickel (Clarebrough *et al.* 1960) and α brass (Clarebrough *et al.* 1960).

Super-purity aluminium (99·991% Al) was used. Ingots approximately 10 cm × 5 cm × 5 cm were cast from smaller ingots supplied by the Aluminium Company of America, deformed 25% in cubic compression and annealed for 1 h at 400°C. The grain size after this treatment was approximately 1 mm. The ingots were deformed 75% in compression and then specimens for the measurement of stored energy, electrical resistivity and hardness were machined from them. The measurements of stored energy were made in the same manner described previously (Clarebrough *et al.* 1952) and the measurements of electrical resistivity were made with a Kelvin double bridge using specimens 9 cm × 0·67 cm × 0·34 cm.

The results of the energy, resistivity and hardness measurements are shown in the figure. The total energy stored is 3·2 cal/g atom. This result is the mean of four measurements, the maximum deviation being 10%. This reproducibility is less than that obtained previously for other metals as the calorimetric method used is less accurate for metals of low density and high specific heat. The ΔP curve shows two stages, a plateau region between 100° and 250°C and a peak between 250° and 360°C. Small decreases in electrical resistivity and hardness occur up to 250°C and these properties then decrease to the values for fully annealed material by 360°C.

Metallographic examination shows that recrystallization does not commence until 250°C and is complete by 360°C. Furthermore, in agreement with the results of Perryman (1954) and Åström (1955), clearly marked sub-grains develop in the range of temperature 100°–250°C. Thus the marked plateau in the ΔP curve can be attributed to recovery involving the rearrangement and annihilation of dislocations.

The value of the total energy stored is less than that reported by Åström for aluminium of similar composition. Although Åström's measurements were made with a calorimeter of the Borelius type (Borelius and Berglund 1951), the difference in techniques is probably not the cause of the difference

in the results since Gordon, using the same type of calorimeter as Åström, obtained excellent agreement with our measurements on copper (Gordon 1955, Clarebrough *et al.* 1960). It is more likely that the main contributory factor to the difference in values for the stored energy is a difference in grain size. Although the grain size of Åström's specimens is not reported it appears from his micrographs that the grain size of our specimens is approximately an order of magnitude larger than his.

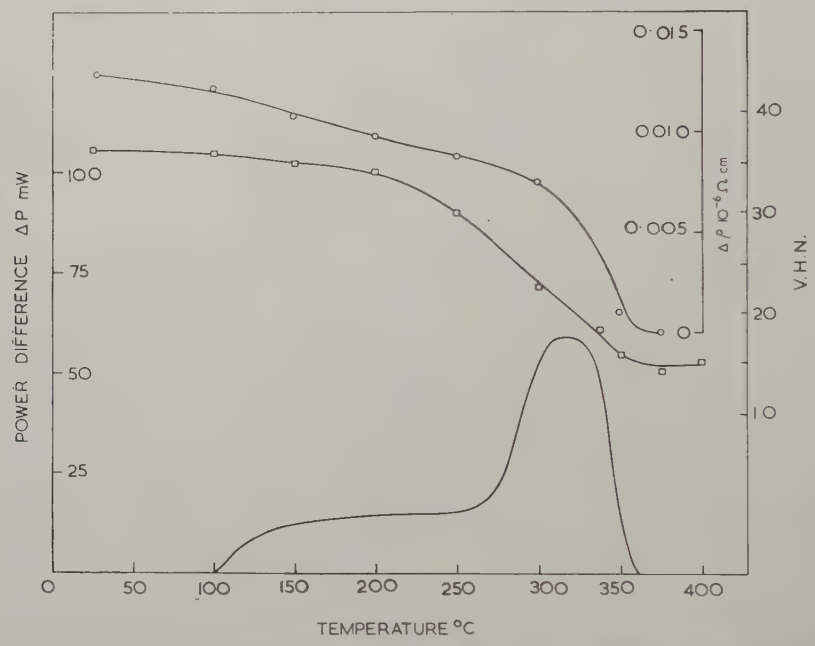

Curves for the power difference, ΔP, as a function of temperature and of the increment in resistivity, $\Delta\rho$, and hardness, V.H.N. after annealing to various temperatures, for specimens of aluminium deformed 75% in compression. The curve for power difference was obtained at a heating rate of 6°C/min and the same rate of heating was used in the annealing treatments.

In the table the values of stored energy and changes in electrical resistivity associated with the annealing of aluminium, copper, nickel and α brass are given. Values for the resistivity of a dislocation (calculated from the energy and resistivity measurements), the stacking-fault energy and the separation of the partial dislocations are also included in the table. The separation, r, of the partial dislocations was calculated from $r = Ga^2/24\pi\gamma$ where G is the shear modulus, a the lattice parameter and γ the stacking-fault energy.

It is apparent that for the metals considered the resistance of a dislocation is more than an order of magnitude greater than that estimated by Hunter and Nabarro (1953) ($0{\cdot}38 \times 10^{-14}\,\mu\Omega\,\text{cm/dislocation line/cm}^2$),

Electrical resistivity of dislocations in metals

Metal	Deformation	Stored energy cal/g atom	Dislocation density, N, lines/cm$^2 \times 10^{11}$	Increment in electrical resistivity $\Delta\rho$ $\mu\Omega$ cm	$\Delta\rho/N$ $\mu\Omega$ cm/dislocation line/cm^2	Stacking-fault energy, γ erg/cm^2	Separation of partials $r/\mathbf{b}$ Burgers vectors
Al	75% compression	3·2	0·40	0·013	33×10^{-14}	200†	~ 1
Cu	70% compression	9·40	1·33	0·037	28×10^{-14}	169‡	~ 1
Ni	70% compression	11·8	1·06	0·10	94×10^{-14}	95§	~ 3
α-brass	60% tension	12·4	1·4	0·251	180×10^{-14}	25‖	~ 10

† Seeger (1957), Seeger *et al.* (1959).
‡ Seeger *et al.* (1959).
§ Thornton and Hirsch (1958).
‖ Hirsch (1958).

Seeger and Stehle (1956) ($0{\cdot}6 \times 10^{-14}\,\mu\Omega\,\mathrm{cm}$/dislocation line/cm^2), or Harrison (1958) ($5 \times 10^{-14}\,\mu\Omega\,\mathrm{cm}$/dislocation line/cm^2). These theoretical estimates do not take into account any scattering due to stacking faults and it has been suggested that the large discrepancy between the experimental and theoretical values for the resistivity of a dislocation arises from such scattering (Seeger 1957, Howie 1960). The increase in resistivity of a dislocation with decreasing stacking fault energy and increasing separation of the partials (see table) may be readily interpreted as an increase in the contribution of the stacking faults to the total scattering. However, to attribute the total discrepancy between theory and experiment to stacking faults requires that faults approximately one atom wide in copper, for example, increase the resistivity from that of an undissociated dislocation by at least an order of magnitude.

References

Åström, H. U., 1955, *Ark. Fys.*, **10**, 197.

Borelius, G., and Berglund, S., 1951, *Ark. Fys.*, **4**, 173.

Clarebrough, L. M., Hargreaves, M. E., and Loretto, M. H., 1960, *Proc. roy. Soc.* A, **257**, 363 ; *Acta Met.*, **8**, 736.

Clarebrough, L. M., Hargreaves, M. E., Loretto, M. H., and West, G. W., 1960, *Acta Met.*, **8**, 797.

Clarebrough, L. M., Hargreaves, M. E., Michell, D., and West, G. W., 1952, *Proc. roy. Soc.* A, **215**, 507.

Clarebrough, L. M., Hargreaves, M. E., and West, G. W., 1957, *Acta Met.*, **5**, 738.

Gordon, P., 1955, *Trans. Amer. Inst. min. (metall.) Engrs*, **203**, 1043.

Harrison, W. A., 1958, *J. Phys. Chem. Solids*, **5**, 44.

Hirsch, P. B., 1958, *Report on Symposium on Internal Stresses and Fatigue in Metals* (New York: Elsevier).

Howie, A., 1960, *Phil. Mag.*, **5**, 251.

Hunter, S. C., and Nabarro, F. R. N., 1953, *Proc. roy. Soc.* A, **220**, 542.

Perryman, E. C. W., 1954, *Acta Met.*, **2**, 26.

Seeger, A., 1957, *Dislocations and Mechanical Properties of Solids* (New York: Wiley), p. 347.

Seeger, A., Berner, R., and Wolf, H., 1959, *Z. Phys.*, **155**, 247.

Seeger, A., and Stehle, H., 1956, *Z. Phys.*, **146**, 242.

Thornton, P. R., and Hirsch, P. B., 1958, *Phil. Mag.*, **3**, 738.

The Direct Observation of Antiphase Boundaries in the Fe_3Al Superlattice

By M. J. Marcinkowski and N. Brown†
Edgar C. Bain Laboratory for Fundamental Research, United States Steel Corporation, Research Center, Monroeville, Pennsylvania

[Received February 9, 1961]

Two distinct types of antiphase boundaries have been observed in thin foils of the ordered Fe_3Al alloy prepared from the bulk material by electrochemical thinning, using transmission electron microscopy techniques. These boundaries are associated with the two types of ordering possible in this alloy. The first ordered arrangement is that which is stable between 560°C and 800°C, and which can be retained at room temperature by rapid quenching. This particular superlattice is an imperfect B2 type, in that one sub-lattice is occupied entirely by iron atoms, while the other one contains a random distribution of equal numbers of iron and aluminium atoms. The antiphase boundary configuration associated with this ordered arrangement is shown in the micrograph of fig. 1‡, where the antiphase boundaries appear as wavy lines which are light or dark depending on the curvature of the foil. This particular domain geometry was obtained by annealing a Fe_3Al sample for 1 hour at 600°C and then quenching. In accordance with what one would anticipate in a superlattice with only two distinct sub-lattices, the arrangement of antiphase domains is such that one type of domain is surrounded entirely by a domain of the other kind. Furthermore, unlike the $AuCu_3$ superlattice (Marcinkowski and Fisher 1960), the antiphase boundaries show no noticeable tendency to lie on any particular crystallographic plane, and this has been attributed to the small difference in antiphase boundary energy between the various planes in this particular superlattice.

Below 560°C, the imperfect B2 type Fe_3Al superlattice undergoes a transformation to the more perfect DO_3 type lattice. The iron and aluminium atoms, which are located originally at random on one of the sub-lattices above 560°C, order in such a manner that the aluminium atoms avoid being second-nearest neighbours. This lower temperature ordering process results in the formation of a second set of domains within the already existing domains formed above 560°C. Such a domain configuration is shown by the micrograph in fig. 2. The specimen was

† Department of Metallurgical Engineering, University of Pennsylvania, Philadelphia, Pennsylvania.

‡ All figures are shown as plates.

first annealed for 1 hour at 600°C to develop the B2 type antiphase domain configuration and then slowly cooled to 250°C at a rate of 3·58°C/hr to develop the DO_3 type antiphase domain arrangement. It is not always apparent from fig. 2 what type of antiphase boundary is associated with a particular ordered configuration. However, close examination of several antiphase boundaries such as that indicated by the arrow at A, shows that it is probably of the DO_3 type since it terminates abruptly on the continuous B2 type antiphase boundary shown by the arrow at B. The difference between these two types of antiphase boundary can be shown by more refined methods using dark field techniques and will be discussed in a future paper. The DO_3 type antiphase boundaries in fig. 2, similar to the B2 type, again show no preference for any particular crystallographic plane, because there is a small difference in antiphase boundary energy among the crystal planes in this structure.

Thus far, consideration has been given to those antiphase boundaries in the Fe_3Al superlattice formed by thermal diffusion. The micrograph of fig. 3, on the other hand, shows a high density of antiphase boundary ribbons, generated on the slip plane by ordinary dislocations, in an alloy possessing an ordered structure similar to that described in fig. 1. Unlike the superlattice dislocations observed in the $AuCu_3$ superlattice (Marcinkowski *et al.* 1960), which are able to move through the lattice with essentially no net creation of disorder, the dislocations present in the Fe_3Al alloy are found to move as ordinary $\frac{1}{2}a_0\langle 111\rangle$ type dislocations. In fig. 3 the paths of the dislocations as delineated by the slip-produced antiphase boundaries, run generally from left to right, but the direction of any one particular ribbon is quite irregular. This has been observed in practically all of the alloys examined, and is postulated to arise from the fact that most of these dislocations are of pure screw type, which are able to move on any plane contained within the $\langle 111\rangle$ zone ; the particular plane at a given point being determined by the direction of the maximum resolved shear stress at that point. Because the slip-produced antiphase boundaries have a relatively low energy and because the dislocations slip easily from one plane to another, it is not expected that superlattice dislocations should be observed in this particular alloy.

Finally, both the thermally- and slip-produced antiphase boundaries in the Fe_3Al superlattice are observed only when the foil is suitably oriented for diffraction by a strong superlattice reflection, because the diffracted waves associated with these particular reflections undergo a change in phase angle α in the region of the antiphase boundary. For the present Fe_3Al type superlattices, this phase angle has been found to be either $\pm\pi$ or $\pm\pi/2$, depending on the particular combination of superlattice reflection and antiphase boundary type. In addition, the extinction distances associated with the superlattice reflections are on the order of 2000 Å, which in most cases results in the elimination of fringe contrast at the antiphase boundaries, so that they appear as solid light

or dark lines with respect to the domains. These rather large extinction distances also lead to very critical orientations at which antiphase boundary contrast can be observed, e.g. within 0·5° of the exact Bragg angle. The details of the results mentioned in this very brief note will be published at a later date in two separate papers.

References

Marcinkowski, M. J., and Fisher, R. M., 1960, *J. appl. Phys.*, **31**, 1687.
Marcinkowski, M. J., Fisher, R. M., and Brown, N., 1960, *J. appl. Phys.*, **31**, 1303.

Thermal Expansion at Low Temperatures
II. Electronic Component in Metals

By G. K. White
Division of Physics, Commonwealth Scientific and Industrial Research Organization, Sydney, Australia

[Received February 27, 1961]

Some years ago Mikura (1941) showed theoretically that the electron gas in a metal should make a contribution β_e to the thermal expansion and that this would be related to the electronic specific heat C_e and the bulk modulus K as follows:

$$\beta_e = \gamma_e C_e / KV$$

where V is the atomic volume and γ_e is a numerical constant. This contribution is of course additional to the usual term β_g arising from the anharmonicity of the crystal lattice:

$$\beta_g = \gamma_g C_g / KV$$

where C_g is the lattice specific heat and γ_g is the Gruneisen constant. Visvanathan (1951) and Varley (1956) each arrived independently at a similar conclusion regarding the existence of the electronic component. In the more general treatment Varley showed that

$$\gamma_e = \left\{ 1 + \left(\frac{\partial \ln n(\epsilon_F)}{\partial \ln V} \right)_{\epsilon_F, T} - \frac{N}{n(\epsilon_F)^2} \left(\frac{\partial n(\epsilon_F)}{\partial \epsilon_F} \right)_V \left(1 + \frac{\partial \ln N}{\partial \ln N} \right)_{\epsilon_F, T} + \frac{C_e}{\alpha V n(\epsilon_F)^3} \left(\frac{\partial n(\epsilon_F)}{\partial \epsilon_F} \right)_V^2 \right\}$$

where $n(\epsilon_F)$ is the total density of states per unit volume at the Fermi energy ϵ_F and N is the number of electrons per unit volume of crystal in the partially filled bands. For the single-band free electron case, γ_e has a value $\frac{2}{3}$.

For a hypothetical metal having

$$V \simeq 10 \text{ cm}^3, \quad C_e \simeq 10^{-3} T \text{ J/mole deg}, \quad K \simeq 10^{12} \text{ dyn/cm}^2,$$

a linear expansion term α_e would be given by

$$3\alpha_e = \gamma_e \times 10^{-9} T,$$

i.e.

$$\alpha_e = 0{\cdot}22 \times 10^{-9} T \text{ per } ^\circ\text{C}$$

and would be comparable in magnitude with the lattice term α_g at temperatures below $\theta/50$.

In an earlier paper (White 1960) it is indicated that modern techniques for comparing small capacitances of the three terminal type are sufficiently sensitive to allow length changes of less than 10^{-8} cm to be detected; these techniques make possible the determination of thermal expansion at these low temperatures. A more detailed paper concerning the method has now been published (White 1961 a) and considerable data has now been compiled on the linear expansivity $\delta l/l_0$ between 1·5° and 25°K of Cu, Fe, Pd, Cr and Al. Some preliminary results for copper and iron were included in the first paper, those for iron indicating the presence of a term $\alpha = AT$, presumably electronic in origin. In all of these elements the data obtained below about 10°K may be analysed to give an expansivity of the form

$$\delta l/l_0 = AT^2 + BT^4$$

from which are deduced values of a, b in the expression

$$\alpha = aT + bT^3.$$

The terms in T and T^3 are respectively identified with the linear components of thermal expansion α_e and α_g and also yield values for γ_e and γ_g using available data for the electronic heat capacity (review by Keesom and Pearlman 1955, also Phillips 1959 (Al) and Rayne and Kemp 1956 (Cr)) and elastic constants (review by Hearmon 1956 and Hughes and Maurette 1956 (Fe), Rayne 1960 (Pd)).

The purpose of this communication is chiefly to present the values of α_e and γ_e so obtained, but values for the lattice parameter of Gruneisen, γ_g, are also included (table). Except in the case of copper, values given for the lattice components α_g, γ_g are still somewhat uncertain. This is because the values of α_g for Pd, Fe, Al, Cr up to 10° or 12°K are usually much smaller than α_e and/or smaller than α for Cu relative to which these measurements have been made. For calibration purposes the α for copper was determined both relative to beryllium, BeO and ruby and absolutely in a specially constructed cell. More closely defined values of α_g will be obtained shortly when detailed analysis of existing results between 12 and 25°K are completed and some further absolute measurements have been made.

Concerning the values for γ_e given in the table, certain facts may be noted:

(*a*) For Cu, the value of 0·7 is not very different from the free-electron value.

(*b*) For Pd, Al, Fe values are in the region of $+2$ suggesting that the volume dependence of the density of states is appreciable and positive (see Varley loc. cit.). In the case of Al measurements by Gross and Olsen (1960) of the change in critical field with pressure suggests a much larger positive value but Olsen (private communication) points out that the value calculated depends rather critically on the form of the critical field curve assumed.

(*c*) For chromium large negative values occur. Varley (loc. cit.) has argued that such negative values would occur where the density of states $n(\epsilon, V)$ increases sharply with energy near the Fermi energy but there is only a weak dependence of $n(\epsilon, V)$ upon volume. And alternatively a density-of-states curve sharply decreasing with energy might

Experimental data for linear thermal expansion. All samples were vacuum annealed excepting Cr3 and Be. (Abreviations are as follows: A.S.R. for 99·999% pure sample from American Smelting and Refining Company, New York; G.D.M. for 99·9% sample from Garrett, Davidson and Matthey, Sydney; B.I.S.R.A. for 99·97% sample from British Iron and Steel Research Association, Sheffield; A.R.L. for 99·98% ductile samples from Aeronautics Research Laboratory, Melbourne; A.A.E.C. for beryllium from Australian Atomic Energy Commission, Sydney.)

Source		$\alpha_e \times 10^{10} T^{-1}$	$\alpha_g \times 10^{11} T^{-3}$	γ_e	γ_g
Cu	A.S.R.	$1{\cdot}6 \pm 0{\cdot}4$	$2{\cdot}9_2 \pm 0{\cdot}0_7$	$0{\cdot}7 \pm 0{\cdot}2$	$1{\cdot}9_3 \pm 0{\cdot}0_6$
Al	A.L.	9 ± 1	$2{\cdot}5 \pm 0{\cdot}2$	$1{\cdot}8 \pm 0{\cdot}2$	$2{\cdot}6 \pm 0{\cdot}2$
Pd	G.D.M.	37 ± 2	$4{\cdot}8 \pm 0{\cdot}8$	$2{\cdot}1 \pm 0{\cdot}1$	$2{\cdot}3 \pm 0{\cdot}4$
Fe	B.I.S.R.A.	29 ± 2	$1{\cdot}0 \pm 0{\cdot}1$	$2{\cdot}2 \pm 0{\cdot}2$	$2{\cdot}0 \pm 0{\cdot}2$
Cr 2	A.R.L.	-39 ± 4	—	$-9{\cdot}7 \pm 1{\cdot}0$	
Cr 3	A.R.L.	-35 ± 3	—	$-8{\cdot}3 \pm 0{\cdot}8$	
Cr 3a	A.R.L.	-31 ± 3	—	$-7{\cdot}8 \pm 0{\cdot}8$	
Be	A.A.E.C.	$2{\cdot}3 \pm 0{\cdot}6$	—	$1{\cdot}9 \pm 0{\cdot}5$	

be associated with sufficiently large and negative values of the volume dependence term. There is an added interest in this large negative coefficient for chromium and its probable sensitivity to band structure because of the anomaly near 38°C, above which the expansion coefficient increases markedly (for example review by Edwards, Nish and Wain 1959, and more recent data of White 1961 b).

(*d*) A value of α_e and γ_e for Be is included in the table arising from an intercomparison of the expansivities of Cu relative to Be and Cu relative to BeO.

Acknowledgments

My thanks are extended to Mr. A. M. Thompson, Dr. P. G. Klemens and Mrs. P. C. Zeleny for their help and to the following for providing samples: Dr. K. Reeve (Metallurgy section of the Australian Atomic Energy Commission, Sydney) for Be and BeO, Dr. H. L. Wain (Aeronautics Research Laboratory, Melbourne) for Cr and the British Iron and Steel Research Association, Sheffield for Fe.

References

Edwards, A. R., Nish, J. I., and Wain, H. L., 1959, *Metallurg. Rev.*, **4,** 403.
Gross, D., and Olsen, J. L., 1960, *Cryogenics*, **1,** 91.
Hearmon, R. F. S., 1956, *Advanc. Phys.*, **5,** 323.
Hughes, D. S., and Maurette, C., 1956, *J. appl. Phys.*, **27,** 1184.
Keesom, P. H., and Pearlman, N., 1955, *Hand. Phys.*, **14,** 282.
Mikura, Z., 1941, *Proc. phys. math. Soc. Japan*, **23,** 309.
Phillips, N. E., 1959, *Phys. Rev.*, **114,** 676.
Rayne, J. A., 1960, *Phys. Rev.*, **118,** 1545.
Rayne, J. A., and Kemp, W. R. G., 1956, *Phil. Mag.*, **1,** 918.
Varley, J. H. O., 1956, *Proc. roy. Soc.*, A, **237,** 413.
Visvanathan, S., 1951, *Phys. Rev.*, **81,** 626.
White, G. K., 1960, *Nature, Lond.*, **187,** 927; 1961 a, *Cryogenics*, **1,** 151; 1961 b, *Aust. J. Phys.* (to be published).

Stored Energy and Flow Stress in Deformed Metals

By L. M. Clarebrough, M. E. Hargreaves, A. K. Head and M. H. Loretto

Division of Tribophysics, C.S.I.R.O., University of Melbourne, Parkville, N.2, Victoria, Australia

[Received September 12, 1960]

The relation between the stored energy and the flow stress for a cold-worked metal is of interest in relation to theories of work hardening. For the model suggested by Friedel (1955) and Seeger *et al.* (1957), in which the flow stress of a work hardened metal arises from long-range stresses associated with piled-up groups of dislocations, Bailey and Hirsch (1960) have calculated the energy stored in silver from flow-stress measurements and compared the results with experimental values. They found that the calculated stored energy was nearly an order of magnitude greater than the experimental value and thus concluded that the theory of flow stress involving piled-up groups could be dismissed, for the case of polycrystalline silver, on the basis of measurements of stored energy and flow stress, without recourse to the results of electron transmission microscopy. This conclusion is also taken as valid for Au, Cu, Al and Ni since no pile-ups are observed in transmission studies on thin foils (Hirsch 1958). However, Bailey and Hirsch consider that long-range stresses may be important in α-brass and stainless steel where pile-ups have been observed (Hirsch 1958, Whelan *et al.* 1957, Whelan 1959). The purpose of this letter is not to argue the merits of various theories of work hardening, but to point out that theories involving piled-up groups cannot be dismissed on the basis of measurements of stored energy and flow stress alone.

Bailey and Hirsch use the expression

$$E_G = \frac{2\pi K}{G} \tau_g^2 \ln\left(\frac{R}{r_0}\right) \quad . \quad . \quad . \quad . \quad . \quad . \quad . \quad . \quad (1)$$

for calculating the stored energy from the flow stress where E_G is the stored energy per unit volume, τ_g is the temperature independent part of the flow stress, R the radius of the volume over which the stress field extends and r_0 the core radius of a dislocation. Equation (1) was obtained by combining the expression

$$\tau_g = \frac{G\mathbf{b}n}{2\pi K} N_G^{1/2} \quad . \quad . \quad . \quad . \quad . \quad . \quad . \quad . \quad (2)$$

due to Seeger *et al.* (1957), where N_G is the density of piled-up groups, with the expression

$$E_G = \frac{G(n\mathbf{b})^2}{4\pi K} 2N_G \ln\left(\frac{R}{r_0}\right). \quad . \quad . \quad . \quad . \quad . \quad . \quad (3)$$

Equation (3) implies that the stored energy per unit volume is essentially the energy of $2N_G$ isolated dislocations of Burgers vector $n\mathbf{b}$, the factor 2 taking account of edge and screw dislocations. It is considered that this gives an incorrect estimate, involving as it does an outer cut-off radius R which should not appear if there is overall equality of dislocations of opposite signs.

The stored energy associated with a model involving piled-up groups of dislocations, taking into account the interaction between groups, has been more accurately calculated by Stroh (1953). This calculation remains valid irrespective of whether the closest groups arise from the same source or not, with a factor near unity to correct for orientation effects, and can therefore be used to calculate the stored energy for the distribution of groups envisaged by Seeger and Friedel. From Stroh's eqns. (10) and (12) it follows that

$$E_G = \frac{n^2\mathbf{b}^2G2N_G}{4\pi K}\left\{\ln\frac{8\pi Ke^{1/2}\tau_g L}{n\mathbf{b}G} - \frac{1}{n}\ln\frac{4\pi K\tau_g r_0}{\mathbf{b}G} + \ldots\right\} \qquad (4)$$

where $2L$ is the distance between nearest groups of piled-up dislocations. Thus eqn. (2) becomes

$$\tau_g = \frac{G\mathbf{b}n}{4\pi KL}. \qquad (5)$$

Taking $r_0 = 2\mathbf{b}$ and $K = 1$ and combining (4) and (5) the expression relating the stored energy to the flow stress becomes

$$E_G = \frac{2\pi\tau_g{}^2}{G}\left\{\ln 2e^{1/2} - \frac{1}{n}\ln\frac{8\pi\tau_g}{G}\right\}. \qquad (6)$$

Using eqn. (6), taking τ_g as half the applied stress (Bailey and Hirsch 1960) and $n = 25$ (Seeger *et al.* 1957) reasonable agreement is obtained between values of stored energy calculated from measurements of flow stress and experimental values for aluminium, copper, nickel and α-brass as indicated in the table. A value of the energy stored in silver recalculated from the measurements of Bailey and Hirsch using eqn. (6) is also included in the table and shows the same agreement. The result is very insensitive to the value chosen for n. In contrast to the results of Bailey and Hirsch all calculated values of the stored energy are close to the experimental values and the agreement is as good as can be expected considering the uncertainty in the estimate of τ_g. It is of interest that the agreement is equally good for those metals (aluminium, copper, nickel and silver), for which no pile-ups have been observed in electron transmission studies, as for α-brass where pile-ups have been observed.

The agreement between the experimental and calculated values of stored energy indicates that theories of hardening involving piled-up groups of dislocations of the type considered by Friedel and Seeger cannot be dismissed on the basis of measurements of flow stress and stored energy alone. However, it should be emphasized that this agreement should not

be taken as proof of the correctness of such theories, which *other* evidence may well show to be based on incorrect models.

Bailey and Hirsch did not detect any significant differences in the distribution and density of dislocations for thin foils of silver before and after a recovery treatment which liberated approximately half of the stored energy in their bulk specimens. The liberation of such a large proportion of the total stored energy during the recovery treatment is very similar to the results obtained with nickel (Clarebrough *et al.* 1955, 1956) where approximately 70% of the total energy stored is released before recrystallization. This large evolution of energy is associated with a large increase in density and a decrease in resistivity and only a small proportion of these changes in properties can be attributed to the annealing of vacancies. The remainder of the energy released and changes

Comparison of calculated and measured values of stored energy

	Flow stress kg/mm^2	Stored energy cal/g atom	
		Calculated	Measured
Aluminium 75% compression	6·1	2·6	3·2†
Copper 70% compression	19·0	12·0	12·1‡
Nickel 70% compression	34·5	18·4	11·8§
α-brass 60% tension	22·5	14·4	12·2‖
Silver 43% tension	11·6	9·6	7·27¶

† Clarebrough, Hargreaves and Loretto (unpublished work).
‡ Clarebrough, Hargreaves and Loretto (1958).
§ Clarebrough, Hargreaves, Loretto and West (1960). (The energy shown refers to the energy evolved during recrystallization.)
‖ Clarebrough, Hargreaves and Loretto (1960). (The energy shown refers to the energy evolved during recovery and recrystallization.)
¶ Bailey and Hirsch (1960).

in other properties are ascribed to the removal of dislocations from within the particles, rearrangement of dislocations and the annihilation of dislocations of opposite sign in the boundary regions. This is in accord with the conclusions on the nature of recovery in general of Gay *et al.* (1954), although these were not based on measurements on nickel. Thus the failure to detect any significant differences in the distribution and density of dislocations in the transmission studies may be due to loss of the dislocations within the particles during thinning down, since the thickness of the foils is small compared to the size of the particles and the inability to detect changes in the boundary regions where the dislocation density is high and very difficult to estimate with any precision (Bailey and Hirsch 1960).

References

Bailey, J. E., and Hirsch, P. B., 1960, *Phil. Mag.*, **5,** 485.

Clarebrough, L. M., Hargreaves, M. E., and Loretto, M. H., 1958, *Acta Met.*, **6,** 725 ; 1960, *Proc. roy. Soc.*, A, **257,** 363.

Clarebrough, L. M., Hargreaves, M. E., Loretto, M. H., and West, G. W., 1960, *Acta Met.*, **8,** 797.

Clarebrough, L. M., Hargreaves, M. E., and West, G. W., 1955, *Proc. roy. Soc.* A, **232,** 252 ; 1956, *Phil. Mag.*, **1,** 528.

Friedel, J., 1955, *Phil. Mag.*, **46,** 1169.

Gay, P., Hirsch, P. B., and Kelly, A., 1954, *Acta cryst., Camb.*, **7,** 41.

Hirsch, P. B., 1958, *Report on Symposium on Internal Stresses and Fatigue in Metals* (New York: Elsevier).

Seeger, A., Diehl, J., Mader, S., and Rebstock, H., 1957, *Phil. Mag.*, **2,** 323.

Stroh, A. N., 1953, *Proc. roy. Soc.* A, **218,** 391.

Whelan, M. J., 1959, *Proc. roy. Soc.* A, **249,** 114.

Whelan, M. J., Hirsch, P. B., Horne, R. W., and Bollman, W., 1957, *Proc. roy. Soc.* A, **240,** 524.

Segregation of Solute Atoms in Copper–Aluminium Alloys

By Koichi Nakazima and Shigeyasu Koda
The Research Institute for Iron, Steel and Other Metals, Tohoku University, Sendai, Japan

[Received January 3, 1961]

It was reported by some workers (for example, Smallman and Westmacott 1957) that the density of stacking faults introduced by cold-working in face-centred cubic solid solutions increased with increasing content of solute atoms, and reached a maximum at the solubility limit of the solution. This fact may be interpreted from the point of view that solute atoms concentrate in the faulted layers, and prevent the movement of the stacking faults at room temperature. In fact, Suzuki (1952) has pointed out that in a face-centred cubic solid solution the state of thermodynamic equilibrium in the faulted layers will be different from that of the matrix, altering the concentration of solute atoms in the faulted layers. If this concept is valid, a small angle scattering due to the inhomogeneity of the structure should be observed. Recently, a weak small angle scattering was actually observed (Nakazima 1959, 1960) in specimens of copper–aluminium alloys with aluminium of 12% or more; and it was seen that in the case of copper-18% aluminium the scattering was little observable after annealing at above 200°C and that these phenomena corresponded to the recovery of asymmetrical line shape as will be mentioned later. Recently, extending the Paterson theory (1952) to the case of segregation of solute atoms around stacking faults, Willis (1959) showed that the principal effect of the segregation was to make the reflections asymmetrical; that is, the change in the diffraction patterns caused by solute concentration in deformation faults gives rise to weak diffuse streaks between reflections, in the columns having $H_1 - H_2 = 3M$, and to asymmetry in the remaining reflections, where H_1 and H_2 are the indices corresponding to the hexagonal indices, and M an integer. In the case of $H_1 - H_2 = 3M$ the combined effects of faulting and segregation on the powder patterns makes this component sharp and undisplaced, whereas in the case of $H_1 - H_2 = 3M \pm 1$ it is broadened asymmetrically and displaced to higher or lower Bragg angles. Therefore the effect of the segregation may be detected from the line profiles of powder diffraction lines.

The present experiment was carried out to calculate the segregation of solute atoms with copper–aluminium alloys by using the theory proposed by Willis. The alloys of various compositions were pulverized at room temperature by using a stamp and a ball mill. The x-ray diffraction was taken with an XRD-5 Geiger counter diffractometer made by General Electric Co., using Cu-Kα radiation. The x-ray tube was used at

25 kv, 15 ma. A nickel filter of about 10 μ in thickness was inserted, and the observation of the counts was made at every 0·01° by handling. Time required for 1000 counts was adopted. Measurements of the profile, and the peak shift of (111) and (200) were made. To correct for instrumental broadening from an observed line broadening Stokes method (1948) was used, and the position of the centre of gravity of diffraction profile was determined graphically.

As the result of the analysis the stacking-fault probability α and the shift of the centre of gravity $\Delta(2\theta)_G$ in the case of copper-18·3% aluminium were 0·08 and 0·05°, respectively. Using these results the factor β relating to the segregation of solute atoms on deformation stacking faults was calculated from the equation proposed by Willis, and as the result $\beta \sim -0{\cdot}06$ was obtained. On the other hand the concentration of solute atoms in stacking faults is calculable by the theory of Suzuki. In the case of copper-18·3% aluminium the solute concentration C_1 at room temperature was 0·33. The segregation factor β can be determined from the value of C_1 and C_0 as shown by

$$\beta = \frac{f_2}{f_1} - 1 = \frac{f_{Cu}(1-C_1)+f_{Al}C_1}{f_{Cu}(1-C_0)+f_{Al}C_0} - 1.$$

From this equation β in the present case was found to be $-0{\cdot}10$. It will be seen that the results from the x-ray analysis is in agreement qualitatively with the result deduced from Suzuki's theory. From these results it is concluded that in the case of copper-18·3% aluminium the average scattering powers of the atoms in the two kinds of layer are different by about 6% owing to cold-working, and this is explained as caused by the segregation of solute atoms on deformation stacking faults. A more detailed investigation on the temperature of the segregation of solute atoms is desirable. The full report will be given before long.

References

Nakazima, K., 1959, *J. phys. Soc., Japan*, **14**, 1825; 1960, *Sci. Rep. res. Inst. Tohoku Univ.*, **12**, 309.
Paterson, M. S., 1952, *J. appl. Phys.*, **23**, 805.
Smallman, B. E., and Westmacott, K. H., 1957, *Phil. Mag.*, **2**, 669.
Stokes, A. R., 1948, *Proc. phys. Soc. Lond.*, **61**, 382.
Suzuki, H., 1952, *Sci. Rep. res. Inst. Tohoku Univ.*, **4**, 455.
Willis, B. T. M., 1959, *Acta cryst., Camb.*, **12**, 683.

Fig. 1

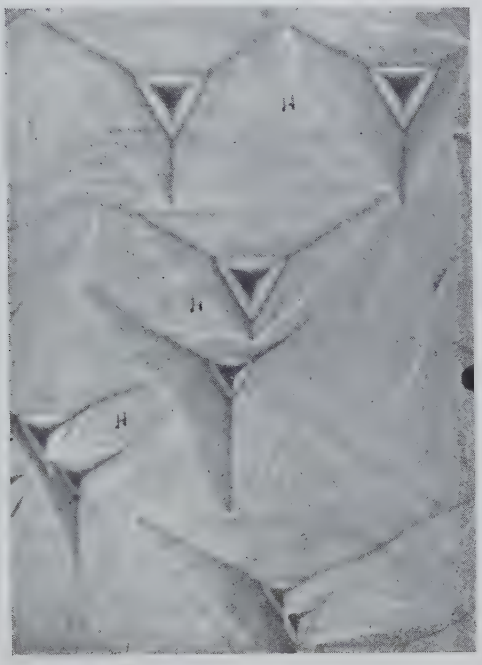

Etched alum. ×120.

Fig 2

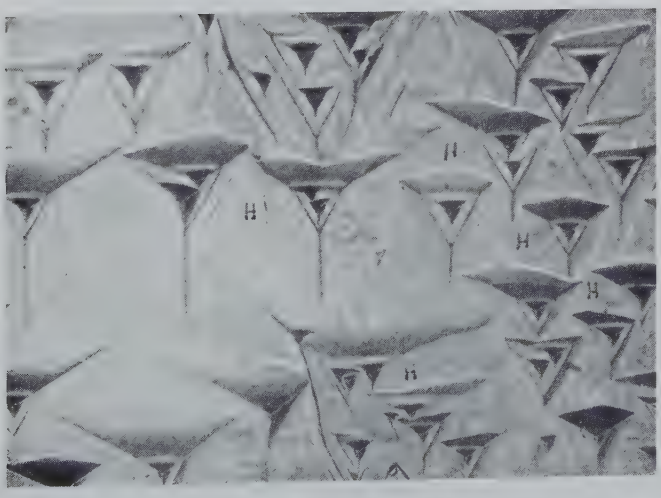

Etched alum. ×105.

Fig. 3

Etched alum. ×65.

Fig. 4

Natural diamond. ×375.

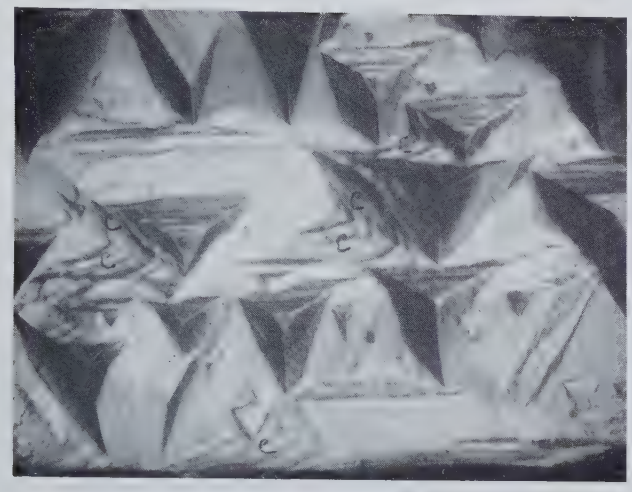

Fig. 5

Etched alum. ×48.

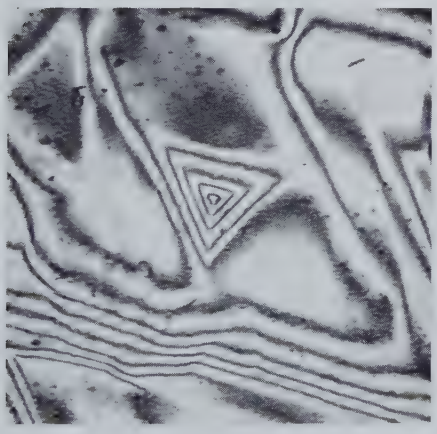

Fig. 6

Etched alum. ×230.

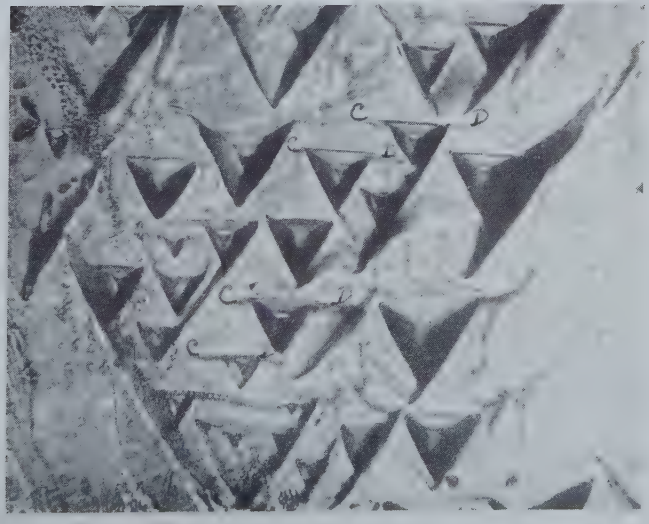

Fig. 7

Etched alum. ×130.

Fig. 1

Antiphase boundaries associated with the B2 type superlattice formed in the Fe_3Al alloy.

Fig. 2

Antiphase boundaries associated with the DO_3 type superlattice formed in the Fe_3Al alloy.

Fig. 3

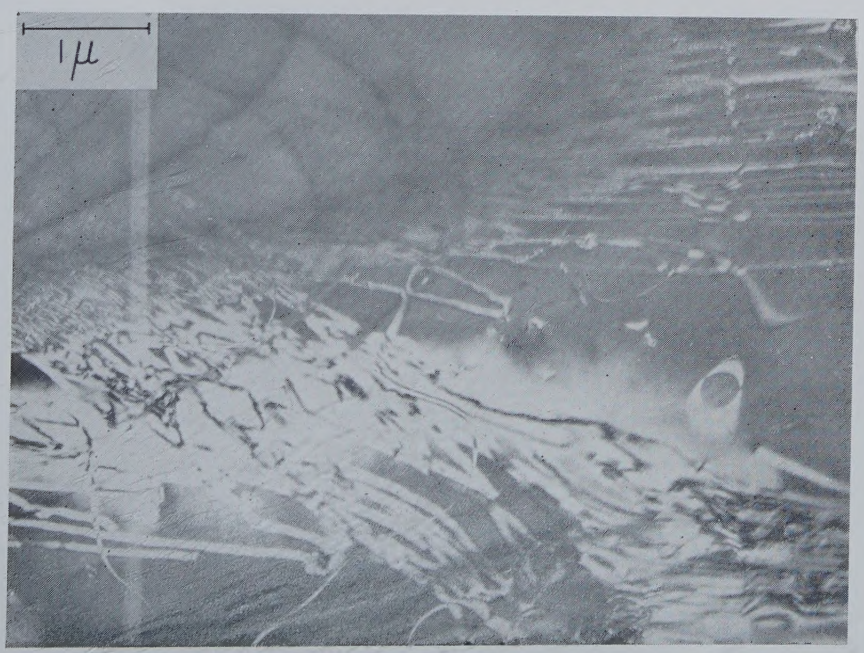

Antiphase boundaries generated by the motion of ordinary dislocations in the Fe_3Al alloy possessing a B2 type ordered lattice.